

The Effect of Hydrogen Addition on Turbocharged Marine Diesel Engines

In search of the catalytic effect of hydrogen addition



MSc. Thesis report

Willem Kes

Student nr: 1517864

Delft University of Technology, Faculty 3mE
Section Ship Design, Production and Operation

Supervisor TU Delft: Ir. K. Visser

Supervisor IHC MTI B.V.: Ir. B.T.W. Mestemaker

TU Delft SDPO Report nr: **SDPO.16.024**

IHC MTI B.V. Report nr: **AO 144**

Graduation date: August 16th 2016

PREFACE

This report is the conclusion of the MSc thesis of Willem Kes. The subject of this thesis is: The effect of hydrogen addition on engine performance and emissions of turbocharged marine diesel engines.

This subject was provided by IHC MTI B.V. in close collaboration with TU Delft.

The graduation committee for this thesis consists of:

Ir. K. Visser (chairman)	TU Delft 3mE, Department M&TT, section Ship Design, Production and Operations
Ir. P. de Vos	TU Delft 3mE, Department M&TT, section Ship Design, Production and Operations
Prof. dr. D.J.E.M. Roekaerts	TU Delft P&E, section Fluid Mechanics
Ir. C.L. Dijkstra	Ministerie van Defensie, Nederlandse Defensie Academie
Ir. B.T.W. Mestemaker	Royal IHC, IHC MTI B.V.

The completion of this thesis is, in no small part, due to a number of people who were closely involved in the entire process.

First and foremost my supervisor at IHC MTI B.V., Benny Mestemaker, for his detailed knowledge regarding the subject and also for helping me keep my focus during the process.

Another special thanks to Klaas Visser, my supervisor at Delft University of Technology. Together with Benny he kept me on track, and provided insightful feedback at numerous progress meetings.

I also want to thank Chris Dijkstra and Sergeant Marcel Roberscheuten at NLDA in Den Helder. During my time there testing both of them were always available for questions and helping out, especially Marcel who was with me continuously during the tests for a period of two weeks.

Finally a thank you to Nikolas Panagakis and his employer Boskalis for providing the emissions measuring equipment.

*Willem Kes
Rotterdam, July 26, 2016*

Table of Contents

PREFACE	2
Chapter 1: Introduction	5
1.1 Background	5
1.2 Research objectives	5
1.3 Thesis outline	6
Chapter 2: Literature review	7
2.1 Introduction	7
2.2 History of hydrogen addition	7
2.3 Properties of hydrogen	11
2.4 Efficiencies	12
2.5 Emissions.....	17
2.6 Pressure, peak pressure and heat release	20
2.7 Combustion limits (knocking)	23
2.8 Conclusions & expectations	24
Chapter 3: Current application	27
3.1 Combustion engine applications.....	27
3.2 Other applications.....	27
Chapter 4: Models and theoretical background	28
4.1 Introduction	28
4.2 Heat release and heat release model	28
4.3 Vibe fit model.....	31
4.4 In-cylinder process simulation model	33
4.5 Seiliger cycle and parameters	35
Chapter 5: Experimental setup and testing	39
5.1 Introduction	39
5.2 Experimental setup and equipment	39
5.3 Hydrogen addition calculations	45
5.4 Map of measured points.....	46
5.5 Testing procedure	48
5.6 Data processing.....	52
Chapter 6: Measurement Results	55
6.1 Introduction	55
6.2 Fuel consumption.....	55

6.3 Correction for hydrogen combustion efficiency and scavenging	58
6.4 Emissions.....	63
6.5 Cylinder pressure	69
Chapter 7: Cylinder pressure analysis results	72
7.1 Introduction	72
7.2 Heat release rate.....	72
7.3 Seiliger fit	87
Chapter 8: Matching results.....	103
8.1 Introduction	103
8.2 Low load scenario's	104
8.3 High load scenario's	107
Chapter 9: Conclusions and recommendations.....	111
9.1 Conclusions	111
9.2 Recommendations	113
References	115
Appendix A: MAN 4L20/27 Technical details and measured parameters	118
Appendix B: Hydrogen addition percentage calculator	121
Appendix C: Vibe parameters	122

Chapter 1: Introduction

1.1 Background

In the search for alternative fuels and means of power generation, hydrogen is a big contender. It can be used directly in internal combustion engines and fuel cells, but is also an energy carrier. When burned it produces no greenhouse gasses, and the only emission is water. It can also be created in a number of different ways, including the electrolysis of water. Given the reserves of water on earth, hydrogen can be considered to be a renewable resource like solar energy.

In terms of energy density however, gasoline and mainly diesel (*HFO* or *heavy fuel oil* in the marine industry) still reign supreme. Due to new environmental legislation the marine sector is slowly converting to other cleaner fuels like LNG, but this is a very slow process and the required infrastructure is not yet available everywhere. An intermediate solution to reduce emissions and convert to renewable energy sources is the addition of hydrogen gas to existing diesel engines. Hydrogen has no inherent greenhouse gas emissions, has wide ignition limits and it burns about seven times faster than gasoline or diesel.

In addition to replacing a part of the diesel fuel with hydrogen, some claim that the addition of hydrogen also has a catalytic effect on the combustion process. The underlying principle is not 100 percent clear, but it is theorized that the hydrogen increases the homogeneity of the mixture, and that due to the high flame speed there is less heat loss to the cylinder walls which results in higher heat loss efficiency. Additionally a shift in combustion from slow, diffuse combustion to fast, pre-mixed combustion could increase thermodynamic efficiency.

It is this supposed catalytic effect of hydrogen addition that is the main focus of this thesis.

1.2 Research objectives

The objective of this thesis is to study the effect of small amounts (max 10% total energy added) of hydrogen addition in turbocharged marine diesel engines on engine performance and emissions. The amount of hydrogen is purposefully kept low, because we are not interested in substituting fuel but rather a catalytic effect that the hydrogen addition will have on the diesel engine.

To reach this objective, both a literature review and engine tests have been performed. The tests have been executed with an experimental hydrogen addition setup on a turbocharged marine diesel engine. The engine used is the MAN 4L20/27, located at the KIM (Koninklijk Instituut voor de Marine) in Den Helder. KIM is part of the Nederlandse Defensie Academie, or NLDA.

Main parameter measured is the in-cylinder pressure, but additional gaseous emissions and various other engine parameters are recorded as well to monitor the full effect of the hydrogen addition.

To characterize the effect of hydrogen addition on combustion and engine performance, both Vibe modelling and the Seiliger process parameters will be used to describe the combustion process and the heat release rate.

The effect of hydrogen addition on emissions will be studied by measuring and analysing the gaseous emissions directly using professional gaseous emissions measurement equipment (Horiba PG-250 provided by Boskalis).

1.3 Thesis outline

Chapter 2 starts with a literature review of previous research done regarding hydrogen addition in internal combustion engines. This will lead to some preliminary expectations regarding the effect of hydrogen addition.

A short overview of currently available applications regarding hydrogen addition will be given in chapter 3.

In chapter 4 the theoretical background required for the models used in this thesis will be explained. This includes the heat release rate, Vibe modelling and the Seiliger cycle and parameters. Additionally the approach of this thesis will be explained, as well as any changes made to the aforementioned models to better handle the hydrogen addition.

In chapter 5 the experimental setup will be reviewed, starting with the engine itself, the water brake and the measurement equipment installed on the engine. Secondly the equipment required for the hydrogen addition is discussed. This chapter will also cover the testing procedures, methodology and the data processing method.

Chapter 6 will cover the results of the direct measurements. Starting with fuel consumption and emissions, and finally the cylinder pressure. This last measurement will also be the base of the next chapter.

Chapter 7 will display the results of the detailed analysis of the cylinder pressure. The heat release has been distilled from the pressure measurement, and has been fitted and analysed using Vibe fitting and the Seiliger parameters. These processes and results will be shown.

Subsequently Chapter 8 will analyse these results, and compare them both against benchmark diesel operation and against each other (Vibe fitting parameters and Seiliger parameters) to see what method can better capture the effects of hydrogen addition.

Finally, chapter 9 will contain the conclusions and recommendations.

Chapter 2: Literature review

2.1 Introduction

In this chapter, the literature available about the addition of hydrogen in the combustion process will be discussed. The different results provided by different sources will be compared and the applicability of this information will be judged based on the application and the consistency of the data in the literature. This chapter will discuss the following topics:

- History of hydrogen addition (paragraph 2.2);
- Properties of hydrogen (paragraph 2.3);
- Efficiencies (paragraph 2.4)
- Emissions (paragraph 2.5);
- Pressure, peak pressures and heat release (paragraph 2.6);
- Combustion limits (knocking) (paragraph 2.7);
- Conclusions & expectations (paragraph 2.8).

2.2 History of hydrogen addition

The use of hydrogen as an additive in both gasoline and diesel engines is not a recent discovery. Research goes as far back as 1974 (Hoehn & Dowdy, 1974), with NASA (National Aeronautics and Space Administration) publishing a paper on the subject in 1977 (Cassidy, 1977). Both papers use tests performed on gasoline engines, but these very first results of hydrogen addition are nonetheless interesting.

Hoehn discussed the use of hydrogen as a fuel additive to run gasoline engines at lean conditions. He found that substituting approx. 15% (by weight) of the total fuel with hydrogen resulted in a mixture with reduced flammability limit and a reduction in engine operating point in terms of equivalence ratio.

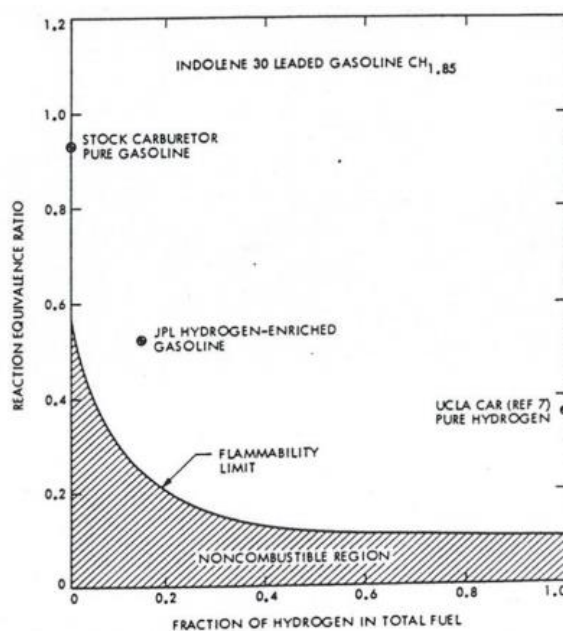


Figure 2.1: calculated flammability limits for hydrogen gasoline mixture, also showing engine design points [Hoehn, 1974]

The flammability limit in figure 1 is expressed in terms of equivalence ratio. Fuel-air equivalence ratio is defined as the fuel-to-air ratio divided by the stoichiometric fuel-to-air ratio (equation 2.1). It is indicated by the Greek letter phi (ϕ) and is the inverse of lambda (λ), the air-to-fuel equivalence ratio (equation 2.2).

$$\phi = \frac{\text{fuel-to-air ratio}}{(\text{fuel-to-air ratio})_{st}} = \frac{\frac{m_{fuel}}{m_{air}}}{(\frac{m_{fuel}}{m_{air}})_{st}} \quad (2.1)$$

$$\phi = \frac{1}{\lambda} \quad (2.1)$$

From figure 2.1 we see that the lean flammability limit of gasoline with 15% hydrogen addition by weight shifts from $\phi = 0.57$ to $\phi = 0.2$. The engine design operating point shifts from $\phi = 0.94$ at pure gasoline to $\phi = 0.57$ with hydrogen addition. Operation at $\phi = 0.57$ with pure gasoline as a fuel would result in engine knock and misfire.

Experimental tests by Hoehn on a 1973 Chevrolet V8 5.7 litre car engine on both a dynamometer and open road showed that at part load (cruising condition), with the aforementioned 15% by weight hydrogen addition and leaning of the operating point, fuel consumption (in terms of energy consumed per mile per ton of vehicle weight) reduced between 25% and 40%. Both CO and NOx emissions were reduced with similar percentages at part load as well, but HC emissions increased significantly. This was attributed to the operation at very lean mixtures, and the consequent risk of misfire and unburned HC.

NASA's research (Cassidy, 1977) also focused on improving efficiency by extending the lean operating range of a gasoline engine by adding hydrogen. Cassidy did a literature review on lean engine operation and found that a fuel with low lean flammability limit and high flame speed might yield low exhaust emissions and increased efficiency at ultra-lean conditions. Hydrogen was identified as such a fuel. Tests were performed to determine the flame speed of a gasoline/hydrogen mixture to confirm the assumption that this value would be greater than the flame speed of a pure gasoline fuel at similar equivalence ratio. The results can be seen in figure 2.2 below.

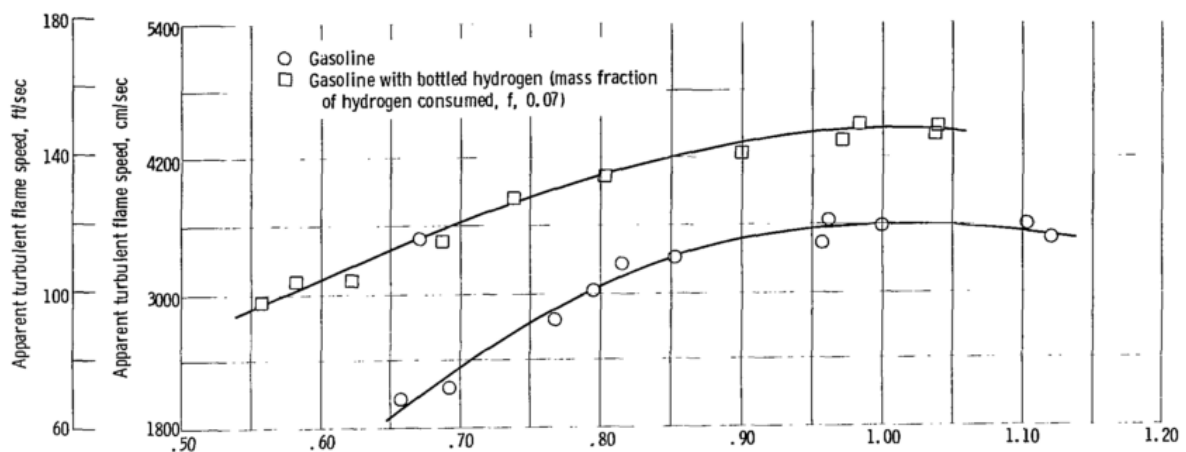


Figure 2.2: Apparent turbulent flame speed as function of equivalence ratio at 2140 rpm and 27 kW [Cassidy, 1977]

It is clear from figure 2.2 that the hydrogen/gasoline mixture (7% hydrogen by weight) has larger flame speed at all equivalence ratios (although the effect is greater at lower ϕ), and also has a lower lean

flammability limit. The flammability limit of gasoline is at an air excess ratio (λ) of 1.54 ($\phi = 0.65$) and when adding 7% hydrogen by mass this limit increases to 1.82 ($\phi = 0.55$).

Cassidy also found a sizeable reduction in ignition delay with hydrogen addition, which he attributed to the advantageous thermal properties of hydrogen. These properties appeared to diminish the thermal loss from the developing flame kernel and to quicken heat release (see figure 2.3 below).

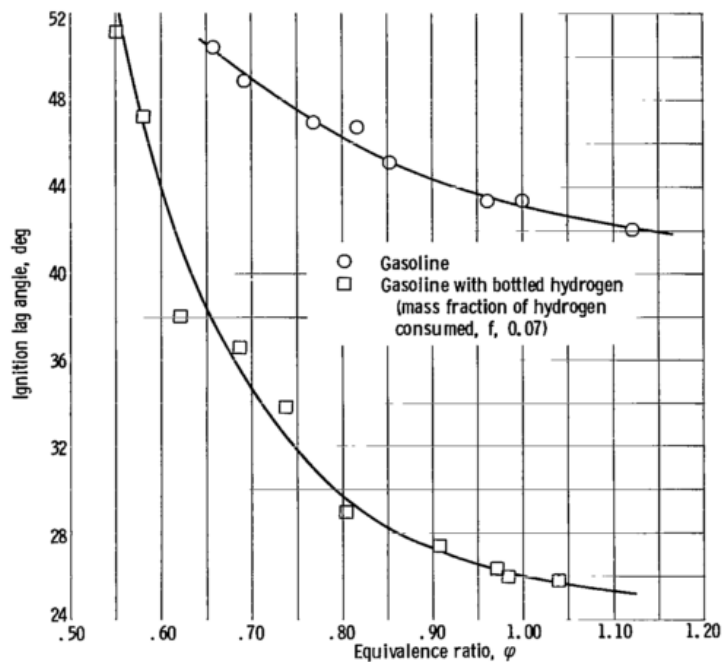


Figure 2.3: Ignition lag as function of equivalence ratio at 2140 rpm and 27 kW [Cassidy, 1977]

In terms of total energy consumption Cassidy found that although the minimum energy consumption is the same for each fuel, this point occurs at a lower equivalence ratio with hydrogen/gasoline mixture as a fuel compared to pure gasoline. At high equivalence ratios (>0.75) the higher flame speed due to hydrogen addition results in higher temperatures which are lost to the cooling system, resulting in higher energy consumption. At low equivalence ratios (<0.70) however, the increase in flame speed is enough to allow smooth and efficient lean operation where this would be impossible with pure gasoline as a fuel. This effect is illustrated in figure 2.4 below.

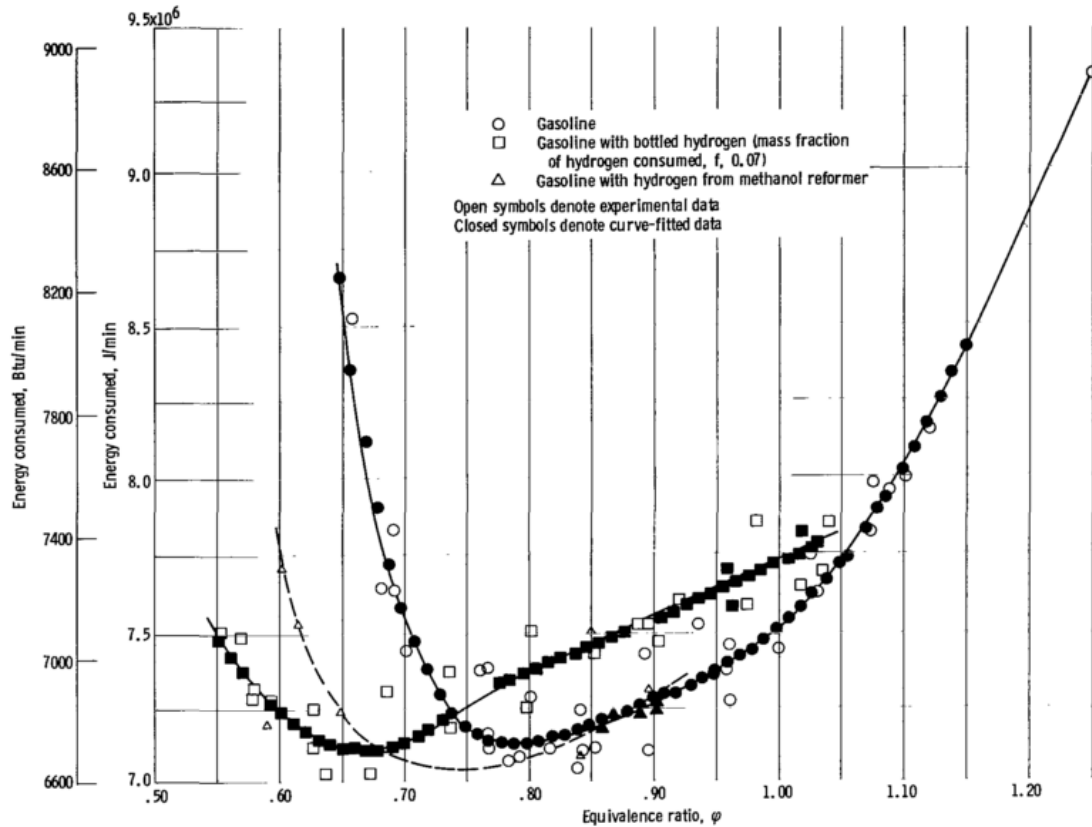


Figure 2.4: Energy consumption as a function of equivalence ratio at 2140 rpm, 27 kW [Cassidy, 1977]

It must be noted that due to the limited capacity of the reformer used in this research the mass flow rate of bottled hydrogen was larger than the mass flow rate of hydrogen from the methanol reformer, resulting in two mixtures with a different percentage of hydrogen addition. This explains why the minimum energy consumption for bottled hydrogen is at a lower equivalence ratio than for the reformed hydrogen in figure 2.4. The fuel mixture with bottled hydrogen is richer in hydrogen and therefore has a higher flame speed which allows it to burn more efficient at even lower equivalence ratios.

As mentioned before the research of both Hoehn and Cassidy was on gasoline engines, not diesel engines. They were summarized to gain some insight into the history of hydrogen addition, and why this subject was first researched.

2.3 Properties of hydrogen

The properties of both diesel and hydrogen that are relevant to combustion in an internal combustion engine are shown (table 2.1). As mentioned before in (Cassidy, 1977) some of these properties make hydrogen an interesting candidate for addition to another fuel like diesel.

Table 2-1: properties of hydrogen and diesel fuel [Tyagi et al., 2013]

Properties	Diesel	Hydrogen
Formula	$C_nH_{1.8n}C_8-C_{20}$	H_2
Auto ignition temperature (K)	530	858
Minimum ignition energy (mJ)	–	0.02
Flammability limits (volume % in air)	0.7–5	4–75
Stoichiometric air fuel ratio on mass basis	14.5	34.3
Molecular weight (g mol)	170	2.016
Limits of flammability (equivalence ratio)	–	0.1–7.1
Density at 160 C and 1.01 bar (kg/m^3)	833–881	0.0838
Net heating value MJ/kg	42.5	119.93
Flame velocity (cm/s)	30	265–325
Quenching gap in NTP air (cm)	–	0.064
Diffusivity in air (cm^2/s)	–	0.63
Octane number		
Research	30	130
Motor	–	–
Cetane number	40–55	–
Boiling point (K)	436–672	20.27
Viscosity at 15.5 °C, centipoise	2.6–4.1	–
Vapour pressure at 38 °C kPa	Negligible	–
Specific gravity	0.83	0.091

One of the main advantages of hydrogen is that it does not produce any major pollutants such as hydrocarbon (HC), carbon monoxide (CO), sulphur dioxide (SO₂), heavy metals, smoke and particulate matter (PM). This is due to the absence of carbon and sulphur in hydrogen. This advantage is relatively small in this thesis, since the focus is on the supposed catalytic effect of hydrogen on the diesel combustion and therefore only small amounts of hydrogen will be added. Additionally hydrogen has high flammability limits (volume % in air) and low ignition energy required, which makes combusting it fairly easy. Diffusivity in air is also very good, making the formation of a homogenous air charge possible and flame speed is very high compared to diesel, which should positively affect the combustion process. Faster combustion means a larger and faster peak pressure which can result in a more effective power stroke of the piston.

The high auto-ignition temperature of hydrogen can be considered both a problem and a perk. In diesel engines this allows for the easy and cheap delivery method of mixing with intake air, instead of adding more fuel injectors to the cylinder. It does however mean that the hydrogen will only be ignited by the burning diesel fuel itself. This increases ignition delay of the hydrogen and the precision with which this ignition can be controlled. In spark ignition engines this is not a problem.

Although the net heating value (unit of MJ/kg) is very high, since hydrogen is a gas its density is very low so overall energy density on a volumetric basis is substantially lower than diesel. This can pose some practical problems with fuel delivery and storage. Hydrogen addition in the charge air replaces oxygen, which reduces volumetric efficiency. This limits the amount of hydrogen that can be added to the intake air. This thesis studies the supposed catalytic effect of hydrogen on the diesel combustion, so only small amounts of hydrogen are added. Therefore this is not a problem in our situation. Additionally, direct injection into the cylinder or intake manifold is also possible but requires expensive

equipment (high-pressure injectors if injected directly into the cylinder) and making substantial changes to the actual engine.

2.4 Efficiencies

The overall efficiency of a diesel engine, often referenced as *brake thermal efficiency* (η_e), is a measure of the engines ability to transform the chemical energy of a fuel (Q_f) into effective mechanical work (W_e), measured at the output shaft. It can be split up into several other partial efficiencies, as shown in equations 2.3 - 2.5 below [Stapersma, 2010]. The suffixes *e* and *i* are used here to indicate *effective* and *indicated* work and/or heat. Effective work is the work developed at the output shaft and is an observable quantity. Indicated work (or heat) is the amount of work (or heat) that can be derived from a P-V respectively a T-S diagram.

$$\eta_e = \eta_m * \eta_{comb} * \eta_{hl} * \eta_{td} \quad (2.3)$$

$$\eta_e = \frac{W_e}{W_i} * \frac{Q_{comb}}{Q_f} * \frac{Q_i}{Q_{comb}} * \frac{W_i}{Q_i} \quad (2.4)$$

$$\eta_e = \frac{W_e}{Q_f} \quad (2.5)$$

Not all of these efficiencies are relevant in this thesis. Mechanical efficiency (η_m) accounts for mechanical losses due to friction of cylinders and bearings, parasitic losses from driving pumps (fuel, cooling water, lube oil), valve operation, etc. It is not impacted by changes in fuel, and thus hydrogen addition will not influence this efficiency. Therefore it will not be covered further.

The other three efficiencies that comprise the brake thermal efficiency are:

- Combustion efficiency (separate for diesel and hydrogen), η_{comb} .

Combustion efficiency is defined as the amount of fuel that is actually burned divided by total fuel injected into the cylinder ($\frac{Q_{comb}}{Q_f}$). In modern diesel engines this efficiency is very close to 100%, but in older engines or at part load this efficiency can drop. It is defined separately for diesel and hydrogen combustion.

- Heat loss efficiency, η_{hl}

Heat loss efficiency corrects for the losses due to heat transfer to cylinder walls, piston heads, etc. It is defined as the heat that is put into the working fluid divided by the total heat released by the fuel during combustion: $\frac{Q_i}{Q_{comb}}$

- Thermodynamic efficiency, η_{td}

The thermodynamic efficiency (η_{td}) is the efficiency of the cycle (Diesel cycle, Otto cycle, Seiliger cycle, etc.) in converting heat to work. Thermodynamic efficiency is defined as $\frac{W_i}{Q_i}$, indicated work divided by indicated heat. For all internal combustion engines (heat engines) this efficiency is limited by the Carnot cycle efficiency:

$$1 - \frac{T_H}{T_C} \quad (2.6)$$

Where T_H is the temperature in the cylinder during combustion, and T_C the condition where waste heat is discharged to.

Other efficiencies can also be defined that are not directly related to the overall efficiency. One of these is the volumetric efficiency:

Volumetric efficiency (η_{vol}) is a measure of how well an engine can move charge into and out of the cylinder. It is the ratio of the amount of air trapped in the cylinder over the theoretical maximum amount of air. By forcing more air into the cylinder (by turbocharging for instance) this efficiency can be increased. The reason this efficiency is interesting when researching hydrogen addition is that the hydrogen (if injected into the intake manifold) will replace some of the air, thus reducing the volumetric efficiency.

Almost all literature covers at least the brake thermal efficiency, while some expand on this further by looking at combustion and heat loss efficiency as well. Continuing on the 1977 research of NASA, in 1983 a similar research was done on a compression ignition diesel engine by the department of Mechanical Engineering of the Banaras Hindu University (Haragopala Rao, 1983). The engine in question was a single cylinder, water-cooled compression ignition engine operating on the four-stroke principle, rated at 3,7 kW (5,0 BHP) at 1500 rpm. Hydrogen was added to the intake air in the manifold, close to the intake valve. The effect of 10% (of total energy input) hydrogen addition (as illustrated at the bottom of figure 2.5) was an increase in brake thermal efficiency at high load, which was attributed to high diffusion rate of hydrogen and faster energy release due to increased flame propagation velocities. This leads to an increased thermodynamic efficiency and thus a higher brake thermal efficiency.

At partial load however, the brake thermal efficiency decreased. This was attributed to incomplete combustion of the added hydrogen, further supported by the observed increase in maximum pressure, which was low at low loads and high at high load.

Another interesting research is the research of the departments of Mechanical Engineering and Applied Physics of the Birla Institute of Technology (Lata, Misra, & Medhekar, 2012). They performed measurements on a fairly large (62,5 kW) gen-set diesel engine with 5-50% hydrogen as secondary fuel. More importantly the engine is turbocharged, and thus comparable to a modern marine diesel engine.

Similarly to Haragopala et al., Lata et al. found that the addition of hydrogen as a secondary fuel enhances the break thermal efficiency at high loads, while it produces reverse effect at low load conditions. They followed the same reasoning as Haragopala et al. as to why this occurred.

While results at low load are consistent, not all research agrees on the effect at high loads. For instance, Gatts et al. of the West Virginia University Department of Mechanical and Aerospace

Engineering (Gatts et al., 2010) performed tests on a 2004 heavy-duty turbocharged diesel engine with

hydrogen supplemented into the intake air. Results on this 265 kW engine were that brake thermal efficiency decreased across the load range with any amount of hydrogen addition (between 0 and 7.5% hydrogen by volume in the intake air, corresponding to between 0 and 60% of total input energy). Diesel flow rate was reduced with increasing hydrogen concentration to maintain constant engine power and torque. The decrease in brake thermal efficiency was minimal for high load, but increasing for lower load and higher hydrogen addition (see figure 2.6 below).

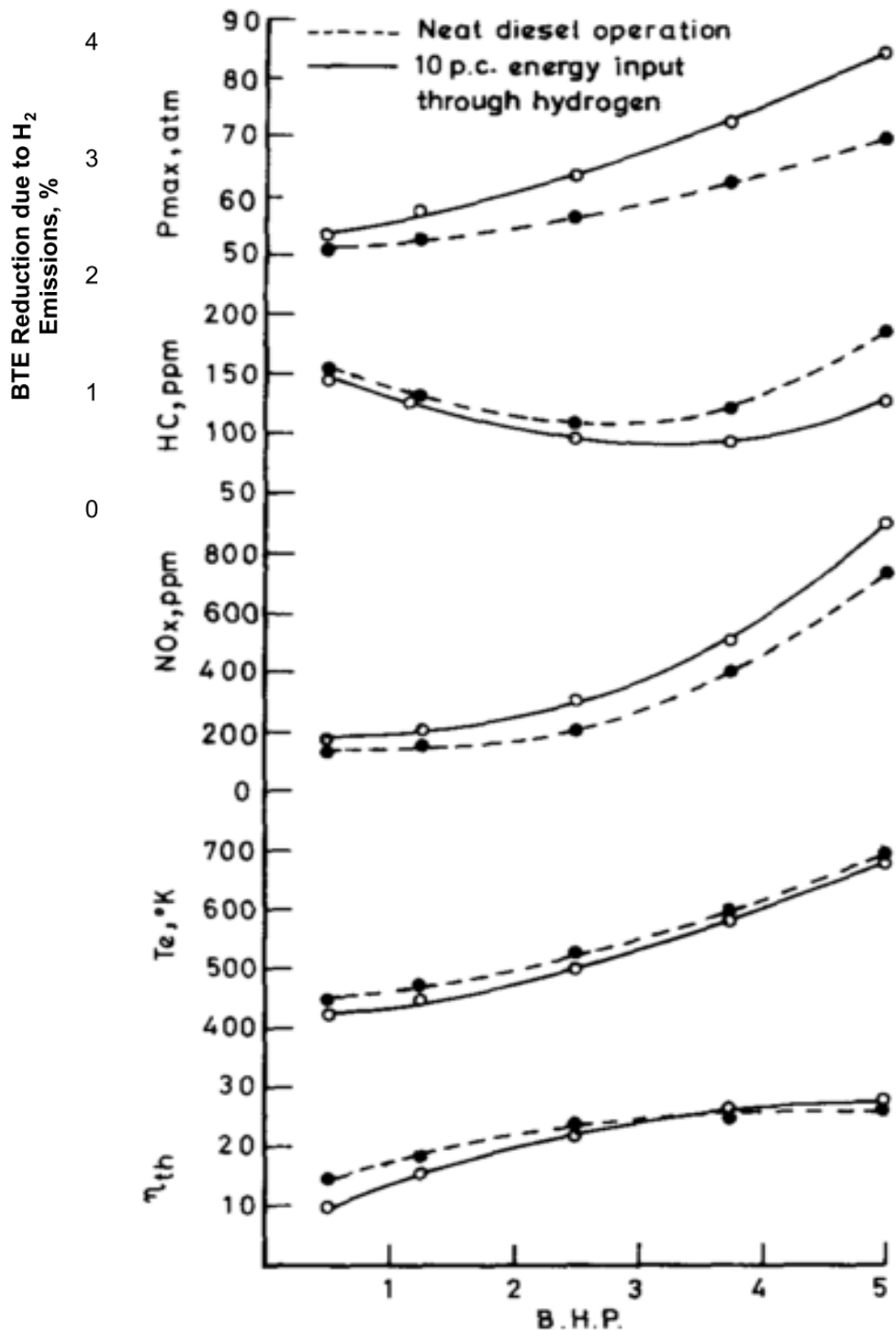


Figure 2.5: Effect of introducing hydrogen into intake air on engine performance and exhaust emissions [Haragopala et al, 1983]

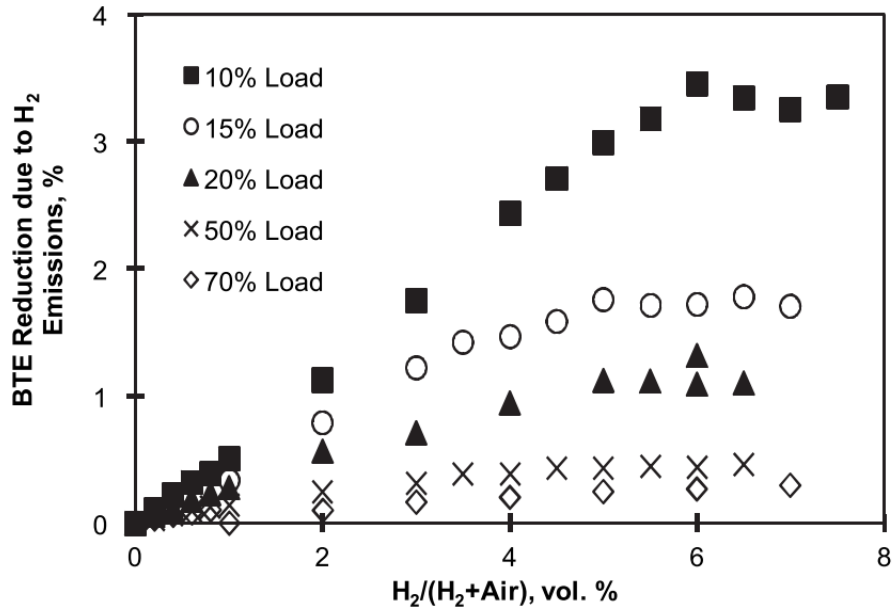


Figure 2.6: Effect of H₂ addition on the reduction of BTE (absolute value) (Gatts et al., 2010)

According to Gatts et al. this reduction of brake thermal efficiency was due to incomplete combustion of H₂. Exhaust gas measurements revealed that unburned hydrogen was present in the exhaust gasses, and the combustion efficiency of hydrogen was determined to be between 75-97%, dependent on engine load and hydrogen addition percentage (see figure 2.7 below).

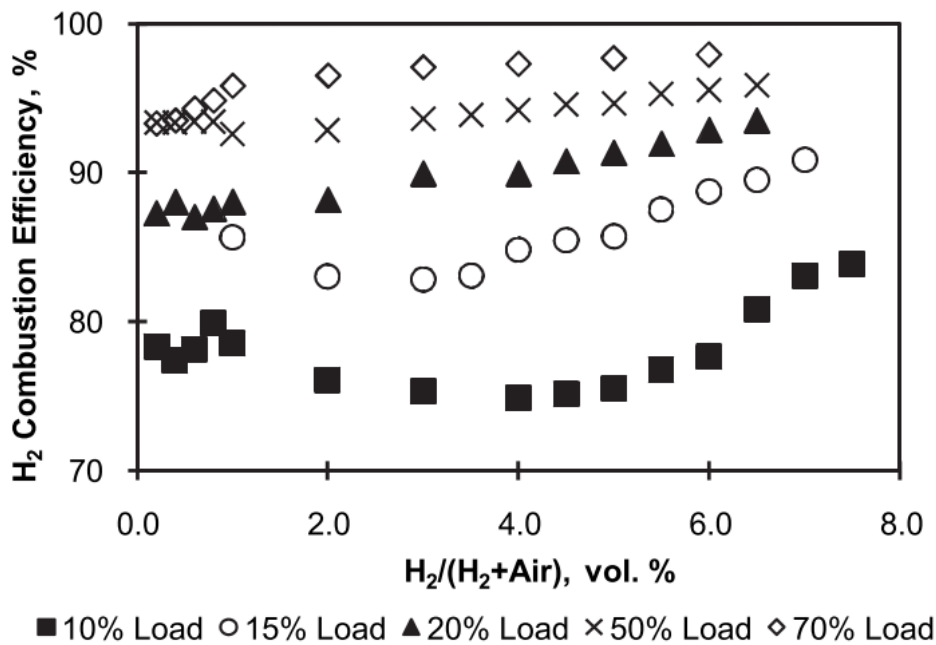


Figure 2.7: Effect of H₂ addition on combustion efficiency of diesel and H₂ at 70% load [Liew et al., 2010]

This reduced hydrogen combustion efficiency was also found by Liew et al. (Liew et al., 2010) who tested on a 6 cylinder, heavy duty, turbo-charged 276 kW diesel engine. The effect of 1,0 – 6,0% hydrogen addition by intake volume at 70% load (corresponding to 5 - 30% of total energy intake) is shown in the figure below. The H₂ combustion efficiencies are similar to what Gatts et al. found at 70% load, but it also interesting to note that the diesel combustion efficiency is negatively affected by large amounts of hydrogen addition (See figure 2.8 below).

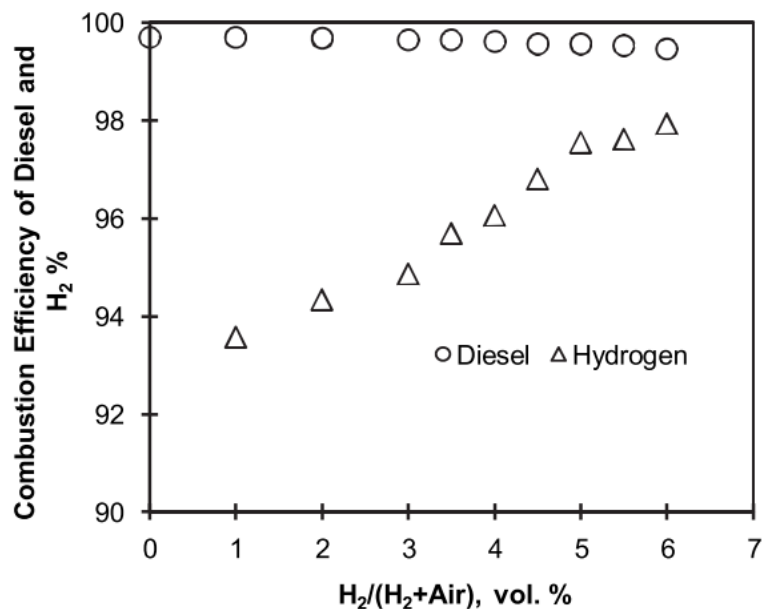


Figure 2.8: Effect of H₂ addition and engine load on combustion efficiency of H₂ (Gatts et al., 2010).

Returning to brake thermal efficiency, a reduction is also found in very recent research by (Sandalcı & Karagöz, 2014). Tests were performed on a small 5.1 kW naturally aspirated diesel engine at 1300 rpm, with hydrogen addition of 16%, 36% and 46% of total energy. This effect is illustrated in figure 2.9 below.

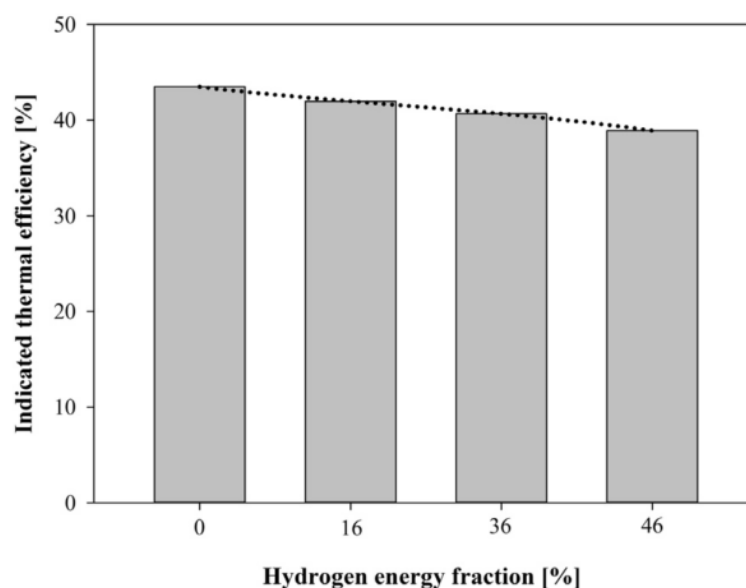


Figure 2.9: Effect of hydrogen addition on thermal efficiency at 1300 rpm and 5.1 kW [Sandalcı et al., 2010]

According to Sandalci et al. this reduction in thermal efficiency is due to two reasons. First of all the change in combustion timing is mentioned, but they also mention a research by Owston et al. [Owston et al., 2007] where it is shown that the wall heat flux of the hydrogen flame is higher than that of diesel combustion. This indicates that higher thermal losses are the reason for the decreased brake thermal efficiency.

Upon further investigation of the heat loss properties of hydrogen combustion there is other research that indicates heat loss for hydrogen combustion is larger compared to diesel combustion, due to higher burning velocity and shorter quenching distance (Shudo & Suzuki, 2002). They also conclude that current equations to calculate this heat loss (for instance Woschni, Nusselt, Eichelberg) are insufficiently accurate for stoichiometric hydrogen combustion. Another research by Demuynck et al. [Demuynck et al., 2012] confirms this result for stoichiometric combustion, but also adds that lean combustion diminishes this effect significantly. This means that the large heat loss of hydrogen combustion will be less of a problem in a turbocharged engine, since it always operates at lean conditions. This effect is illustrated in figure 2.10 below.

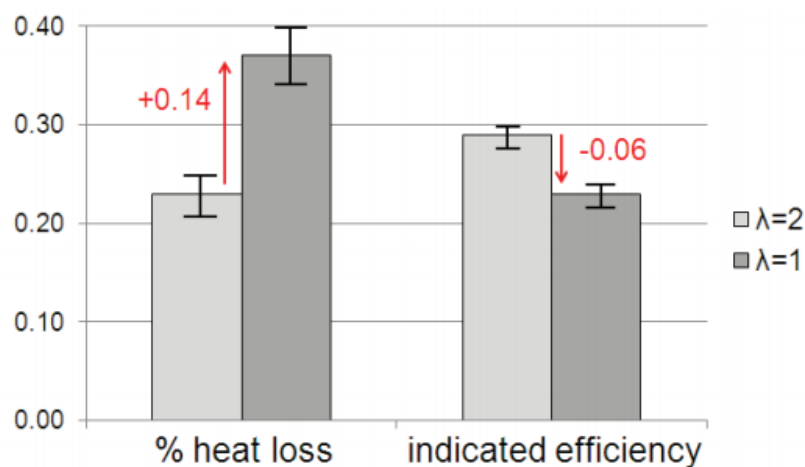


Figure 2.10: Heat loss and indicated efficiency for hydrogen combustion at stoichiometric ($\lambda=1$) and lean ($\lambda=2$) operation [Demuynck et al., 2012].

2.5 Emissions

Emissions are a very important aspect of diesel engine operation, especially with new emission regulations for the marine industry mentioned before. While the combustion of hydrogen itself does not emit any harmful emissions (in fact, the only emission is water), the effect the hydrogen has on the combustion process could result in other emissions increasing or decreasing. Extensive research has been done on this topic, but the focus is mostly on the following emissions:

- NO_x (sometimes split in NO and NO_2)
- CO/CO_2
- (Total) Unburned Hydrocarbons (THC)
- Particulate Matter (PM)

While CO_2 emissions form a large percentage of the actual exhaust gasses, they are also purely fuel dependant. This means that simply substituting a carbon based fuel (diesel) for a non-carbon based

one like hydrogen will reduce these emissions almost linearly with the percentage of carbon based fuel that is removed. This is also partially true for unburned hydrocarbons (UHC), although these also tell something about the combustion efficiency. CO₂ results are therefore rarely reported, and in the cases they are reported show no surprising results.

The results of Haragopala et al. concerning emissions are shown above in figure 2.5. As can be expected with reduced hydrocarbon fuel (diesel replaced by hydrogen) the total amount of hydrocarbons in the exhaust is also decreased relative to the pure diesel operation. This effect is not constant though, but increases with increasing load indicating that at low loads the combustion efficiency of diesel is lower than at full load.

The effect of hydrogen addition on NO_x emissions is an increase over the entire operating range. The formation of (thermal) NO_x is mostly determined by peak temperature and residence time in the cylinder, and according to Haragopala et al. the increase in NO_x emissions in this case was due to an increase in peak cycle temperature caused by faster energy release.

Research by Lilik et al. in 2010 (Lilik, Zhang, Herreros, Haworth, & Boehman, 2010) puts the focus on NO_x emissions. The engine used in their research is a 2.5L 4-cylinder turbocharged light-duty diesel engine. Hydrogen was substituted for diesel fuel on an energy basis of 0%, 2.5%, 5%, 7.5%, 10% and 15% by aspiration into the intake air. 4 operational points were tested, 25% and 75% power at 1800 rpm and 25% and 75% power at 3600 rpm.

When looking at NO_x emissions, Lilik et al. measured both NO_x, NO and NO₂ emissions separately. This led to the discovery that while brake specific NO_x emissions increase slightly across almost all load points with increasing hydrogen addition (see figure 2.11), there is also a shift in the composition of the NO_x.

Note that the reduction of NO_x at 1800 rpm and 25% load is actually due to the use of 12% exhaust gas recycling (EGR). All other points utilize less than 2% EGR. This was done automatically by the engine ECU.

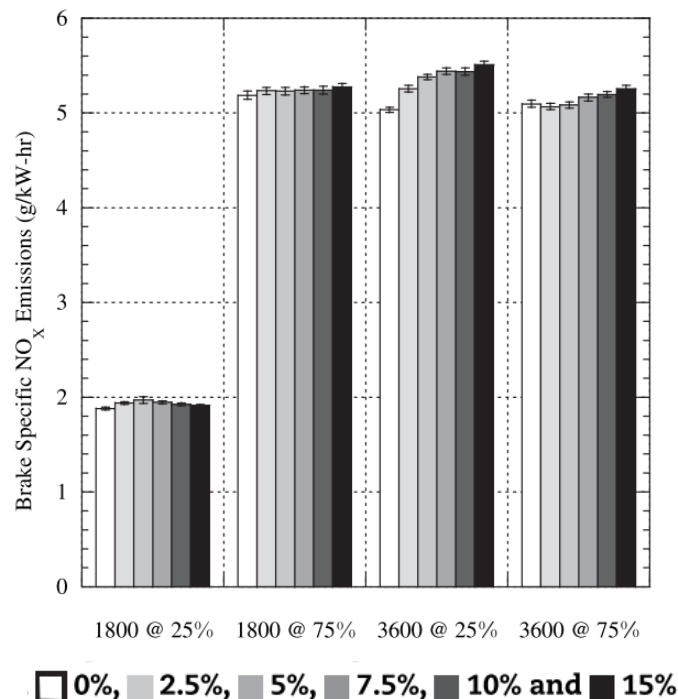


Figure 2.11: Brake specific NO_x emissions with 0% - 15% hydrogen substitution on energy basis [Lilik et al., 2010]

When looking at the specific emissions for NO and NO₂ (figures 2.12 and 2.13), we see that due to the addition of hydrogen the balance shifts towards NO₂. The increase of NO₂ is more pronounced at high loads, while the decrease in NO is particularly evident at lower loads. Again, the emissions are generally lower at 1800 rpm and 25% power due to 12% EGR, as opposed to approx. 1-2% at all other points.

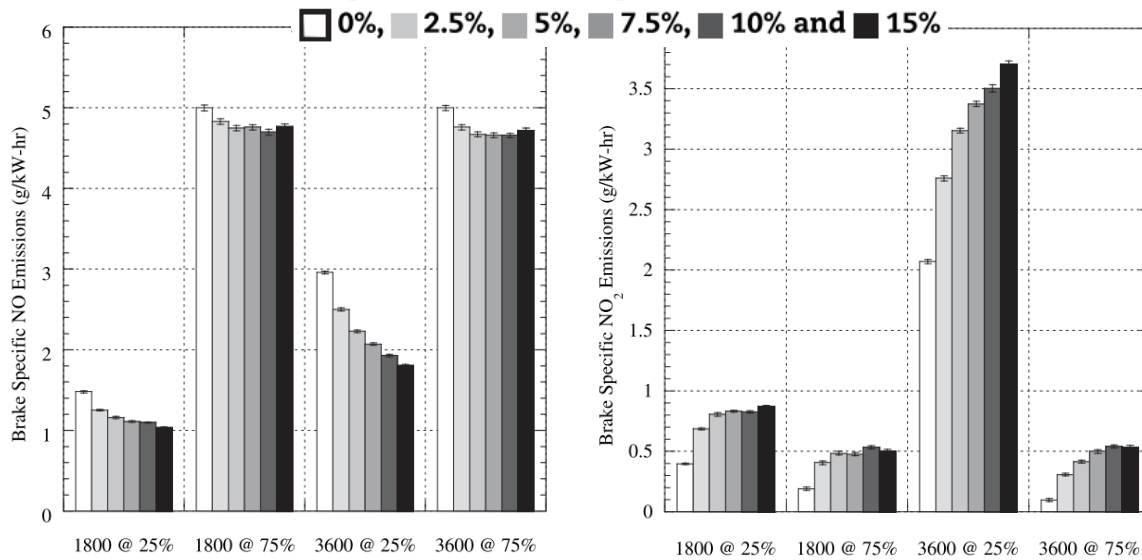


Figure 2.12: Brake specific NO emissions [Lilik et al., 2010]

Figure 2.13: Brake specific NO₂ emissions [Lilik et al., 2010]

CFD calculations confirmed that the addition of hydrogen increased the in-cylinder levels of HO₂, which in turn enhanced the conversion of NO to NO₂. While this is not directly relevant since regulations regarding nitrogen-oxide emissions are based on NO_x measurements, it is nonetheless interesting to see the effect that adding hydrogen has on the formation process of NO and NO₂.

There are several very recent researches ([Sandalci et al., 2014], [Zhou et al., 2014], [Pan et al., 2014]) where emissions are reviewed as well. These are not all on turbo-charged engines but overall they come to the same conclusions. All this recent research agrees that both CO and CO₂ emissions decline linearly with hydrogen addition percentage (figure 2.14) simply due to the reduction of carbon in the fuel. Emission of NO_x is either slightly reduced or similar to that of diesel at low loads, but significantly higher at high loads due to increased in-cylinder peak temperature.

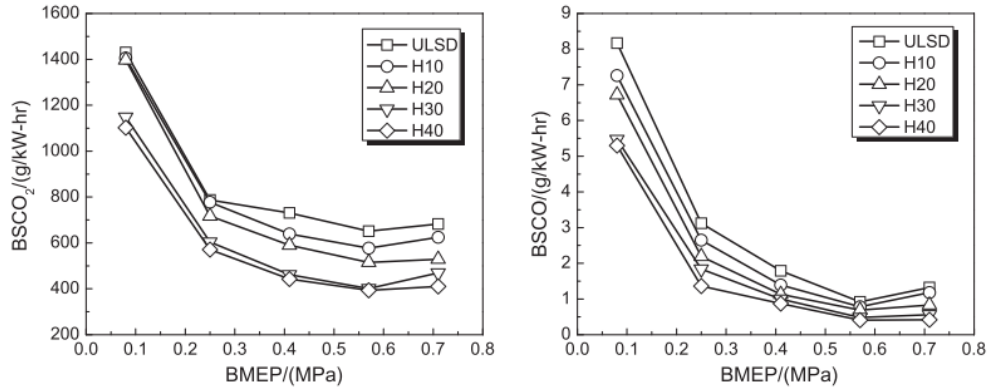


Figure 2.14: Effect of 10-40% hydrogen addition on brake specific CO and CO₂ emissions [Zhou et al., 2010]

2.6 Pressure, peak pressure and heat release

In addition to tests on an small diesel engine, Haragopala et al. also performed a number of closed vessel explosion tests to study the effect of adding a hydrocarbon fuel to hydrogen-air mixtures. The total amount of energy was kept constant, so increasing hydrocarbon fraction meant reduced hydrogen fraction.

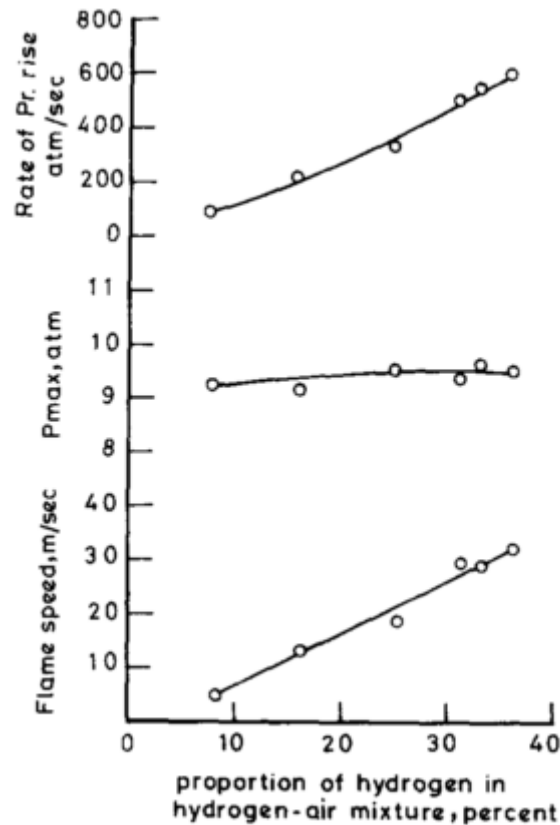


Figure 2.15: Variation of flame speed with composition of hydrogen-gasoline-air mixture under constant energy content conditions [Haragopala et al, 1983]

From figure 2.15 it can be seen that the effect of increasing the hydrogen proportion results in higher flame propagation velocities, increased rate of pressure rise, but relatively stable maximum pressure. This stable maximum pressure is due to the nature of the closed vessel explosion tests, where the energy input to the mixture is essentially the same.

In more recent research pressure traces and heat release rate measurements are also included. As mentioned before Haragopala et al. found increased rate of pressure rise when adding hydrogen, but did not provide a graph of either pressure or heat release rate over time (or against crank angle). More modern measurement equipment in the more recent researches can provide this information.

In figure 2.19 below the pressure and heat release rate of Sandalci et al. are shown. Sandalci et al. managed to add up to 46% of total energy with hydrogen, a very substantial amount. The engine these tests were performed on is a single cylinder 4-stroke diesel engine rated at 7.5 kW, naturally aspirated. The hydrogen was injected into the intake manifold. This engine is normally used for cooperative fuel research and can be setup as both a compression ignition and as a spark ignition engine.

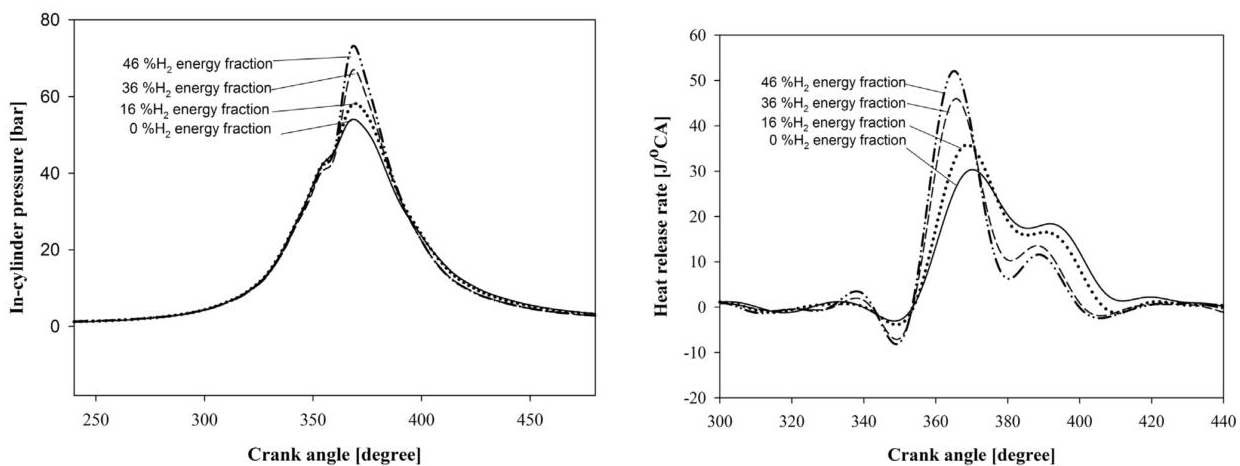


Figure 2.16: In-cylinder pressure and heat release rate against crank angle at 1300 rpm and 5.1 kW

From the figures we see that the peak pressure increases with increasing hydrogen addition. While Haragopala et al. found that maximum pressure was stable with increasing hydrogen addition percentage, this result was from a closed vessel explosion experiment. In an actual combustion cycle diesel fuel is continuously injected, and this results in the increased peak pressure. From the pressure plot we see no evidence of the combustion shifting, but the heat release rate figure tells a different story. The initial peak (premixed combustion) is both higher and the incline is steeper, again similar to what Haragopala reported (increase in rate of pressure rise). Naturally the diffuse and late combustion are reduced, since the total energy input of the cycle is the same. These effect are especially visible with large hydrogen addition percentages of 30%-50%.

Zhou et al. performed similar tests, where up to 40% of total energy was provided by hydrogen. Their engine was a naturally aspirated, 4-cylinder inline engine with rated power of 88 kW. Hydrogen was

aspirated into the intake manifold through a mixing chamber, to allow the formation of a homogenous air-hydrogen mixture. 5 engine load points were tested, 10%, 30%, 50%, 70% and 90% power at 1800 rpm. The hydrogen addition percentage was varied between 10%, 20%, 30% and 40%.

Unfortunately no pressure traces were provided, but heat release rates for 10% through 90% load are shown in the figure below. Operation at 30% and 50% load was almost identical, so only one of those is plotted below.

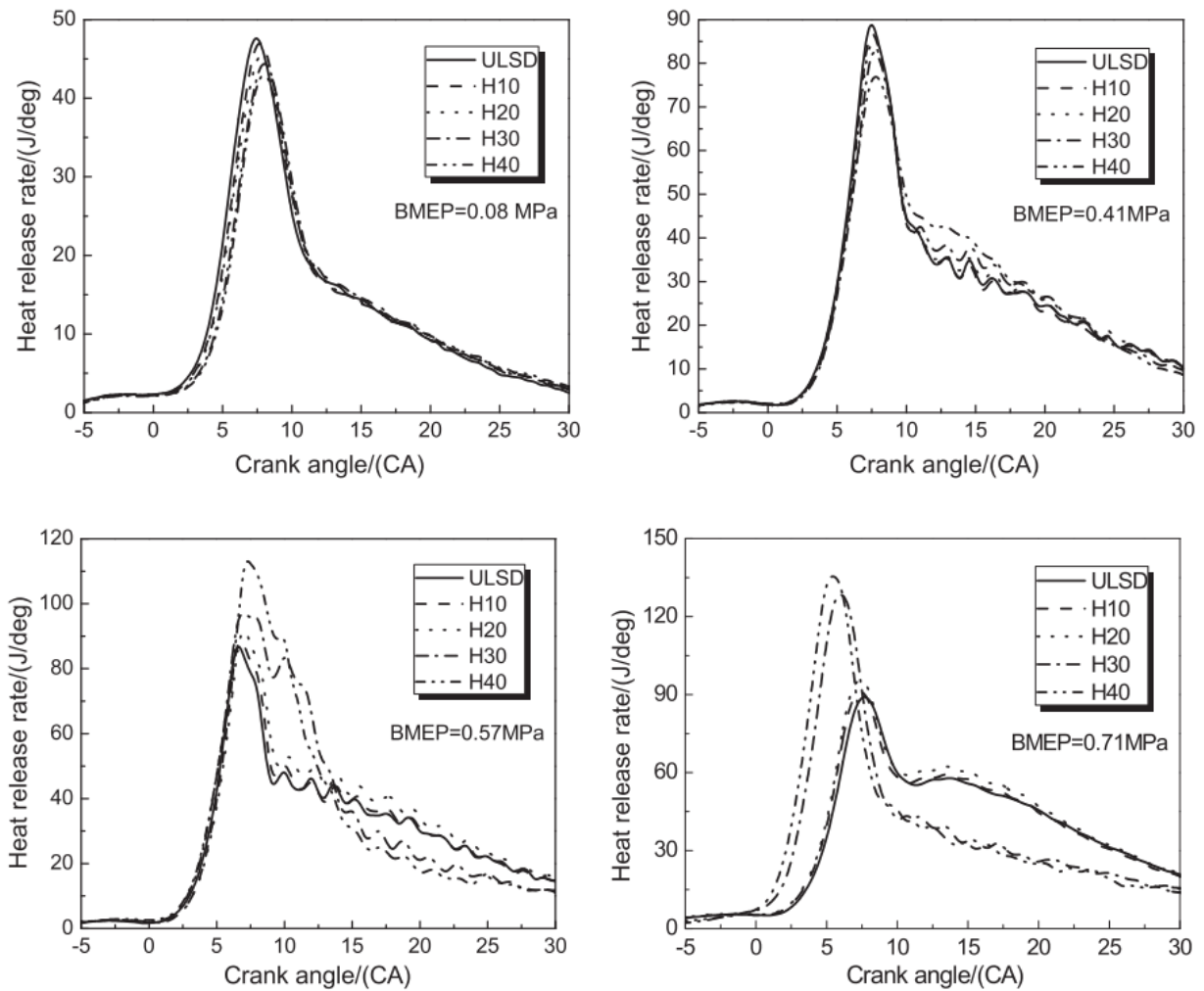


Figure 2.17: Heat release rate at 10% load (BMEP =0.08 MPa), 50% (BMEP = 0.41 MPa), 70% (BMEP = 0.57 MPa) and 90% (BMEP = 0.71 MPa) (Zhou et al., 2014)

From the heat release rate at 10% load (top left figure 2.17) we see that increasing hydrogen addition percentage retards combustion slightly and has a small negative effect on peak pressure. This is likely due to the bad combustion efficiency of hydrogen at this very low load, as mentioned before by Gatts et al.

At 30% and 50% load (top right figure 2.17) hydrogen combustion efficiency increases, but peak pressure is still lower than pure diesel operation with increased hydrogen addition. Zhou et al. theorized that the reduced amount of pilot diesel fuel that ignites the hydrogen, combined with low

hydrogen combustion efficiency at low loads causes lower peak pressure. Once the hydrogen ignites an increase in diffuse combustion is visible between 10 and 15 degrees crank angle at 40% hydrogen addition.

At 70% load (bottom left figure 2.17) the hydrogen combustion efficiency is quite high (Gatts et al., 2010) so even small amounts of hydrogen addition ignite quickly and lead to increased peak pressure and heat release rate. There is however no sign of advanced or retarded combustion. The increase in pre-mixed combustion and reduction of diffuse combustion are similar to the results of Sandalci et al.

At 90% load (bottom right figure 2.17) and higher hydrogen addition percentages (30% and 40%) we do see the combustion advance. The initial pre-mixed peak is very substantial and the diffuse combustion is significantly reduced. The advancement of combustion is both substantial and quite sudden, since all other points do not show this behaviour. Zhou et al. interpreted this as auto-ignition of the hydrogen due to hot-spots (carbon deposits, cylinder wall, piston bowl, etc.) in the cylinder. Normally this is very unlikely due to the high auto-ignition temperature of hydrogen (858 degrees K), but at these high loads and hydrogen addition percentages some unexpected behaviour can occur.

2.7 Combustion limits (knocking)

While in this thesis the focus is on the effect of small amounts of hydrogen addition, it is of course also possible to add larger amounts of hydrogen, effectively substituting part of the diesel fuel. There is however an upper limit to how much hydrogen can be added before abnormal combustion occurs. This abnormal combustion is referred to as knocking, due to the characteristic sound it makes. [Kersting, 2014] performed tests to find the maximum hydrogen addition percentage at each operating point before knocking occurs. This is shown in the figure below.

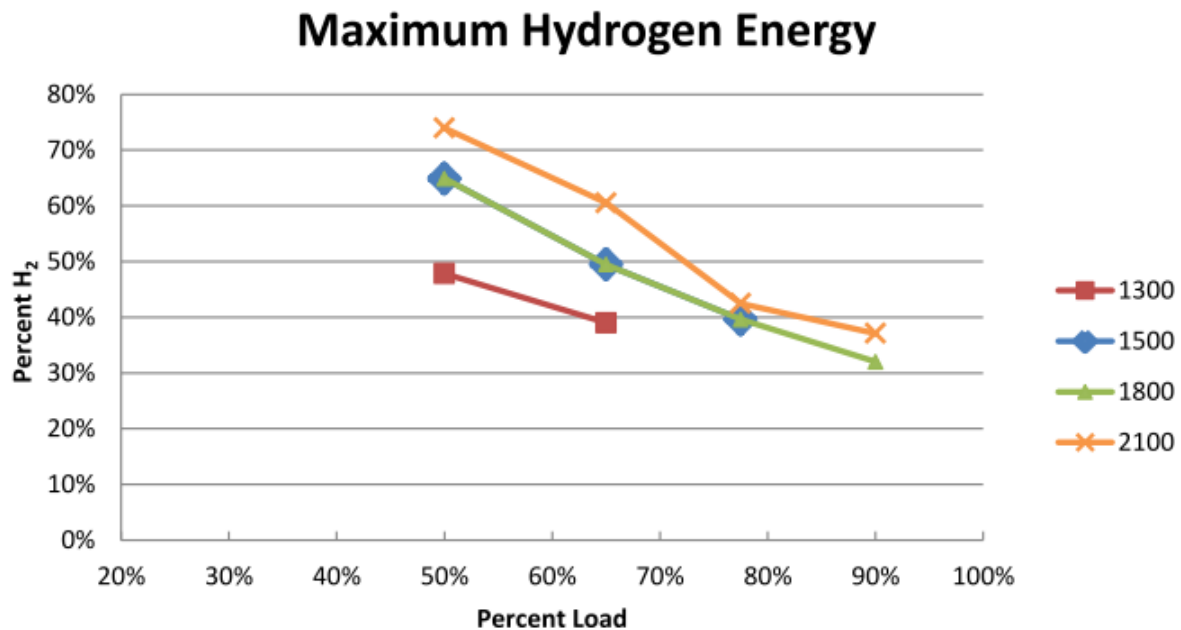


Figure 2.18: hydrogen addition percentage at the knock limit (percentage of total energy added)

It is clear that both engine power and RPM influence the maximum amount of hydrogen that can be added. This is linked to the maximum rate of pressure rise. As seen before in paragraph 2.6 both increasing load and adding hydrogen increases the rate of pressure rise. This means that at higher loads less hydrogen can be added before the limit in terms of rate of pressure rise is reached, and knock occurs.

2.8 Conclusions & expectations

Based on the literature review there are a number of expectations. Almost all researchers agree that hydrogen addition will increase peak pressure and rate of pressure rise. This will be taken into consideration while designing the testing procedures for our own tests, so the testing engine will not be at risk of damage. In terms of efficiency and fuel consumption the expectations are that at low loads efficiency will reduce and specific fuel consumption will increase. As load increases this effect will become smaller, but the effect at high load remains difficult to predict. It is expected that the result here will be very similar to pure diesel operation, with large amounts of hydrogen addition possibly resulting in slightly improved efficiency and fuel consumption.

In terms of emissions it is clear that the substitution of a carbon fuel with a non-carbon fuel will result in reduced CO₂ emissions. CO emissions will likely follow the same trend, but one of the biggest uncertainties is the emission of NO_x. Research has shown varying results, although the trend seems to be that at low loads NO_x emissions is slightly lower or similar to pure diesel, while at high loads the NO_x emissions are fairly substantially increased.

Regarding the effect on combustion the addition of hydrogen in the intake air will likely result in increased pre-mix combustion and (since total energy added is constant) reduced diffuse combustion. This is due to the fact that all the hydrogen is pre-mixed into the intake air, and is

immediately available for combustion. This is however very dependent on the operation point of the engine, in terms of cylinder temperature, amount of diesel fuel, ignition timing, etc. As mentioned before also an increase in rate of pressure rise is expected.

These expectations are summarized in the table below. The parameters that are expected to change are listed on the left side, and a rough separation of low/high load and low/high hydrogen addition percentage is made at the top. A plus symbol indicated an expected increase of that parameter, a minus sign an expected reduction and an equality sign indicates no expected change. When the expected result is unclear, a question mark is shown.

Table 2-2: Expected results at various loads and hydrogen addition percentages

	Low (partial) load		High (full) load	
	Low H ₂ addition	High H ₂ addition	Low H ₂ addition	High H ₂ addition
Brake thermal efficiency, η_e	-	-	=	?/+
Peak pressure, p_{max}	=/+	=/+	++	++
Start of combustion, SOC	=	=	=	-
Ignition delay	=/?	=/?	-	-
CO ₂ emissions	-	-	-	-
CO emissions	-	-	-	-
NO _x emissions	-	-	+	+
Pre-mixed combustion	+	+	+	+
Diffuse combustion	-	-	-	-

Chapter 3: Current application

Currently hydrogen addition to diesel engines is not applied commercially on a big scale in any type of application. There are some small companies and individuals who provide small kits or instructions to build such a kit, which can be installed in cars and trucks and claim to reduce fuel consumption.

3.1 Combustion engine applications

Ecowell Energy (<http://www.ecowell-energy.com/>) is such a company, and the product they sell (EcowellPower) can be installed in a gasoline or diesel car and converts water to something they call 'hydroxygeen gas' on demand. This is a mixture of hydrogen and oxygen, the two products of an electrolysis reaction. They claim that adding this mixture to the combustion process via inlet air will result in more complete combustion, and therefore reduced emissions. They guarantee a 10% reduction in fuel consumption.

Additionally they offer a service to clean the internals of the combustion engine, by adding a substantial amount of this 'hydroxygeen gas' combined with steam to the inlet air. This cleaning effect is again contributed to a more complete combustion.

The Dutch Hydroxide Organisation (<http://www.tdho.eu/>) does something similar, but focuses on heavy diesel engines in inland shipping vessels. On demand 'hydroxygeen gas', here called 'HHO', is produced and supplemented into the intake air. This supposedly has a catalytic effect on diesel combustion, resulting in more complete combustion. Additionally the combustion speed increases, which according to THDO results in greater pressure and due to the earlier end of combustion, a cooling effect as the piston completes its descent. The cumulative effect of this faster and more complete burn is greater energy transferred to the crankshaft with reduced emissions.

3.2 Other applications

Another application of the previously mentioned 'HHO' gas is the cutting of steel and other materials using flame cutting. The Dutch company FEY (*Free E Yourself*, <http://www.freeeyourself.com/>) has developed a cutting torch using 'HHO' gas, and claims that this method is faster, cleaner and required less additional oxygen than conventional acetylene torches (since the gas itself contains oxygen). Again the gas is produced on demand using electrolysis, removing the need for transporting bottled, pressurised gas. This results in a very compact and clean (in terms of emissions) cutting solution.

the Dutch website www.watergas.nu has bundled some information and provides links to companies that are currently working with hydrogen (or 'hydroxygeen/HHO gas') addition in all types of applications, but unfortunately most websites they provide are offline or unavailable and actual information is practically non-existent. Most of these companies appear to be small start-ups, and are in the process of acquiring funding through either investors or government subsidies.

Chapter 4: Models and theoretical background

4.1 Introduction

In this chapter the models and theoretical background of the models will be discussed. The following subjects are discussed in this chapter:

- Heat release and heat release mode (paragraph 4.2);
- Vibe fit model (paragraph 4.3);
- Seiliger cycle and parameters (paragraph 4.4);
- Modelling approach (paragraph 4.5).

4.2 Heat release and heat release model

There are a number of parameters from which we observe the effect of hydrogen addition to the engine. One of the most important ones is the Heat Release Rate (HRR), as it can tell us a lot about the combustion process in the cylinder. Both heat release theory and the model used to obtain the HRR will be discussed below. Most information is from Stapersma's *Diesel Engines Volume 3: Combustion* [Stapersma, 2009].

Heat Release Rate (HRR) is defined as the rate at which chemical energy of the fuel is released by the combustion process [Heywood, 1988]. There are several ways of expressing the HRR, but the 3 main definitions used are the Net Apparent Heat Release Rate (NAHRR), Gross Apparent Heat Release Rate (GAHRR) and the Combustion Reaction Rate (CRR). These are displayed below in equations 1 through 3.

$$NAHHR = \dot{Q}_{comb} - \dot{Q}_{loss} = m \cdot c_v \cdot \frac{dT}{dt} + p \cdot \frac{dV}{dt} \quad (4.1)$$

$$GAHHR = \dot{Q}_{comb} = m \cdot c_v \cdot \frac{dT}{dt} + p \cdot \frac{dV}{dt} + \dot{Q}_{loss} \quad (4.2)$$

$$CRR = \xi = \frac{m \cdot c_v \cdot \frac{dT}{dt} + p \cdot \frac{dV}{dt} + \dot{Q}_{loss}}{u_{comb}^{ref} - \Delta u_{comb}^{ref}} \quad (4.3)$$

The NAHRR is the net heat as observed from temperature and volume evolution during the combustion cycle. This is however not all of the heat produced from the fuel, since the losses are neglected.

For this we have the GAHRR, where the heat loss to the walls is added. This heat loss is not measured but estimated using a model, making it susceptible to errors. An accurate estimate is essential to the accuracy of the entire HRR.

Finally the CRR introduces the effect of temperature dependent effective heat. Additionally it is also in another dimension, kg/s instead of kJ/s.

The terms on the right side of equations 1-1 through 1-3 also correlate to a physical meaning. The first term in the HRR's corresponds to the change in internal energy due to temperature changes. The second term is the work done by the piston, and the third term is the heat loss to the cylinder walls.

In the CRR we have additional terms in the denominator, the first being the reference internal energy (for a closed system) and the second term the change in internal energy due to temperature change from the reference condition.

The model that is being used to calculate the heat release rate is displayed in figure 1 below. The main inputs in this model are the crank angle (to calculate volume) and the pressure in the cylinder.

The other main parts of this model are the temperature calculation (based on the Ideal Gas Law), the Woschni heat loss model and the Properties Library where the internal energy of the reaction components is calculated each step based on pressure and temperature. From figure 1 we can also clearly differentiate the NAHHR, the GAHHR when losses are added and the CRR when varying internal energy is taken into account.

At first sight it might seem like this model has an algebraic loop, since the output (CRR) is also one of the main inputs to the model, defining the composition in the cylinder and therefore indirectly the temperature and internal energy calculations. However, in the "Mass Balance and Composition" block an integration of CRR takes place (breaking the algebraic loop) to calculate how much fuel has been burned. In addition with an initial value of mass in the cylinder to start the calculation, there is a new value available after each calculation step.

Finally the CRR is integrated to gain the reaction coordinate (RCO). Since CRR is calculated based on a measured pressure, it fluctuates quite heavily. The integration to CRO smooths out most of the fluctuation. Additionally it is a monotonously increasing function, very suited to curve fitting.

Another option would have been to smooth the pressure signal itself before using it as input to the HRR calculation model, but this would possibly remove information from the pressure signal and introduce a great deal of uncertainty in the HRR calculation model.

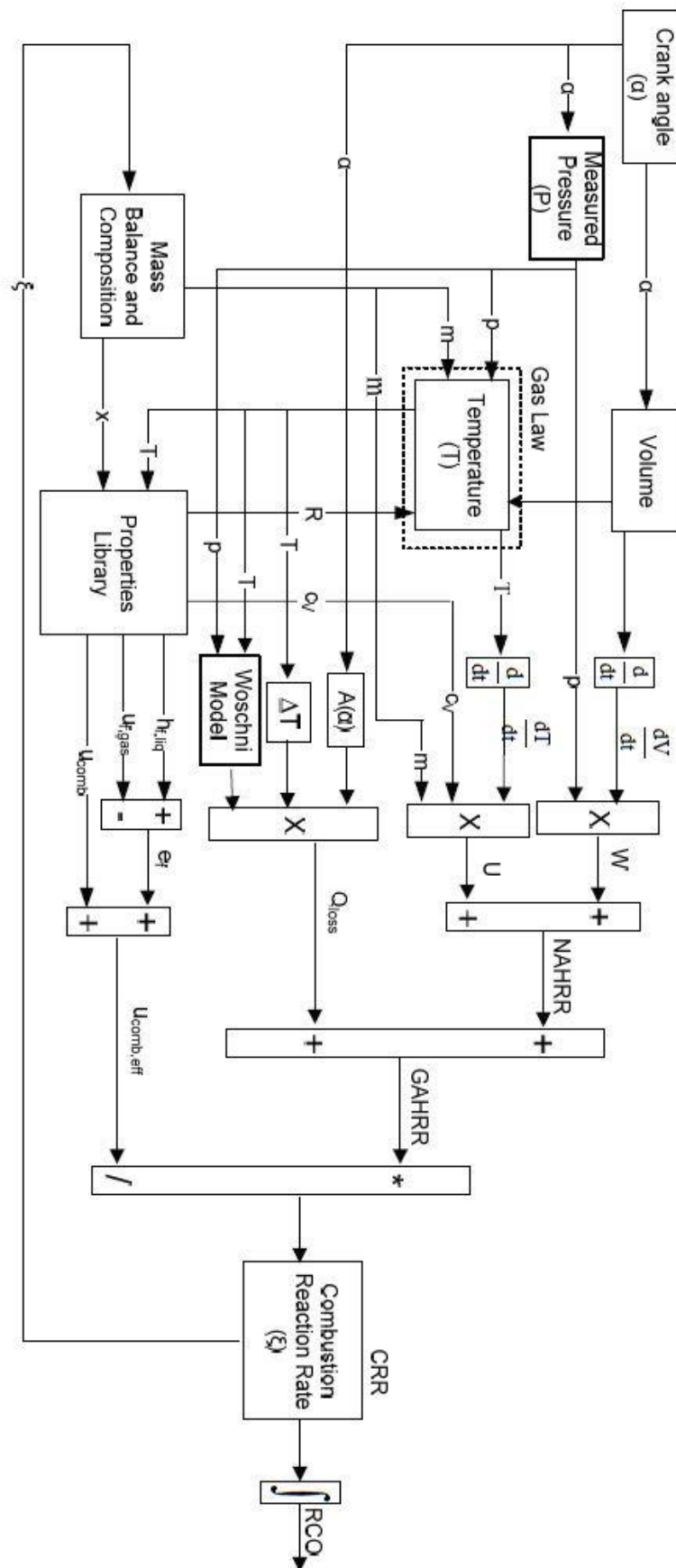


Figure 4.1: Block diagram of Heat Release Calculation Model [Ding, 2011]

4.3 Vibe fit model

To fit the HRR a Vibe fit function will be used. The Vibe combustion profile was originally presented in [Vibe, 1970] but has found widespread use since. Distinction can be made between the linear and non-linear Vibe model, and furthermore the distinction between single, double or multiple Vibe models. Vibe fitting is especially suited to fitting a combustion process since the formula is based on the principals of chain reactions, as explained further below.

As a basis for the combustion process it is assumed that the fuel molecules are “attacked” by oxygen molecules, and break up into free radicals. It is also assumed that the reaction rate for the formation of free radicals is proportional to the amount of fuel:

$$\frac{dm_f^+}{dt} = k \cdot m_f \quad (4.4)$$

Additionally the increase of radicals is proportional to the decrease in fuel:

$$dm_f^+ = -\mu \cdot dm_f \quad (4.5)$$

Combining these 2 formulas results in the reaction rate.

$$\xi = \frac{dm_f}{dt} = -\frac{k}{\mu} \cdot m_f \quad (4.6)$$

The question now is what value we choose for k and μ . The simplest assumption, the linear Vibe model, assumes that $\frac{k}{\mu}$ is constant. In general this linear Vibe model offers too little freedom in shaping the heat release. A more promising solution is the non-linear Vibe model, where we assume that the reaction rate is dependent on time and not on instantaneous amount of number of molecules or radicals.

This assumption implies that the reaction rate starts at zero and ends at (or near) zero, which makes more sense when looking at the physical combustion process itself. This behavior is something the linear model did not incorporate, since the reaction rate had its maximum value at $t=0$.

Introducing the normalized combustion progression X and the normalized rate of combustion Z :

$$X = \frac{\text{number of fuel molecules broken up}}{\text{initial number of fuel molecules}} = \frac{m_f}{m_{f,0}} \quad (4.7)$$

$$Z = \frac{dX}{dt} = \xi \cdot \frac{t}{m_{f,0}} \quad (4.8)$$

Where τ is defined as the normalized combustion time (0 at SOC, 1 at EOC)

$$\tau = \frac{t}{t_{comb}} \quad (4.9)$$

Simplifying further leads to these formulas for X and Z:

$$X = 1 - e^{-\alpha \cdot \tau^{m+1}} \quad (4.10)$$

$$Z = a \cdot (m + 1) \cdot \tau^m \cdot e^{-\alpha \cdot \tau^{m+1}} \quad (4.11)$$

If the duration of combustion and the total injected fuel are given, the Combustion Reaction Rate (CRR) can be acquired after selecting parameters m and α . Parameter m is a form parameter, used to shape the Vibe function. The parameter α can be easily linked to combustion efficiency:

$$1 - e^{-\alpha} = \eta_{comb} \quad (4.12)$$

For almost all engines and operating points this value approaches unity, and will be set as 0.999. This is the same value used for this specific engine before by Ding [Ding, 2011].

A single Vibe function is often not enough to accurately fit a combustion cycle. Therefore a double or even multiple Vibe function can be used. Weight factors are assigned to each Vibe function, and each function can be shaped using the form parameter m . Parameter α is taken equal for all Vibe functions. Finally, the sum of all weight factors b needs to be 1.

X and Z for a double Vibe function are shown below.

$$X = b_1 \cdot (1 - e^{-\alpha \cdot \tau^{m+1}}) + b_2 \cdot (1 - e^{-\alpha \cdot \tau^{m+1}}) \quad (4.13)$$

$$Z = b_1 \cdot (a \cdot (m + 1) \cdot \tau^m \cdot e^{-\alpha \cdot \tau^{m+1}}) + b_2 \cdot (a \cdot (m + 1) \cdot \tau^m \cdot e^{-\alpha \cdot \tau^{m+1}}) \quad (4.14)$$

4.4 In-cylinder process simulation model

After having obtained the vibe parameters that describe the combustion process and heat release rate, we would like to know the actual in-cylinder process (pressure, temperature, etc.) given this specific combustion profile. Then we can compare to the measured pressure and results of the heat release model described earlier in 4.2, and should arrive at the same values if the Vibe fit was accurate.

The in-cylinder process model and heat release model can be seen as opposites, and are anti-causal. Figure 4.2 below illustrates the in-cylinder process model [Ding, 2010]. The final output is the in-cylinder temperature, based on the first law of thermodynamics. The heat release is based on the Vibe fit that was obtained earlier using the Vibe fit model.

Similarly to the heat release model a Properties Library block calculates all (temperature dependant) properties of air, stoichiometric gas and fuel, and a Woschni model is used to model the heat loss to the walls, cylinder, etc. The ideal gas law is used to calculate the in-cylinder pressure.

From the block-diagram (figure 4.2) the similarities between the heat release model and in-cylinder process model are even more clear. In overall structure the models are very similar, and are complimentary to eachother. This is very helpful in checking results of either model, since running the data through its partner should result in the original input.

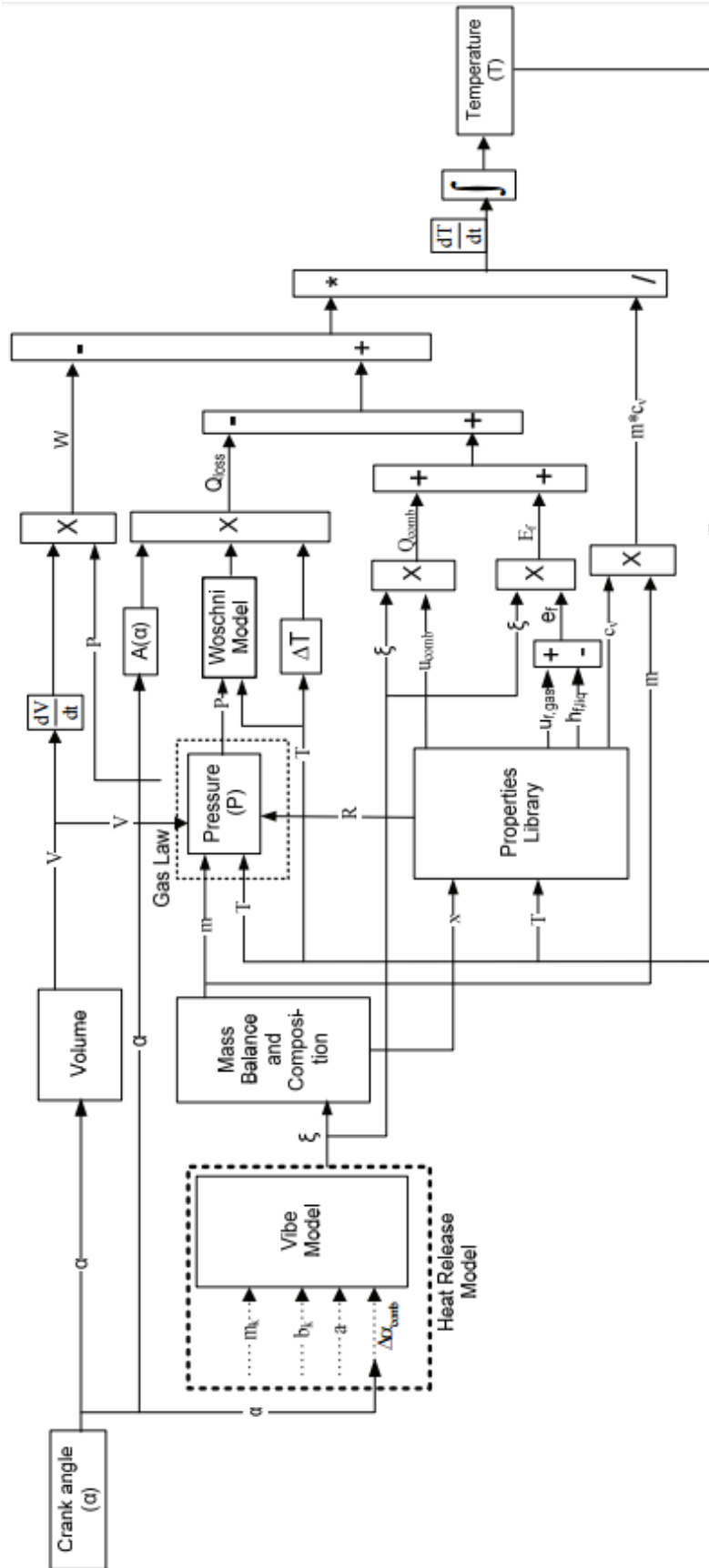


Figure 4.2: General block diagram of in-cylinder process model [Ding, 2010]

4.5 Seiliger cycle and parameters

In addition to the Vibe fitting and corresponding Vibe parameters, there is another method to characterize an engine and its performance using performance parameters, the Seiliger cycle.

The Seiliger cycle is one of the more popular methods developed to calculate the thermodynamic process in the engine and to predict its performance. Originally published by M. Seiliger in 1922, the Seiliger process attempts to approximate the real thermodynamic process by an ideal cycle process. Seiliger proposed a number of cycles, of which the “5-point” or “dual” cycle is the most popular and bears his name.

In this thesis the Seiliger cycle will be used as a way to characterize the combustion process (similar to the Vibe model), but not the popular 5-point cycle. Stapersma [Stapersma, 2009] has modified the *original* 6-point Seiliger to better represent the main features of diesel engine combustion, i.e. pre-mix, diffusive and late combustion. The compression and expansion stages are normally modelled adiabatic, but in the version modified by Stapersma are changed into polytropic processes. This allows for some heat loss from the working medium to the wall, something that was missing in the original Seiliger cycle. This version will be called the *basic Seiliger process*.

Today more sophisticated methods are also available to calculate and evaluate the combustion process, but they generally require a lot of processing power and a lot of engine parameters that are not generally known. These methods are often based on differential equations for mass and internal energy in the cylinder, and are known as “filling and emptying” methods. Of course the result is also more accurate, so both methods will be useful in specific situations. For this thesis the simpler and easier to use method will suffice.

The results of both the Vibe fit and the Seiliger fit will be compared in Chapter 8.

4.5.1 Definition of basic Seiliger process

Figure 2 below shows the six-point basic Seiliger process. The stages can be described as follows:

- 1-2: Polytropic compression (instead of adiabatic as in original Seiliger process);
- 2-3: isovolumetric combustion;
- 3-4: isobaric combustion and expansion;
- 4-5: isothermal combustion and expansion
- 5-6: polytropic expansion (instead of adiabatic as in original Seiliger process);

As mentioned before, heat loss can now be modelled into stage 1-2 and 5-6, due to their polytropic nature.

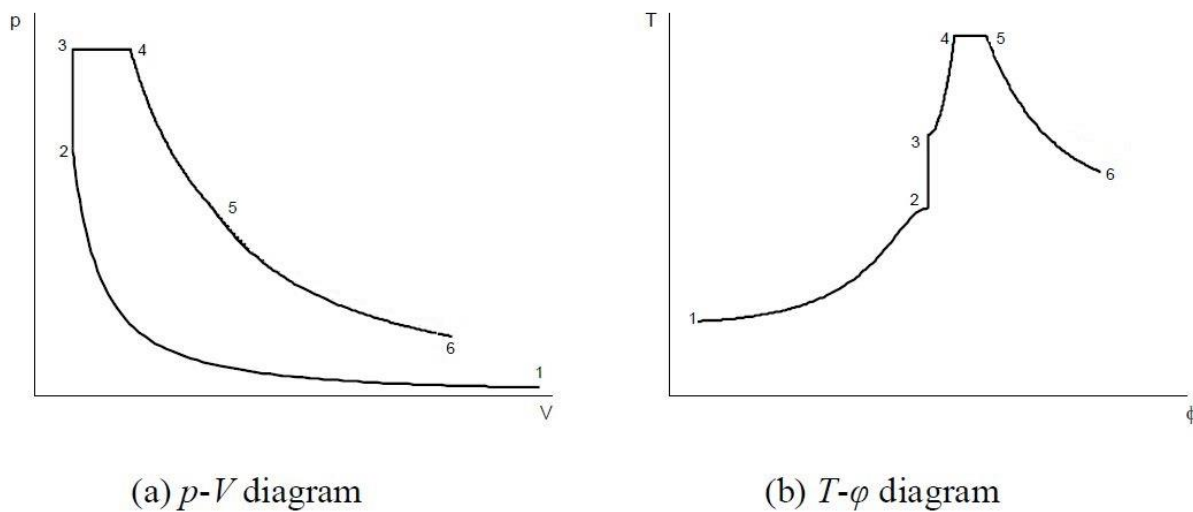


Figure 4.3: Six-point Seiliger process definition

The basic Seiliger cycle can be described by a number of parameters that, together with the initial condition and the properties of the working medium, fully describe the process. Especially interesting are the parameters that describe the ‘shape’ of the heat release, a , b and c . These parameters have a similar function as the Vibe shape parameters b and m in the Vibe fit model mentioned earlier. Table 1 gives the definition of the Seiliger parameters and stages [Ding, 2010].

Table 4-1: Seiliger process definition and parameters

Seiliger stage	Seiliger definition	Parameter definition	Seiliger parameters
1-2	$\frac{p_2}{p_1} = r_c^{n_{comp}}$	$\frac{V_1}{V_2} = r_c$	r_c, n_{comp}
2-3	$\frac{V_2}{V_3} = 1$	$\frac{p_3}{p_2} = a$	a
3-4	$\frac{p_4}{p_3} = 1$	$\frac{V_4}{V_3} = b$	b
4-5	$\frac{T_5}{T_4} = 1$	$\frac{V_5}{V_4} = c$	c
5-6 (5-6')	$\frac{p_6}{p_5} = r_e^{n_{exp}}$	$\frac{V_5}{V_6} = r_e$	r_e, n_{exp}

In addition to the shape parameter a , b and c we have the two parameters that model heat loss in the polytropic processes 1-2 and 5-6, n_{comp} and n_{exp} . The other 2 parameters, r_c and r_e are determined by the geometry of the cylinder (equations 3.15 and 3.16 below). V_1 is determined by inlet valve timing and V_2 is the volume at TDC, thus defining r_c . Similarly r_e is defined by V_6 , thus by the exhaust valve timing, and the product of b , c and r_{26} .

$$r_c = \frac{V_1}{V_2} \quad (3.15)$$

$$r_e = \frac{V_5}{V_6} = \frac{V_2 \cdot b \cdot c}{V_6} = b * c * r_{26} \quad (3.16)$$

$$r_{26} = \frac{V_2}{V_6} \quad (3.17)$$

Based on the Seiliger parameters and the initial conditions, the state parameters in the 6 station points can be calculated based on Seiliger definitions and the gas law. Figure 4.3 – 4.5 below show various forms of pressure, temperature and entropy in cylinder [Ding, 2010]. Stage 5-6 is the basic Seiliger process where there is heat loss in this segment, and stage '5'-6 represents an advanced Seiliger cycle, where there is heat input (combustion) in this stage.

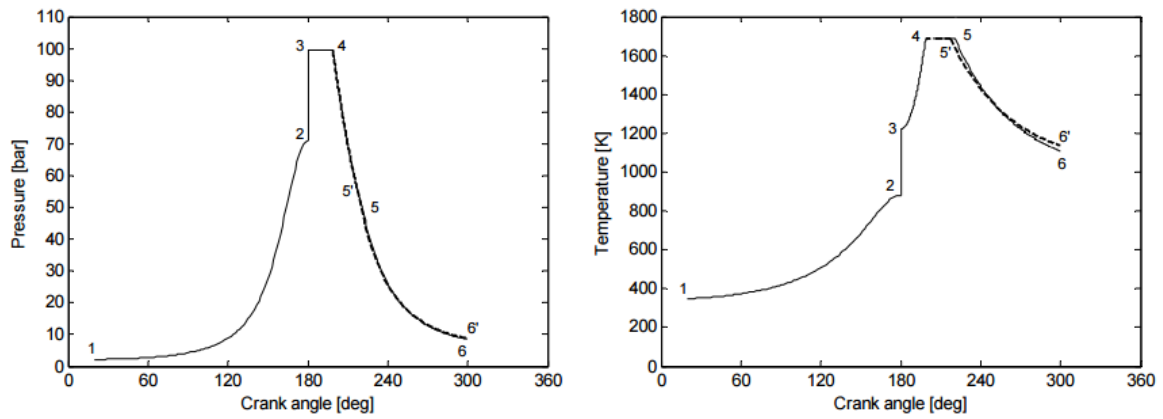


Figure 4.4: Seiliger process p- ϕ and T- ϕ diagram

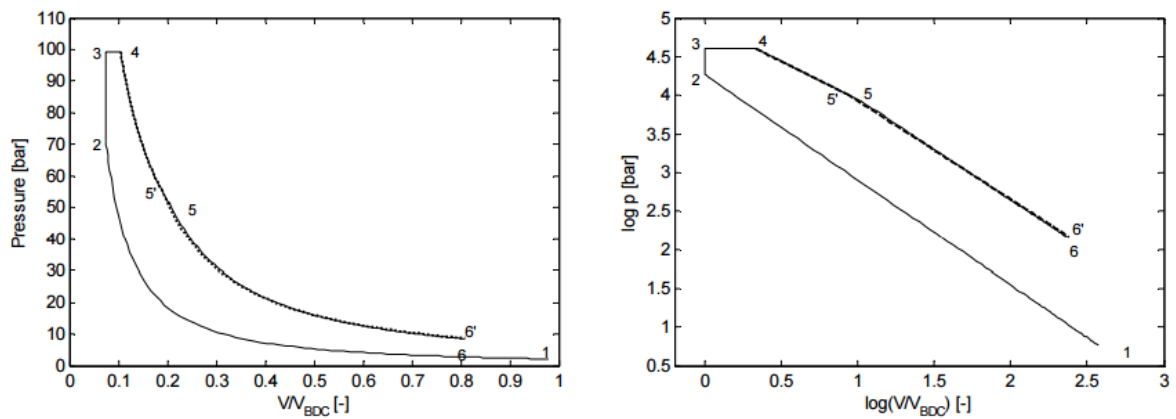


Figure 4.5: Seiliger process p-V and $\log(p-V)$ diagram

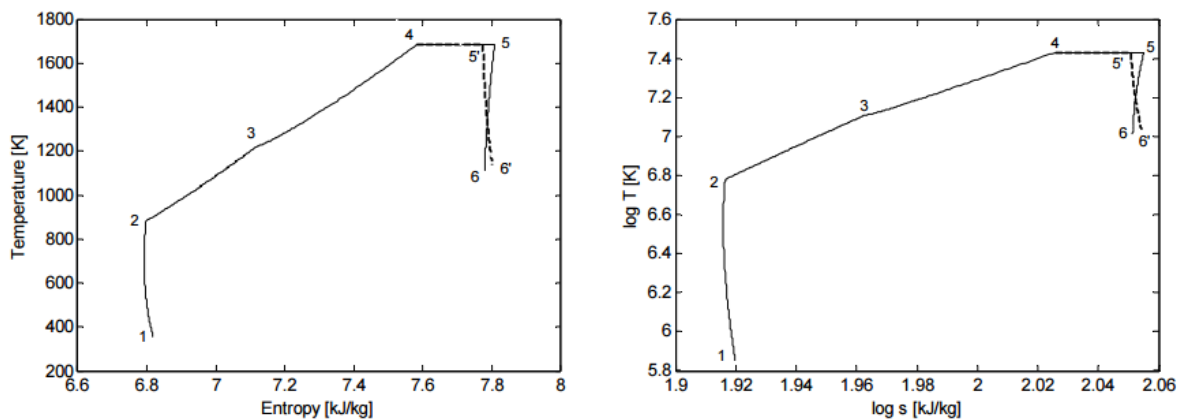


Figure 4.6: Seiliger process T-s and $\log(T-s)$ diagram

Chapter 5: Experimental setup and testing

5.1 Introduction

In this chapter the experimental setup will be discussed, as well as the testing procedures that were developed and used during the experiments. The following subjects are discussed:

- Experimental setup and equipment (paragraph 5.2);
- Hydrogen addition calculations (paragraph 5.3);
- Map of testing points (paragraph 5.4);
- Testing procedures (paragraph 5.5);
- Data processing (paragraph 5.6).

5.2 Experimental setup and equipment

The experimental setup consists of the test engine, water brake, various measuring equipment and the hydrogen addition equipment.

5.2.1 Test engine

The test engine is the MAN 4L 20/27, stationed at KIM (Koninklijk Instituut voor de Marine) in Den Helder. Basic engine data is provided in the table below (table 5.1). This engine is fairly old, but has been used in numerous researches and MSc Theses for the TU Delft and is very well documented. It is also fitted with a range of measurement equipment, which greatly simplifies the process of preparing the engine for tests. Additionally it is quite a large engine in terms of power compared to engines used in other researches, and therefore more representative of an actual marine diesel engine.

Table 5-1: MAN 4L 20/27 basic engine data

Engine Data	
Name	Brons/MAN 4L20/27
Number of cylinders	4 in line (4 stroke)
Bore	0,20 [m]
Stroke	0,27 [m]
Min. rpm	700 [rpm]
Max. rpm	1000 [rpm]
Maximum brake power	350 [kW]
Fuel	NATO F76 diesel fuel
Compression ratio	13,4 [-]
Charge air pressure (max)	0.5 [bar]

5.2.2 Water brake

To apply a load to the engine, a water brake is connected to the output shaft of the engine. The water brake consists of a rotor mounted in an enclosure filled with water. The rotor is connected to the engine shaft, and when it rotates mechanical energy is transferred to the water. This energy heats the water due to friction. Therefore, water must constantly move through the water brake, the flow depending on the amount of energy that needs to be absorbed. The loading of the engine can be varied by adjusting the amount of water in the enclosure. More water equals more friction and thus a bigger load. See figure 3 for a schematic overview of a water brake.

The water brake is controlled from outside the engine room, by providing a torque set point. During startup or when changing settings between measurements the torque setting is manually adjusted in small intervals to make sure the engine does not stall. This process can be compared to slowly engaging the clutch in your car.

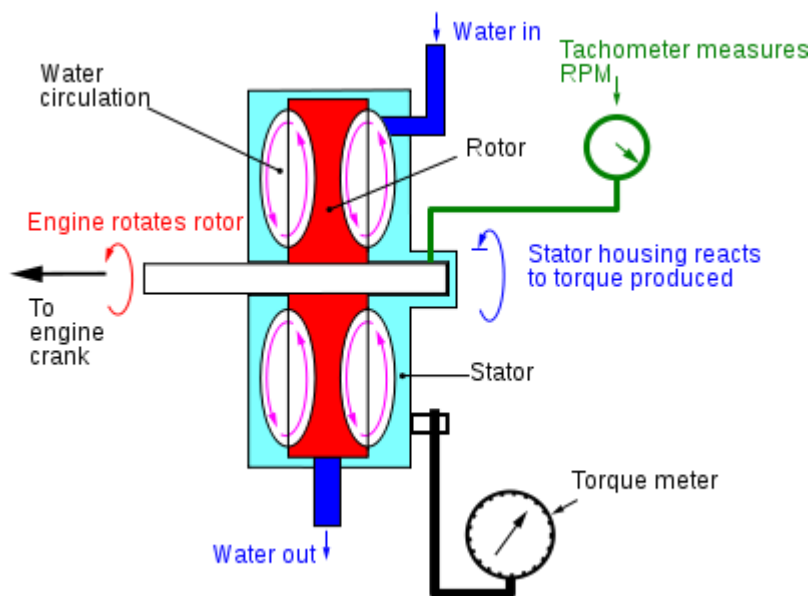


Figure 5.1: Schematic overview of water brake

5.2.3 Measurement equipment

The MAN 4L 20/27 is already equipped with a large selection of measurement equipment. A complete list of measured parameters is provided in appendix A. Almost all measuring equipment is connected to a PC via a data logger, and can be accessed through a graphical user interface (GUI). This GUI shows real time data, and can also be used to start recording data for a given period of time. The data can be stored in both .txt and .mat file formats. In the figure below a screenshot of the GUI is given. Every colored block can be selected to provide further and detailed information on that specific subsystem. The subsystems are:

- Fuel system
- Lubrication oil system
- Intake air
- Exhaust gasses
- Central cooling system
- Cylinder cooling system
- Fuel weighing system (not operational)

Some additional, mostly unused systems (in the small colored blocks in the top left):

- Brackish water system
- Starting air system
- Water brake system

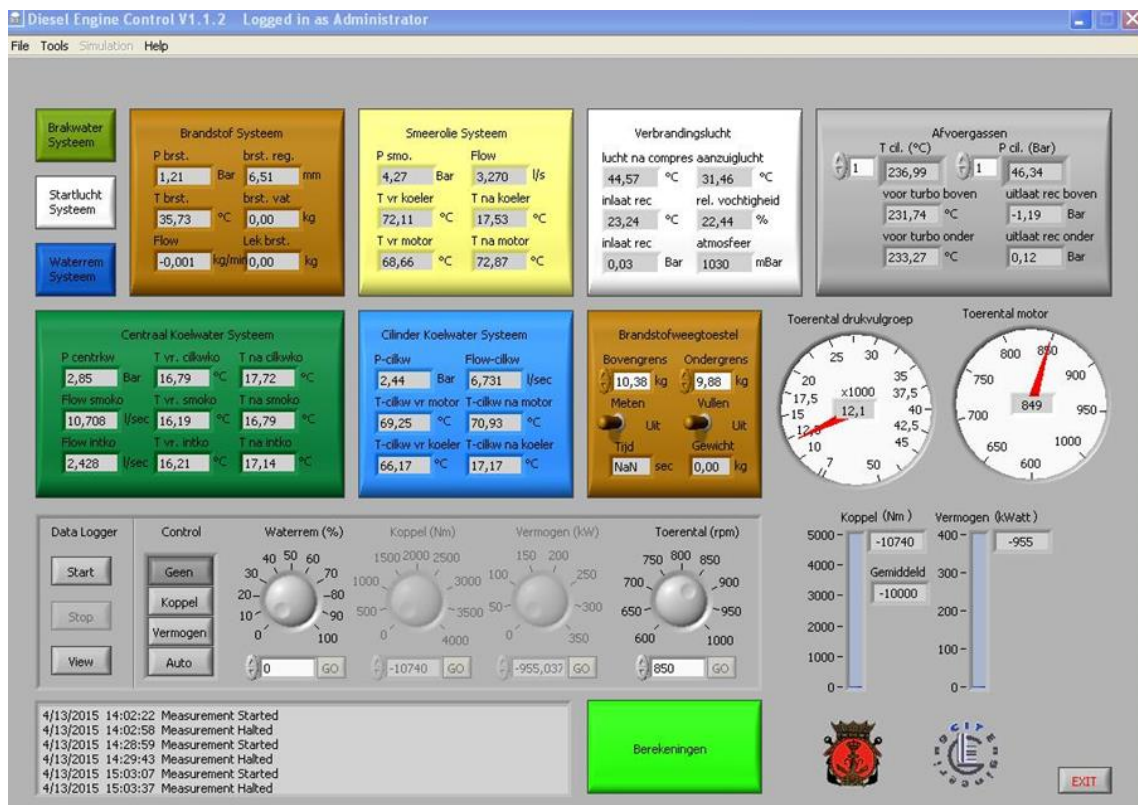


Figure 5.2: Overview of data logger GUI

5.2.3.1 In-cylinder pressure

One of the most important measurements is the in-cylinder pressure, and therefore we will go into a bit more detail concerning that particular sensor. The pressure sensor used is the Kistler 7061B, which is a water-cooled precision pressure sensor especially suited for duty in internal combustion engines for high-precision thermodynamic measurements. Technical data of this sensor is provided in appendix A. The pressure sensor is used in combination with a charge amplifier. This charge amplifier (Kistler 5011B) converts the electrical charge produced by the piezoelectric pressure sensors into a proportional voltage signal.



Figure 5.3: Kistler 7061B Pressure sensor

5.2.3.2 Emissions

To measure the gaseous emissions in the exhaust gas, a Horiba PG-250 portable emissions analyzer was used. This analyzer measured the concentration of O₂, CO, CO₂, SO₂ and NO_x particles in the exhaust gas flow using a number of analysis principles. For the NO_x measurement the chemiluminescence detection method (CLD) is used, while the SO₂, CO and CO₂ concentrations are measured using non-dispersive infrared absorption (NDIR). O₂ concentration is measured using a galvanic cell. The device was calibrated every morning using span gas and ambient air. Data from this device was written down manually during measurements, as there was no possibility to attach it to the data logger digitally.



Figure 5.4: Horiba PG-250 portable emission analyser

5.2.3.3 Fuel consumption

To monitor the fuel consumption of the engine, the amount of fuel used in a certain amount of time was recorded using a precision balance and a chronometer. Normally this system would be connected to the data logger, but unfortunately that was not possible at the time of testing so the results were collected manually. The amount of fuel was chosen such that the time to burn this amount of fuel was in excess of 2 minutes. This to ensure accurate results over the entire range of operating points. Leakage fuel was also measured to correct fuel consumption.

5.2.4 Hydrogen addition equipment

To add the hydrogen gas to the engine, some additional equipment is required. Most importantly a flow meter, to set and monitor the precise amount of hydrogen that is being fed into the engine. For this purpose the F-113AC Mass Flow Meter (MFM) from Bronkhorst Nederland was used. The MFM consists of a thermal mass flow sensor and a microprocessor based pc-board with signal and fieldbus conversion and a PID controller for optional mass flow control by means of a separately mounted control valve. The mass flow is provided as either analog or, in our case, digital input via RS232. The MFM was specifically calibrated by Bronkhorst for operation with hydrogen gas with flow rates between 0.01 and 0.5 m³n / min. Accuracy is +/- 0.5% of measured value. Software was also provided, which allowed the setting and monitoring of a set point in both percentage of maximum flow rate and in m³n/min. m³n/min stands for cubic meters at normal condition per minute.



Figure 5.5: F-113AC Mass Flow Meter

The hydrogen itself is provided by Linde Gas B.V. They offer a number of different solutions, varying in purity of the hydrogen gas. This varies from the lowest purity of 99.5 volume %, up to the highest purity of 99,9999 volume %. For operation in an internal combustion engine the highest grade is not required, but to make sure that any impurities in the hydrogen would not play a factor in any following calculations or results, the choice was made for "Waterstof droog 3.0". This grade has a purity of 99,9 volume % hydrogen, and is guaranteed to contain less than 30 ppmv H₂O.

This gas is provided in cylinders containing 50 litres of hydrogen gas at 200 bar pressure. Our MFM mentioned above has a maximum inlet pressure at the primary side of 10 bar, and thus a pressure reducing valve is necessary. A suitable valve was also ordered from Linde Gas B.V., after ensuring it would not restrict the flow of hydrogen in any meaningful way.

Finally, safety regulations also require a flame arrester to be installed. A flame arrester is a device which allows gas to pass through it, but stops an actual flame. This prevents backfiring of a flame to the hydrogen cylinder in the case of an accident. Again it was checked that the flame arrester would not restrict the flow of hydrogen. A schematic overview of a flame arrester is shown in the figure below.

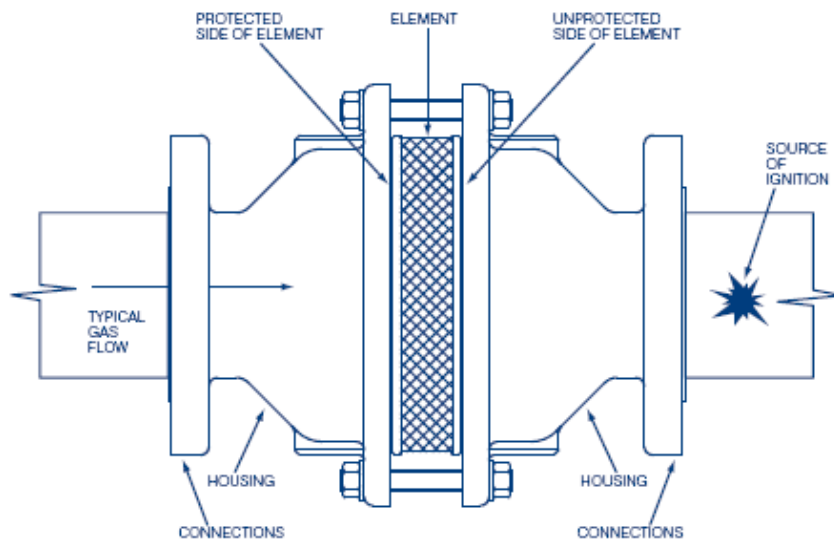


Figure 5.6: Schematic overview flame arrester

From the MFM, the hydrogen needs to be transported to the engine. Due to safety regulations the hydrogen cylinder cannot be placed in the same room as the engine itself, and was placed in the adjacent (empty, well ventilated) room with the MFM. This left a considerable distance (approx. 15 meters) to be covered between the cylinder and MFM, and the engine itself. To cover this distance specialized tubing was used (made from ethylene polyfluoroethylene, or PTFE. Commonly known as Teflon). Due to its small molecular size hydrogen is prone to leaking, and using correct tubing is essential to minimizing this leakage. Other reasons for using PTFE tubing are temperature related: at the point where hydrogen enters the engine, temperatures can reach values up to 80-100 degrees Celsius. Since PTFE has operational limits of -190 to 260 degrees Celsius, this does not pose a problem.

Additionally hydrogen transport poses some problems due to hydrogen embrittlement and corrosion. Hydrogen embrittlement is the process by which metals become brittle and fracture due to diffusion of hydrogen into the metal. Corrosion can occur since hydrogen has an active electron, and therefore behaves somewhat similar to a halogen. Since composite tubing instead of metal piping was used this was not an issue.

5.3 Hydrogen addition calculations

The amount of hydrogen that needs to be added to the engine at each testing point is based on a percentage of total energy going into the engine. To find out this total energy, baseline measurements are performed simply with pure diesel operation. From the diesel fuel consumption (kg/sec) at this baseline we convert to energy consumption (MJ/sec) by multiplying with the lower heating value (LHV, unit of MJ/kg) of the diesel fuel. Then we calculate the mass flow of hydrogen required by multiplying with the desired percentage of hydrogen addition and dividing by the LHV of hydrogen. See formula below:

$$\dot{m}_H = \frac{\dot{m}_{diesel} \cdot LHV_{diesel} \cdot x}{LHV_H} \quad (4.1)$$

In this formula x is the percentage of hydrogen addition.

The mass flow meter is controlled in units of $\frac{m^3n}{min}$, which is defined as cubic meters at normal condition per minute. "Normal condition" is defined as:

- 1,01325 bar pressure
- 15 degrees Celsius temperature (288,15 degrees Kelvin).

This definition is necessary since hydrogen is used in gas form, and the density of a gas changes with temperature and pressure according to the ideal gas law:

$$P \cdot V = N \cdot R \cdot T \quad (4.2)$$

Where P is pressure in Pascal, V is volume in cubic meters, N is the total amount of substance in moles, R is the universal gas constant (8,314 J/K·mole) and T is the temperature in degrees Kelvin.

This formula can be rewritten further by introducing the formula below

$$N = \frac{m}{M} \quad (4.3)$$

Where m is the mass in grams and M the molar mass in grams per mole. For hydrogen this value is 2,016 g/mol. Density is defined as mass divided by volume, resulting in the following formula for density:

$$P \cdot V = \frac{m}{M} \cdot R \cdot T \gg \rho = \frac{P \cdot M}{R \cdot T} \quad (4.4)$$

When we fill in the values for pressure and temperature at normal conditions, the molecular mass of hydrogen and the universal gas constant, we get the density of hydrogen at this condition: 0,085 kg/m³. With this density we can convert our mass flow of hydrogen to a volume flow, and set our flow meter correspondingly.

This process has been automated in an excel sheet, where the amount of hydrogen and corresponding flow meter settings are calculated for each test point. Additionally this model was used to predict the total amount of hydrogen required beforehand using estimates for the diesel fuel consumption. In this case not the “normal conditions” were used, but the estimated actual conditions at which the hydrogen is injected into the engine (around 30 degrees Celsius and 1,3 bar(a)).

An overview of the excel model is available in Appendix B. Here only the sheet for a single set of measurements is shown (propeller curve), but the sheet is identical for the other sets (700, 850 and 1000 RPM generator curves).

5.4 Map of measured points

During selection of what engine operating points were to be tested, a number of factors influenced this decision. In no particular order they are:

- Total number of points
- How often to repeat tests at a certain operating point
- Hydrogen consumption at specific point
- Engine operating limits

Of course the operating points are mainly chosen based on how likely it is that an actual engine would operate in a certain area. Therefore testing points were chosen along both the propeller curve and a number of generator curves, two of the most likely applications on board a vessel.

Since a limited amount of time was available for tests, keeping the total number of testing points manageable was of importance. Additionally hydrogen is consumed at a considerable rate, especially at high loads and high percentages of addition. While no limitations were set as to the amount of hydrogen that could be used or purchased, common sense dictates that needlessly increasing costs is not desirable. Additionally, storage location that meets the safety requirements was available, but only for about 6 cylinders. This means that if more hydrogen was required, deliveries would need to be frequent and logistics might also become an issue. More reasons to keep the total amount of hydrogen required low.

Originally, the MAN 4L20/27 was rated for 350 kW at 1000 RPM nominal operation. Given the engines age and the expected results of adding hydrogen to the engine (increased peak pressure) it was decided that the engine would not be loaded further than 300 kW at 1000 RPM. The experience and expertise of the engine’s mechanic, sergeant Marcel Roberscheuten, was instrumental to this decision.

Based on this new nominal point a new propeller curve was drawn. The original Technical Data of the engine was also consulted to make sure operation would remain within the operational envelope at all times.

For the generator curves we decided on 3 sets of measurements. One at 700 RPM, one at 850 RPM and one at 1000 RPM. Although it was possible to run the engine at even lower RPM, the power range that could be produced at this setting was fairly low without exceeding the operating envelope. Therefore the minimum RPM was set at 700, and the maximum at the nominal RPM of 1000. One intermediate point was chosen in the middle, at 850 RPM. The decision for only 1 intermediate generator curve was made to keep the total number of testing points down.

The operating envelope and the test curves and points are shown in the figures below.

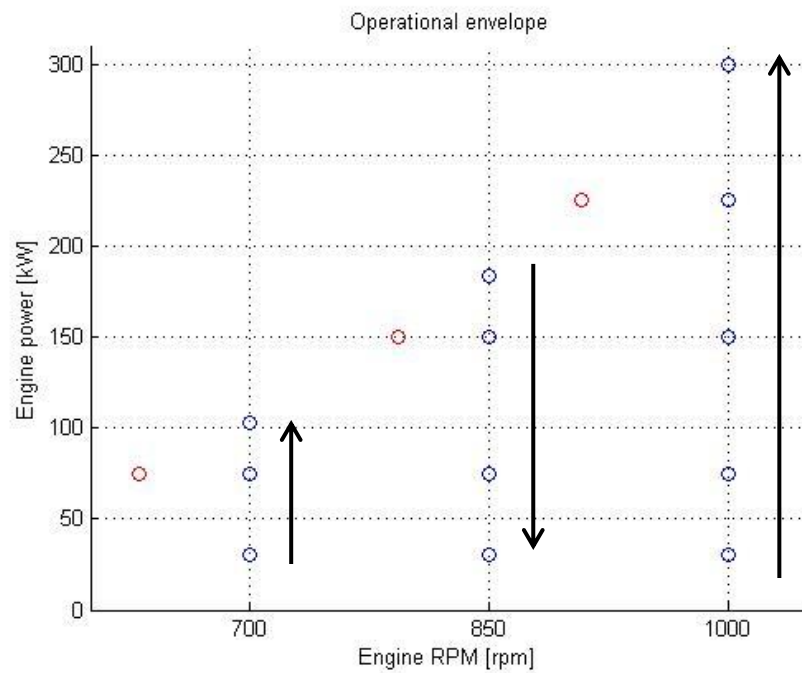


Figure 5.7: Test series 1, generator curves (blue points)

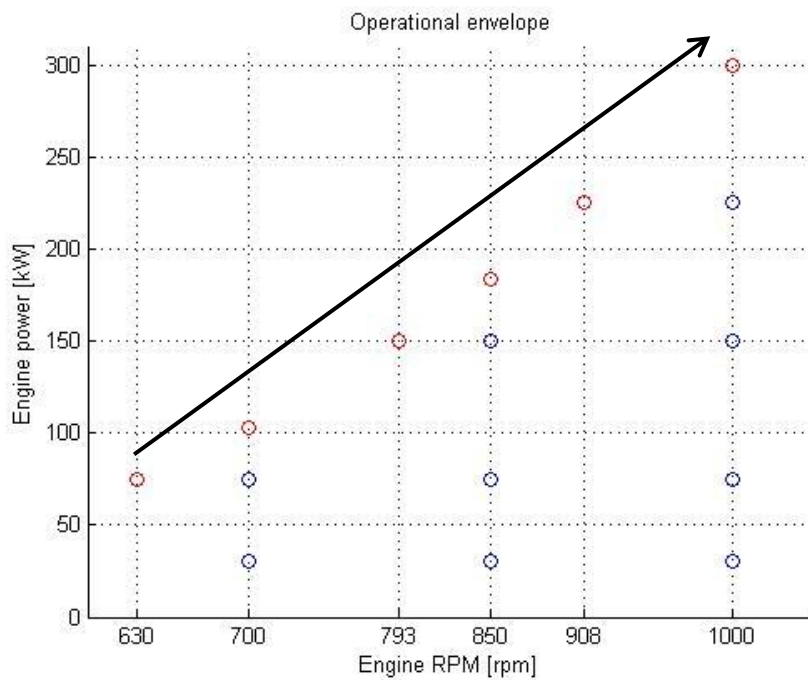


Figure 5.8: Test series 2, propeller curve (red points)

Another consideration was how often to repeat tests at a certain operational point. There is always some variation in test results due to any number of factors: test equipment, engine performance, ambient conditions, slight differences in fuel, etc. Therefore repeating tests multiple times and averaging the results or checking for outliers and strange data is essential. Of course this poses the same problems as mentioned before when discussing the total number of testing points, mainly constraints in terms of available time for testing. It was decided that ideally all tests should be performed 3 times. For all the benchmark tests (without hydrogen addition) tests results were already available, so these were performed an additional 2 times. For most of the hydrogen testing points 3 sessions were recorded, but a number of points were only measured twice due to time constraints. Since the results of these 2 tests were fairly consistent, it was decided to use them anyway.

To keep testing time-efficient, the first generator curve is traversed from the lowest to the highest load, and the subsequent one from highest to lowest. This kind of “S-shaped” testing order results in the shortest time required between tests to let the engine reach stable temperatures.

5.5 Testing procedure

To streamline the actual testing, a procedure has been developed with clear step-by-step instructions and templates to write down results. These steps are detailed below, and the templates are included.

5.5.1 Start-up

At the beginning of the day the test setup has to be started, preferably as early as possible to allow the engine to reach stable temperatures. This takes up to an hour, therefore the sooner this is done the sooner actual testing can commence. Starting the engine and preparing all equipment for measurements consists of the following steps.

First step is a visual check of the engine and engine room. This is simply to make sure everything is as it was left the previous day, a basic precaution for obvious problems. The next step is to start up the PC with data acquisition software and monitoring software, and set the engine RPM to approx. 700 RPM. The water brake is not yet engaged. After this the engine can be physically started, using the key on the engine block itself. While the engine is heating up, emissions measurement equipment is checked and recalibrated using span gas and ambient air.

After approx. 20 minutes, the water brake can be engaged to apply a load, and the engine can be set to the first testing point of the day and continue to reach stable temperatures. Additionally the laptop connected to hydrogen flow meter can be started, and hydrogen levels checked. When the engine has reached stable temperature, testing can commence.

5.5.2 Testing

After the engine has reached stable temperatures at the desired test point, actual testing can commence. The first test of the series is always the benchmark, where no hydrogen is added to the engine.

The first step is to start recording the digital data set from the data acquisition system. Duration of recording is 1 minute. File size increases rapidly with test duration, and since the sample rate is fairly high (approx. 2 Hz), 1 minute of continuous measurement provides plenty of data.

After stopping the data recording (from the control room), 2 people enter the engine room. Both have stopwatches. During the next couple of minutes both fuel consumption and emissions will be checked. Fuel consumption is checked by monitoring the time required to burn a specific amount of fuel. A precision scale is used for this purpose. The amount of fuel varies between testing points, to make sure the measurement always takes about 3 to 4 minutes. To calculate the air consumption of the engine a pair of venturi tubes are connected to the air inlet, filled with water. The emissions measurements are done in the same timeframe, periodically writing down the value on the display of the Horiba PG-250. The templates used for the emission and fuel consumption measurements can be found below.

Meetpunt:					
Datum:					
Brandstofmeting					
Hoeveelheid brandstof:		[kg]			
Tijd:		minuten		seconden	
Venturi buis					
Hoogte buis 1:					[cm]
Hoogte buis 2:					[cm]

Figure 5.9: Fuel and air consumption measurement template

Meetpunt:					
Datum:					
	00:00	01:00	02:00	03:00	04:00
CO [ppm]					
CO2 [ppm]					
NOx [ppm]					
O2 [%]					

Figure 5.10: Emission measurement template

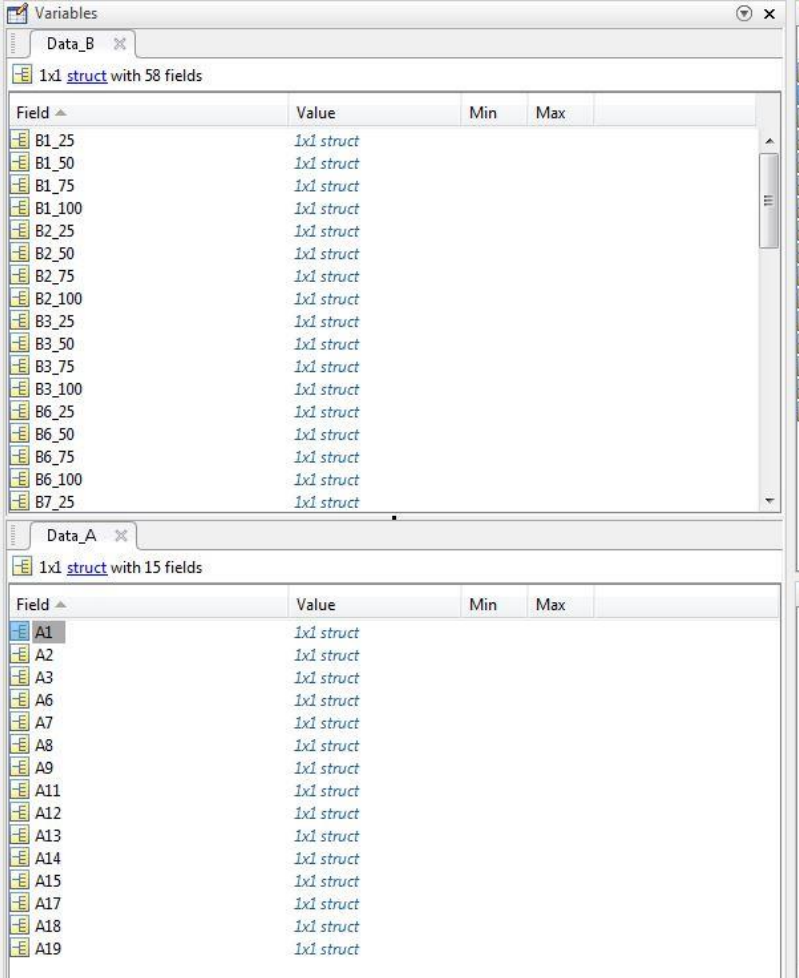
When these benchmark measurements are done, both persons can return to the control room. With the measured fuel consumption the correct setting of the hydrogen flowmeter can be calculated, starting at the lowest percentage of hydrogen addition and working up.

The hydrogen flowmeter is set to the correct value, after which the engine is given 5 minutes to stabilize. During this time the digital data recorded from the previous test can be saved and the log cleared. After 5 minutes of stabilizing, the procedure is repeated.

5.6 Data processing

Before we can use the data we gathered from the engine, we must first convert it into a usable format. First step is to import the data files into Matlab, to see what we are working with. This was very easy, since the output of the data acquisition computer could be chosen as either a table in .txt format, or (very conveniently) the Matlab .mat format. First of all, the data is a continuous measurement over the course of a minute. A lot of the measured parameters barely fluctuate at all over time, since the engine was given time to stabilize at each operating point. Therefore the continuous measurements are condensed into a mean value. Additionally some sensors were defect or nothing was connected to a certain channel, resulting in values reading NaN or negative values where this would be impossible. These faulty readings were removed. Additionally the measurements for emissions and fuel consumption were done manually with pen and paper, so these needed to be added to the correct digital file. Emission measurements were taken periodically during testing from the Horiba emission analyser, and the mean of these measurements was used.

Finally this data was stored into two separate arrays in Matlab. One for the benchmark data files, and one for the data files with hydrogen addition (see figure 5.11).



The screenshot shows the MATLAB Variables window with two tabs: Data_B and Data_A. Data_B is a 1x1 struct with 58 fields, and Data_A is a 1x1 struct with 15 fields. Both are displayed as tables with columns for Field, Value, Min, and Max.

Field	Value	Min	Max
B1_25	1x1 struct		
B1_50	1x1 struct		
B1_75	1x1 struct		
B1_100	1x1 struct		
B2_25	1x1 struct		
B2_50	1x1 struct		
B2_75	1x1 struct		
B2_100	1x1 struct		
B3_25	1x1 struct		
B3_50	1x1 struct		
B3_75	1x1 struct		
B3_100	1x1 struct		
B6_25	1x1 struct		
B6_50	1x1 struct		
B6_75	1x1 struct		
B6_100	1x1 struct		
B7_25	1x1 struct		

Field	Value	Min	Max
A1	1x1 struct		
A2	1x1 struct		
A3	1x1 struct		
A6	1x1 struct		
A7	1x1 struct		
A8	1x1 struct		
A9	1x1 struct		
A11	1x1 struct		
A12	1x1 struct		
A13	1x1 struct		
A14	1x1 struct		
A15	1x1 struct		
A17	1x1 struct		
A18	1x1 struct		
A19	1x1 struct		

Figure 5.11: Data stored in 2 structures for benchmark and hydrogen addition

The in-cylinder pressure data also required some work before it could be used in the various models. First of all the pressure was recorded for a set amount of time, resulting in a continuous signal with multiple cycles (see figure 5.12 below).

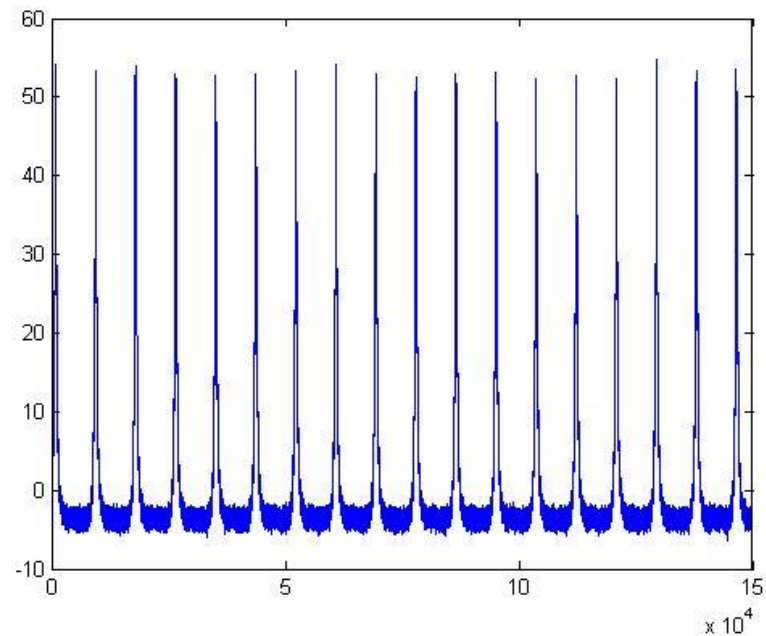


Figure 5.12: Raw pressure data (1 cylinder)

From this figure we can also see that there is some vertical error, since the pressure drops to approx. -5 bar. A number of processing steps were applied to this raw signal:

- Synchronizing the pressure trace to the top dead centre signal (horizontal sync.)
- Determining the vertical shift of the pressure signal and correcting this
- Averaging the cycles together to reduce some noise

Additionally some no-fuel measurements were done at all RPM's, since this was required for the TDC synchronization. This results in a lot cleaner pressure trace, correctly synchronized to crank angle and inlet pressure. Not all noise in the pressure trace could be removed, but this was due to the way the pressure was measured. The sensor is located in a fairly narrow channel, and this results in the pressure wave bouncing around in this channel before hitting the sensor. Since all cycles have this effect, averaging the cycles together does not remove this noise. The result of the processing is shown in figure 5.13 below.

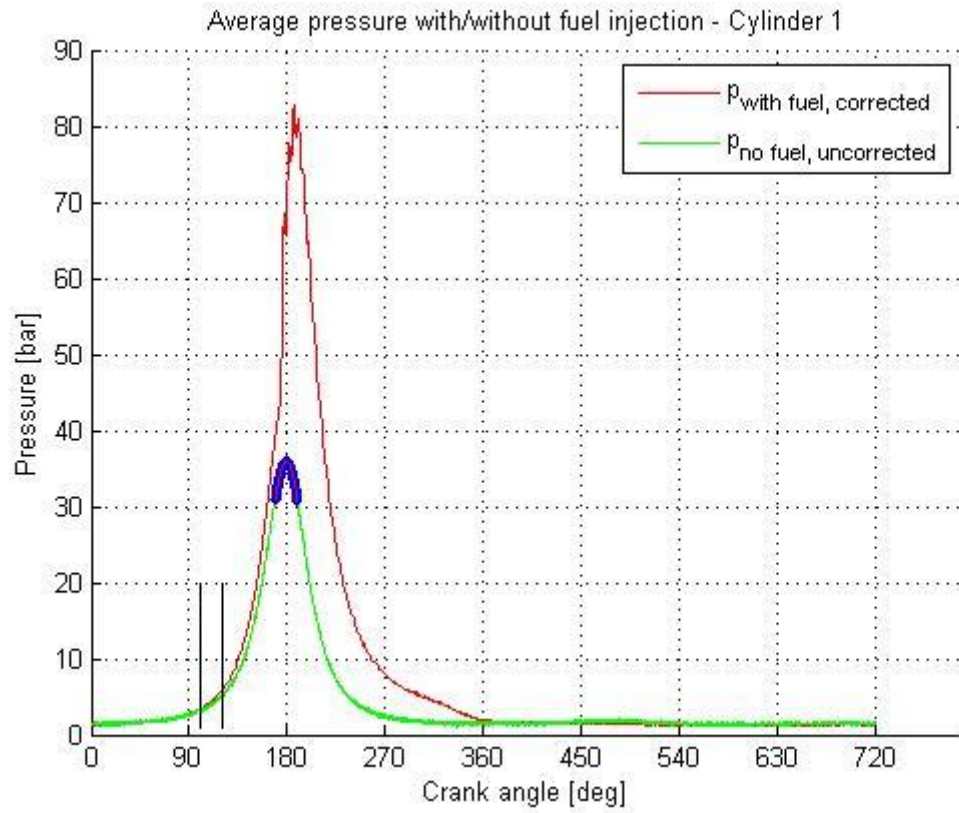


Figure 5.13: Processed pressure trace with no-fuel measurement

Chapter 6: Measurement Results

6.1 Introduction

In this chapter the results of the direct measurements will be shown. This chapter covers:

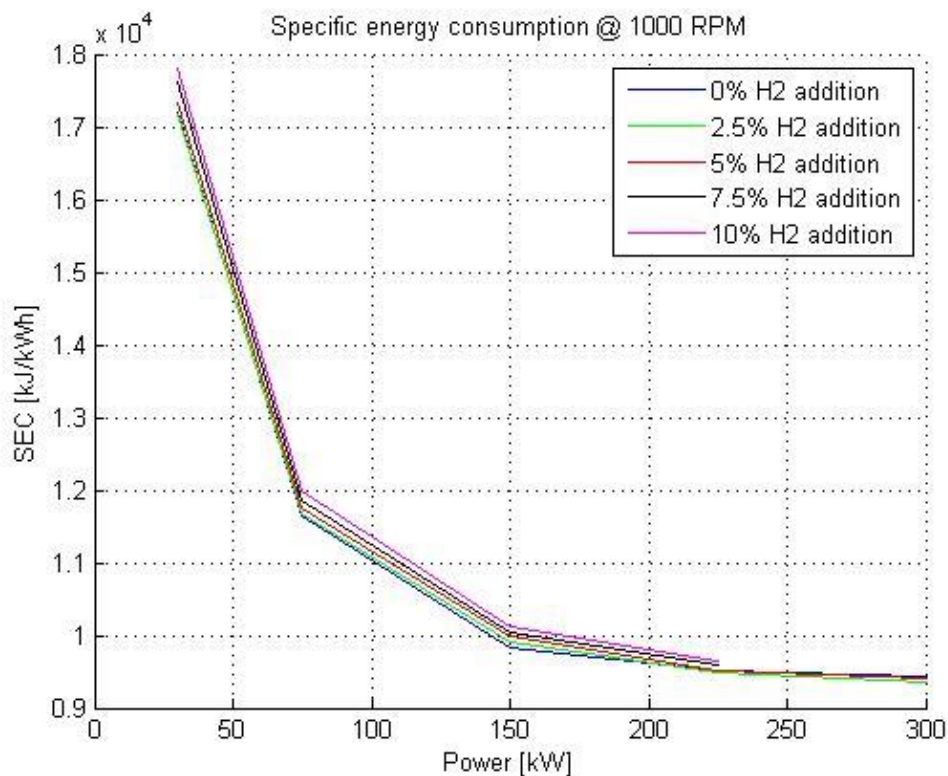
- Fuel consumption (paragraph 6.2);
- Corrections for hydrogen combustion efficiency and scavenging (paragraph 6.3);
- Emissions (paragraph 6.4);
- Cylinder pressure (paragraph 6.5).

6.2 Fuel consumption

Fuel consumption consists of two parts: diesel and hydrogen consumption. To make a fair comparison between pure diesel and diesel/hydrogen operation, we cannot use specific fuel consumption (SFC, unit of g/kWh). Instead we will convert to energy (Joules), and compare the specific energy consumption (SEC) of the engine. This way we can compare apples to apples. To do this we use the LHV of both diesel (42,7 MJ/kg) and hydrogen (120 MJ/kg) to convert both the measured mass flow of diesel and the massflow set at the massflow meter for hydrogen to energy.

$$SEC = \frac{(\dot{m}_{diesel} * LHV_{diesel}) + (\dot{m}_H * LHV_H)}{kWh} \quad (6.1)$$

This results in the following plots.



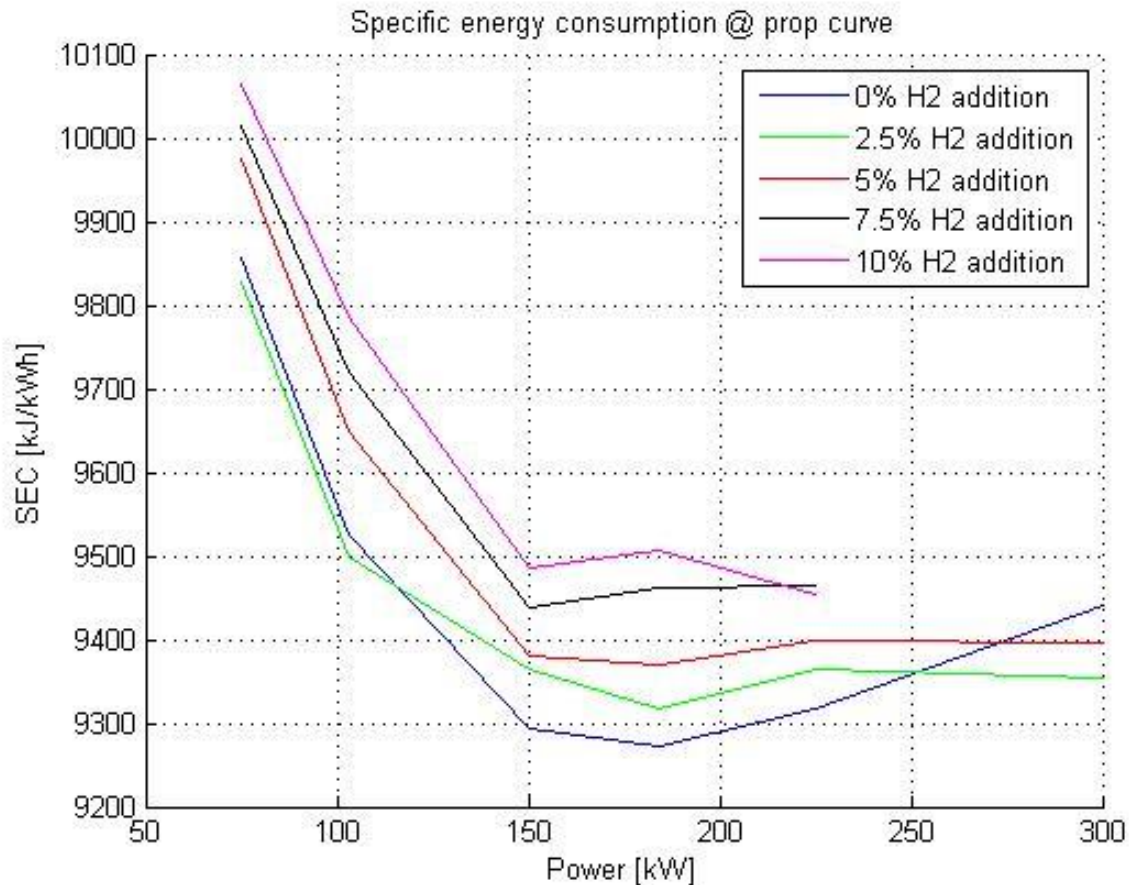


Figure 6.2: SEC @ propeller curve

These plots show that more energy is consumed to produce the same amount of work if hydrogen is added, both for operation at the propeller curve and at a constant RPM of 1000. The only point where the addition of hydrogen seems to result in more efficient operation (e.g. less energy consumed to produce a certain amount of work) is at 300 kW. This is the same point in both graphs, since the propeller curve intersects 1000 RPM at 300 kW. Interestingly enough, this seems to be only true for low percentages of hydrogen addition.

Unfortunately there are no tests results for 7,5 and 10% hydrogen addition at this load, because of practical issues during testing. At this load point hydrogen consumption is quite substantial (30-40 gram/minute), and hydrogen was only available in 50L cylinders at 200 bar pressure. Including time to stabilize, the cylinder would be empty before the testing cycle was complete, resulting in unusable data.

Normalizing the plots results in a clearer overview, and shows that percentage-wise the differences are fairly small. This new view also shows that the 2.5% hydrogen addition curve dips below the benchmark line at very low loads. This difference (less than 1%) is too small to conclude anything from, however.

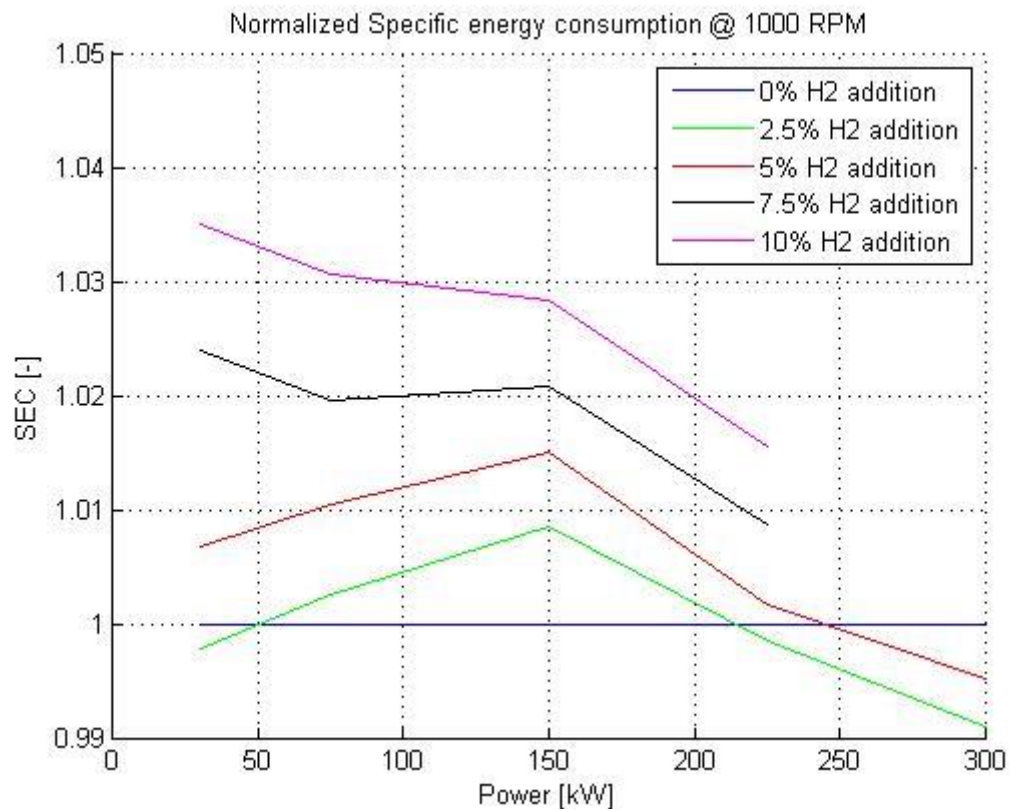


Figure 6.3: Normalized SEC @ 1000 RPM

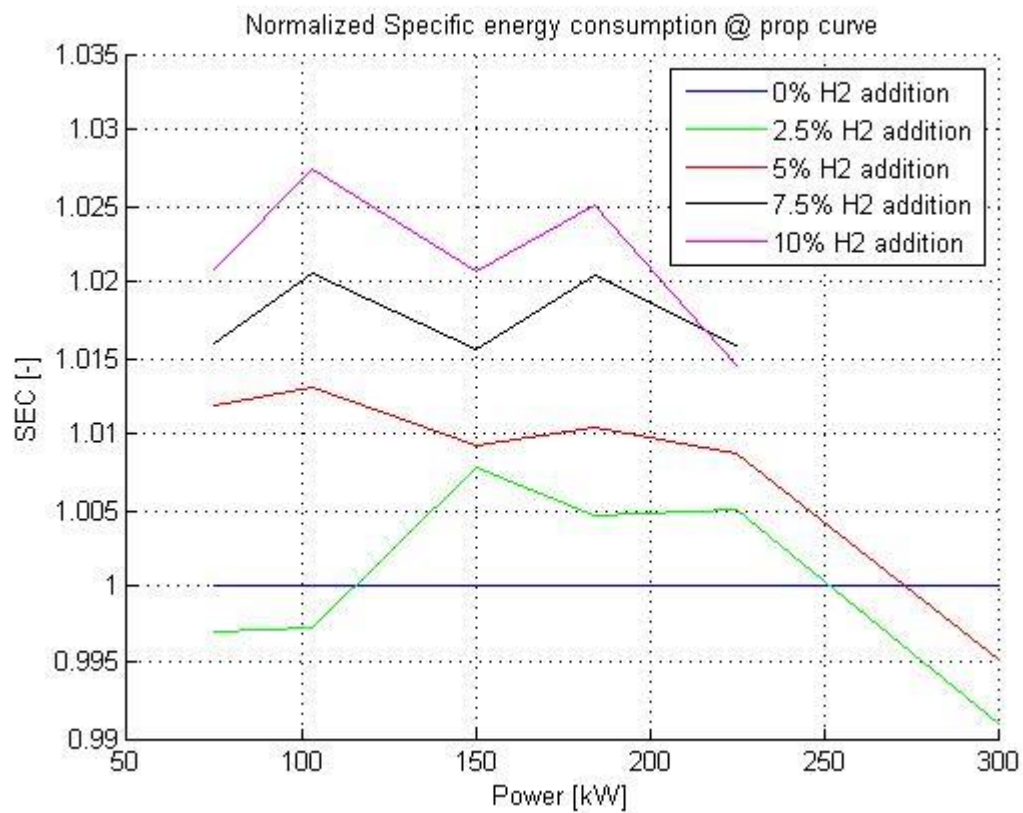


Figure 6.4: Normalized SEC @ propeller curve

6.3 Correction for hydrogen combustion efficiency and scavenging

While the graphs above correctly show the fuel consumption of the engine in terms of total fuel entering the engine, they do not take into account combustion efficiency and scavenging.

Normally for diesel fuel the combustion efficiency is so high (99.9%) that this is not an issue, and scavenging losses do not influence the diesel fuel since it is injected after the ports are closed. Therefore specific fuel consumption gives an accurate view of the engines performance and fuel consumption. For hydrogen however the literature review in paragraph 2.4 has shown that hydrogen combustion does not always have this same high combustion efficiency, and additionally in our case it is present in the intake air and therefore susceptible to fuel loss due to scavenging.

These factors have potentially reduced the effect of the hydrogen addition as shown in paragraph 6.2. While the results that were shown are valid for this particular engine, it is important to correct these factors if possible to separate between what is purely the effect of the hydrogen addition, and additionally what is caused by this specific engine.

Based on research by Gatts et al. and Liew et al. ([Gatts et al, 2010, [Liew et al., 2010]) mentioned before in paragraph 2.4, the combustion efficiency is reported to be 75%-85% (increasing with hydrogen addition percentage) at very low loads (10%) and increases rapidly. At 20% load combustion efficiency is already approx. 88%, and from 50% load and above the efficiency rises to 93% and above.

A static hydrogen combustion efficiency for all points is preferred over varying values per operating point to keep the calculations and the figures simple. Since most of our measured points are at 25% load or higher, and the higher load points appear to be the most interesting, the hydrogen combustion efficiency will be set at 92%.

The valve overlap where both intake and exhaust valves are open of the MAN 4L20/27 engine is both reported by the manufacturer and directly measured at the engine. Results are shown in the table below. For this research the measured values will be used. An overlap of 92 degrees crank angle over a total of 256 degrees crankangle of time that the inlet port is open (56° before TDC to 20° after BDC) means that 36% of the time the inlet valve is open, the exhaust valve is open as well. Not all of this time is effectively used for scavenging due to varying pressure gradients, choking, etc. We will assume that 20% of the fuel is lost due to scavenging.

Table 6-1: Valve overlap for MAN 4L20/27 engine

	Inlet opens	Exhaust closes	overlap
Reported by manufacturer	50° before TDC	50° after TDC	100°
Measured	56° before TDC	36° after TDC	92°

Combining the hydrogen combustion efficiency and losses due to scavenging results in a total effective correction factor of $0.92 * 0.8 = 0.736$. This means that approx. 26% less hydrogen is being combusted than previously assumed, which influences the results shown before in paragraph 6.2. The corrected figures are shown below.

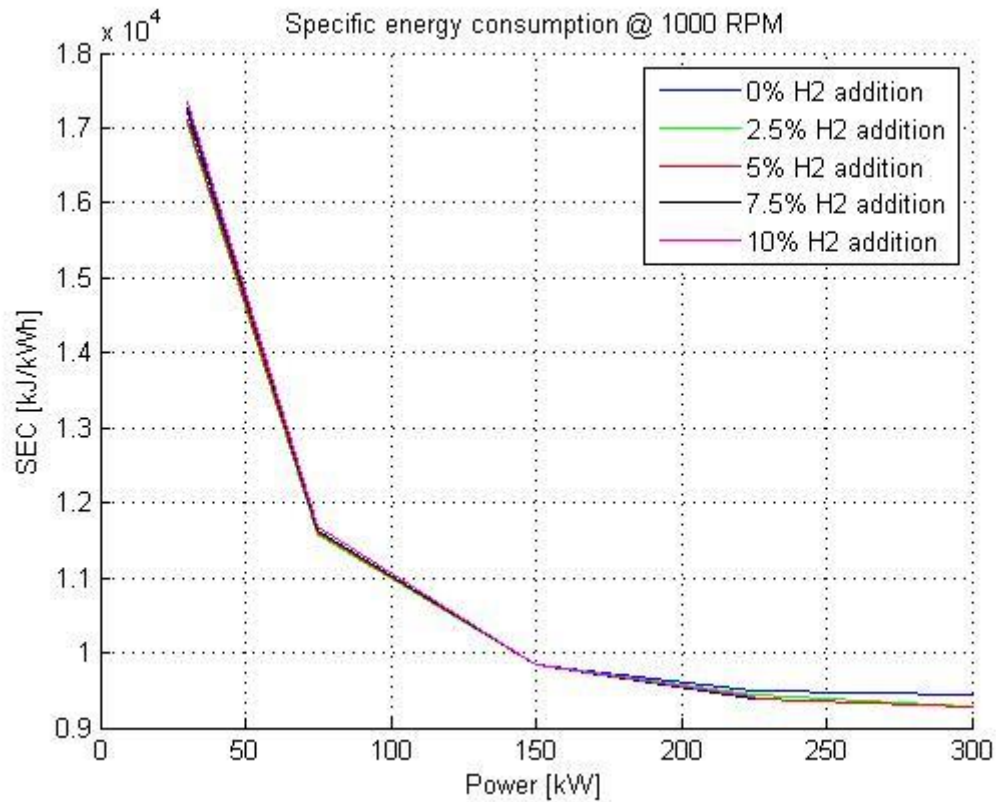


Figure 6.5: Corrected SEC @ 1000 RPM

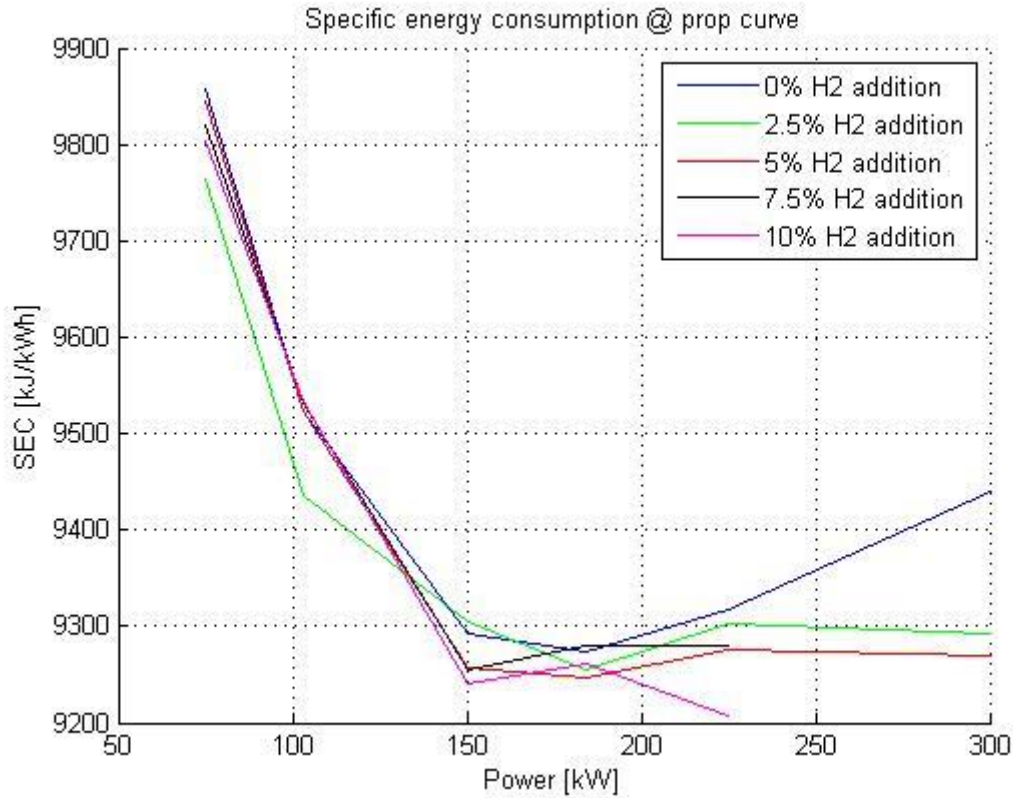


Figure 6.6: Corrected SEC @ propeller curve

In these corrected figures the benchmark and hydrogen operating points are very close together at almost all points. Only at high loads of 225 kW and 300 kW it becomes clear that hydrogen addition has a beneficial effect in energy consumption. In the propeller curve plot the ordering of 2.5% up to 10% is no longer visible, something that was the case previously in figure 6.2.

Normalizing the plots gives a clearer view, and shows that percentage-wise the differences between benchmark operation and hydrogen addition at low loads are very small indeed (almost always less than 1%). The differences at high loads however are now more in the region of 1.5%-2%, compared to 0.5%-1% in the uncorrected figures.

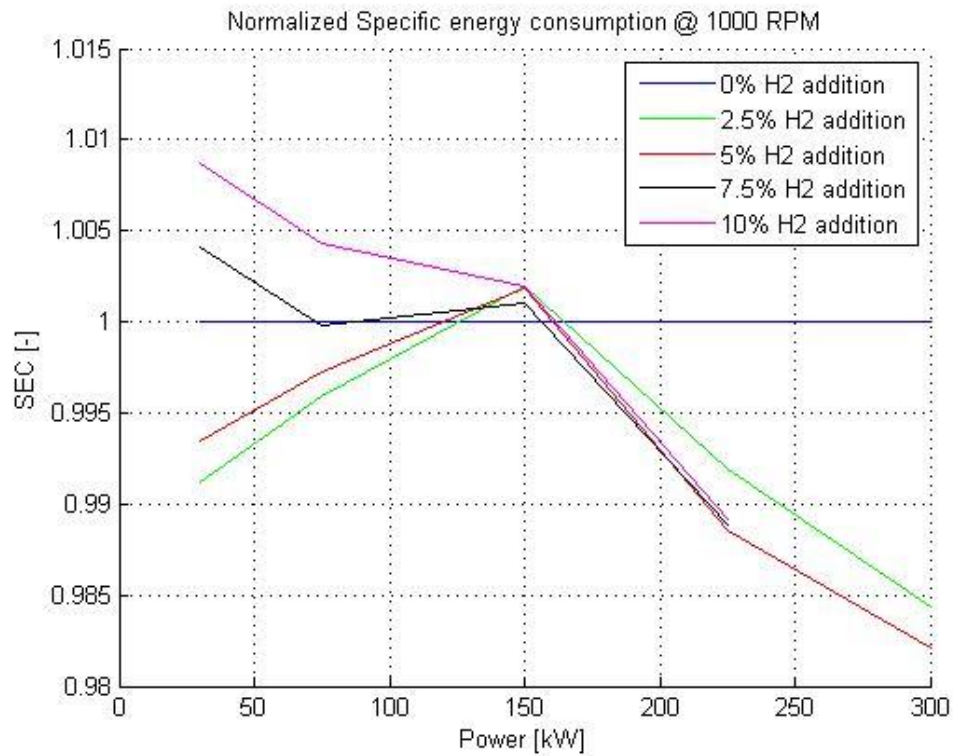


Figure 6.7: Normalized corrected SEC @ 1000 RPM

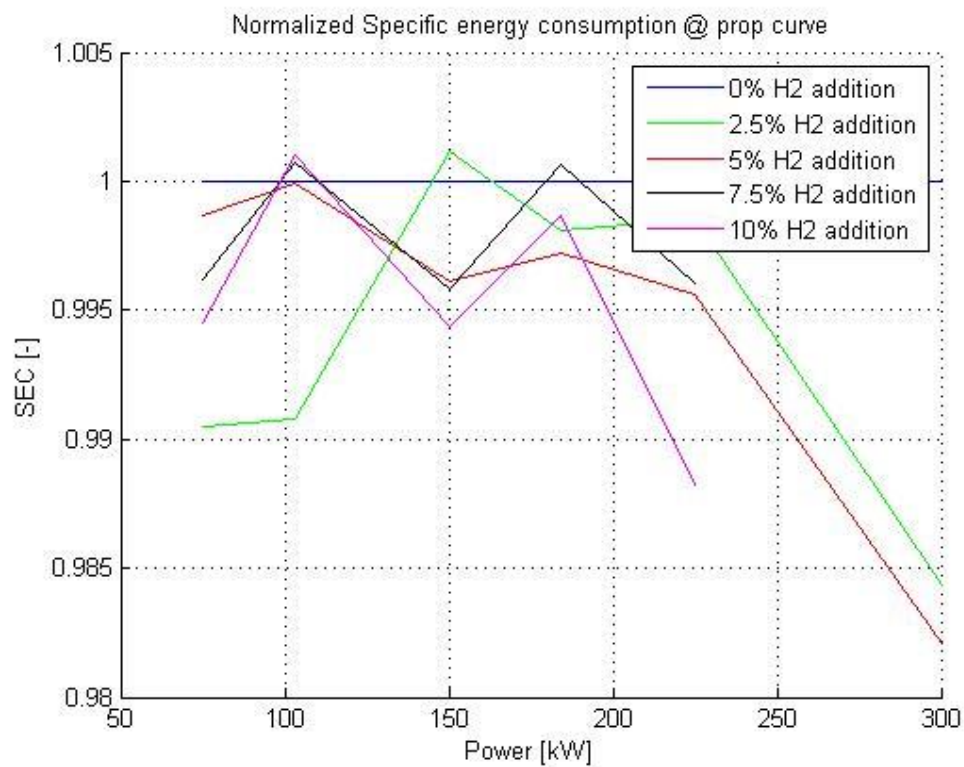


Figure 6.8: Normalized corrected SEC @ propeller curve

It is important to remember that these corrected figures are based on estimates for both hydrogen combustion efficiency and scavenging losses. By varying these estimates the results can vary quite substantially, but the current estimates are as accurate as possible. It is unfortunate that no measuring equipment was available to measure unburned hydrogen in the exhaust gasses, as this could have helped to acquire a more accurate estimate.

Nonetheless the overall results seem clear. At low loads differences in energy consumption between benchmark operation and operation with hydrogen addition (at all percentages) are insignificant, and overall differ only around 0.5%. At high loads however, the addition of hydrogen at rates of 2.5% and 5% of total energy (and presumably also when adding 7,5 and 10%, although this is extrapolated data) leads to an overall lower specific energy consumption, of approx. 1.5 to 2%.

These results indicate that while hydrogen addition in this particular engine was not very effective, it might prove more usefull in cases where the scavenging losses can be reduced or removed. Enhancing hydrogen combustion efficiency might prove to be more complicated, since this is (at least for the most part) a parameter of the hydrogen itself, and not so much of the engine used during testing.

6.4 Emissions

As mentioned before, the emissions measured with the Horiba PG-250 are O₂, CO, CO₂ and NO_x. O₂ and CO₂ are measured as a volume percentage of exhaust gas flow, while CO and NO_x are measured in ppmv (parts per million volume). The emissions were also converted to a normalized view, similarly to the fuel consumption. The graphs presented are the results for the 1000 RPM curve.

6.4.1 CO₂

We can clearly see from the graphs that percentage CO₂ in the exhaust drops a constant amount with the addition of increasing amounts of hydrogen. This was expected, since less carbon in (replacing diesel with hydrogen) means less carbon out. The reduction in CO₂ is constant throughout the power range, and proportional to the reduction in diesel fuel. With one exception: the effect at 300 kW. Similarly to the fuel consumption, we see that CO₂ emissions drop more than expected. This is particularly clear in the normalized view. We see the percentage decrease of CO₂ almost double, from approx. 2% to 4% at 2.5 % hydrogen addition, and from 3,75% to 6% at 5% hydrogen addition. Unfortunately the results for 7,5 and 10% hydrogen addition were not recorded due to the same practical problems as mentioned before.

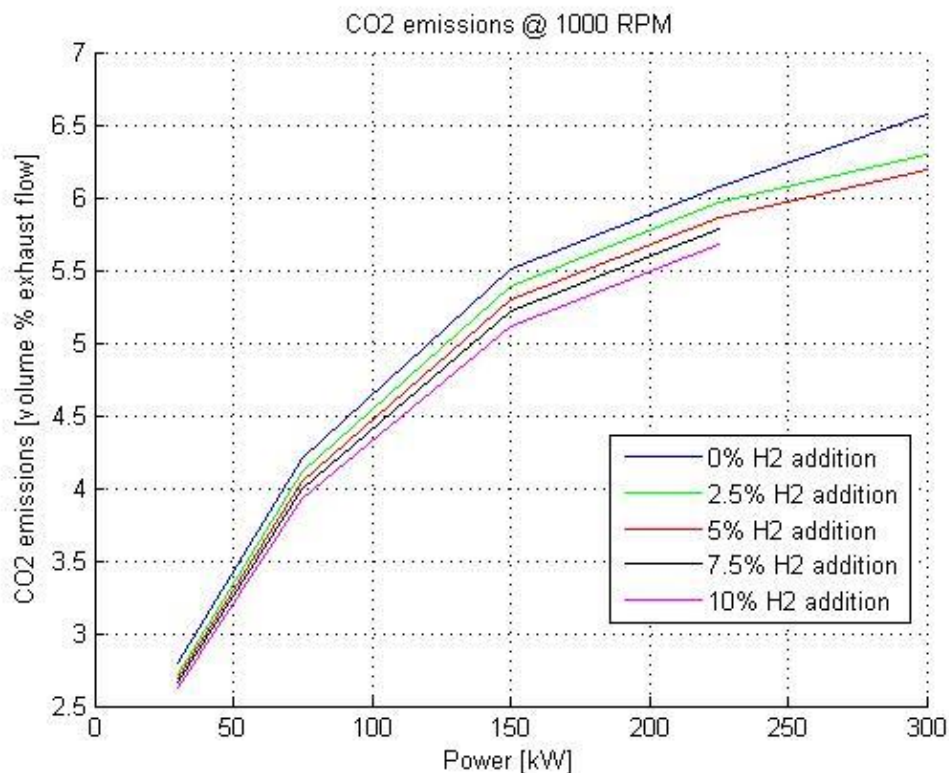


Figure 6.9: CO₂ emissions at 1000 RPM

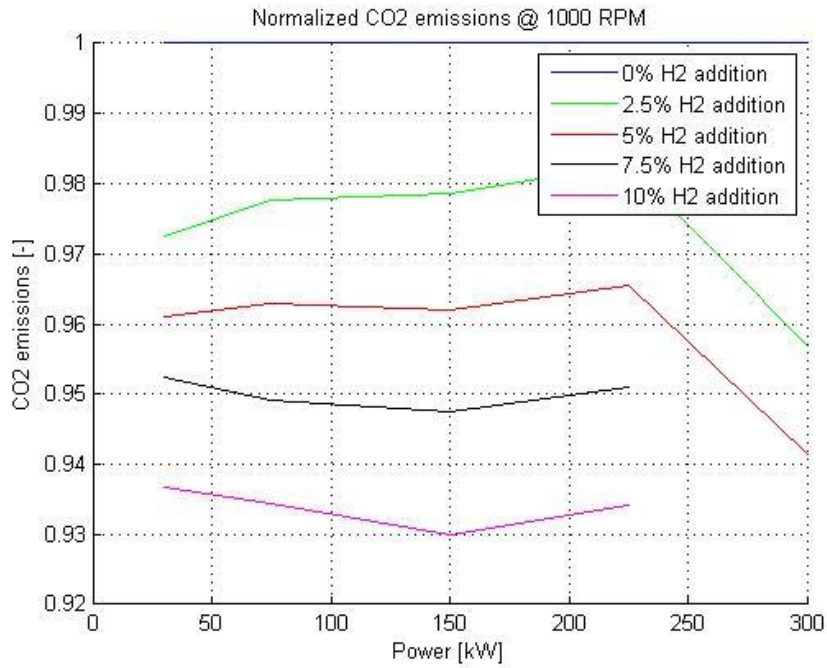


Figure 6.10: Normalized CO2 emissions at 1000 RPM

6.4.2 CO

The effect for CO emissions looks somewhat strange at first sight. At low loads the effect is quite strong, reducing CO emissions by 14 to 22%. This effect diminishes with increasing load to <5% at 150-200 kW, but ultimately seems to return at full load (300 kW). Again, the 7,5 and 10 % results at 300 kW are missing. The results at 225 kW seem somewhat strange, as the lines all swap around with 10% hydrogen having the most and 2,5% the least CO emissions.

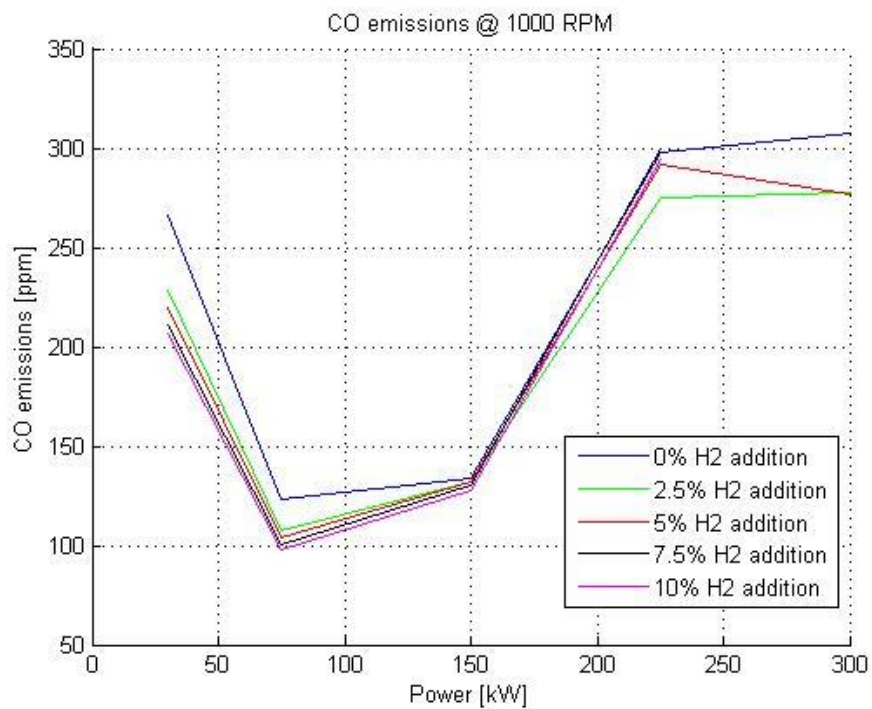


Figure 6.11: CO emissions at 1000 RPM

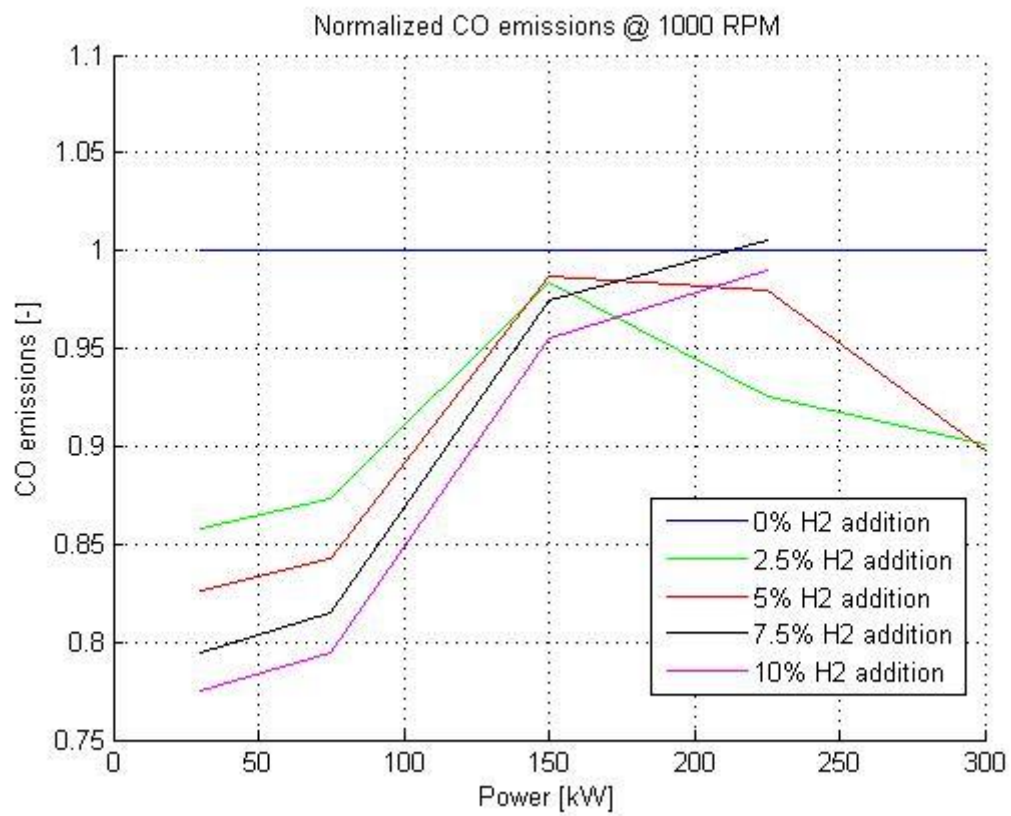


Figure 6.12: Normalized CO emissions at 1000 RPM

6.4.3 O₂

At almost all points O₂ emissions are similar to the benchmark situation, as values are within a .25% band. As seen before, the 300 kW point is an exception with O₂ values spiking up to about 1,5 -2% higher than the benchmark.

Only the normalized graph is shown in this case, since the regular data was very clustered and did not provide any extra insight.

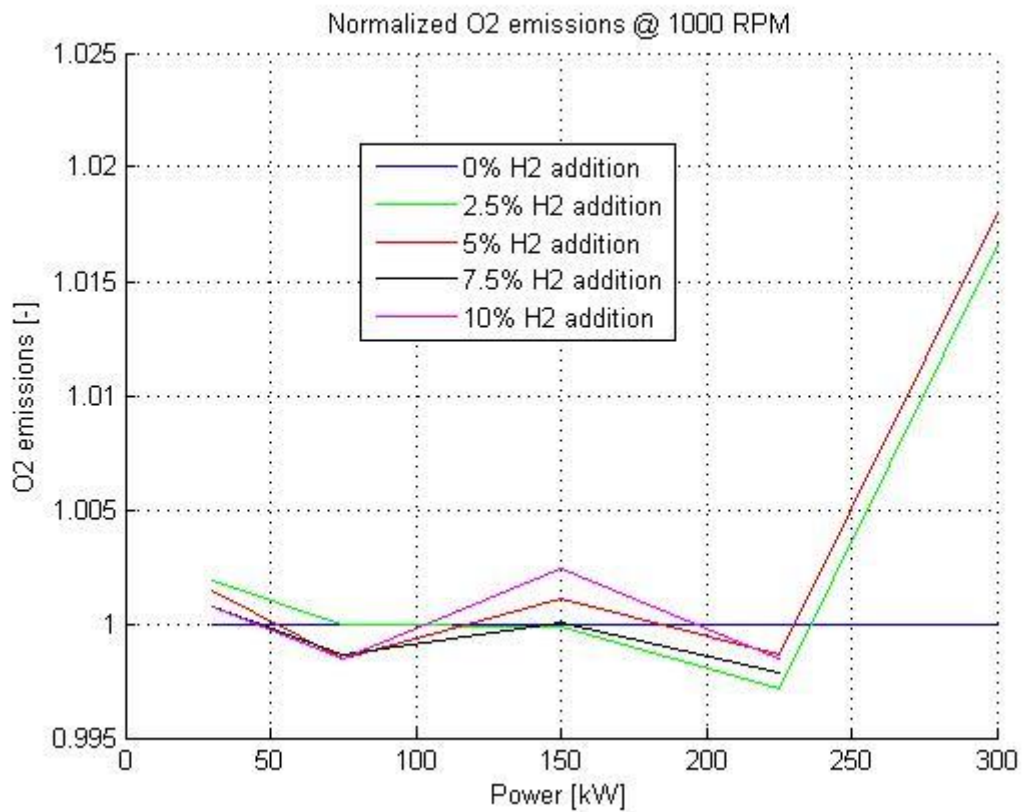


Figure 6.13: Normalized O₂ emissions at 1000 RPM

6.4.4 NO_x

NO_x emissions are slightly different than the other emissions, since they have had some calculations done on them. All other emissions are just the raw data from the Horiba PG-250 analyser, but for NO_x we converted from the ppmv values to specific NO_x emissions. This is a similar calculation as was done for the diesel fuel consumption, and results in a value with a unit of g/kWh NO_x emissions. This was done mainly because it is the common method of presenting NO_x emissions, and because it provides the ability to compare with other research results and legislation (which is also prescribed in g/kWh).

At low loads NO_x emissions are greatly diminished, proportionally to the reduction in diesel fuel. This effect becomes smaller as load increases, and at maximum load (300 kW) NO_x emissions rise 2-3% above the benchmark scenario.

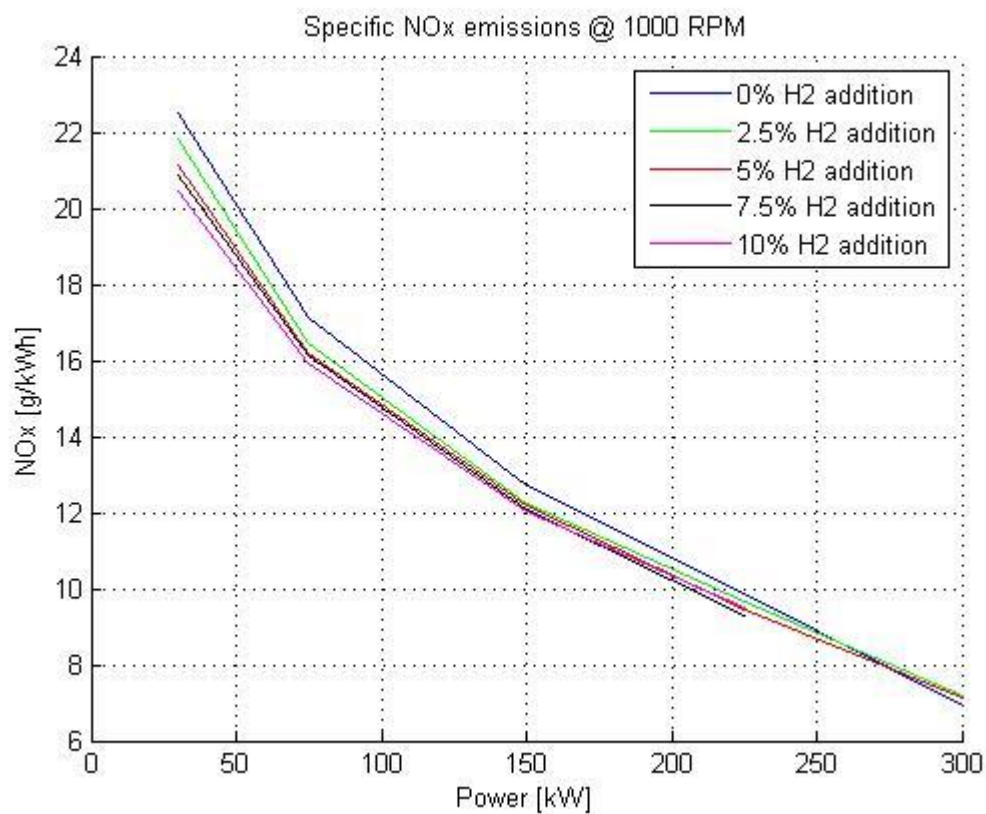


Figure 6.14: Specific NO_x emissions at 1000 RPM

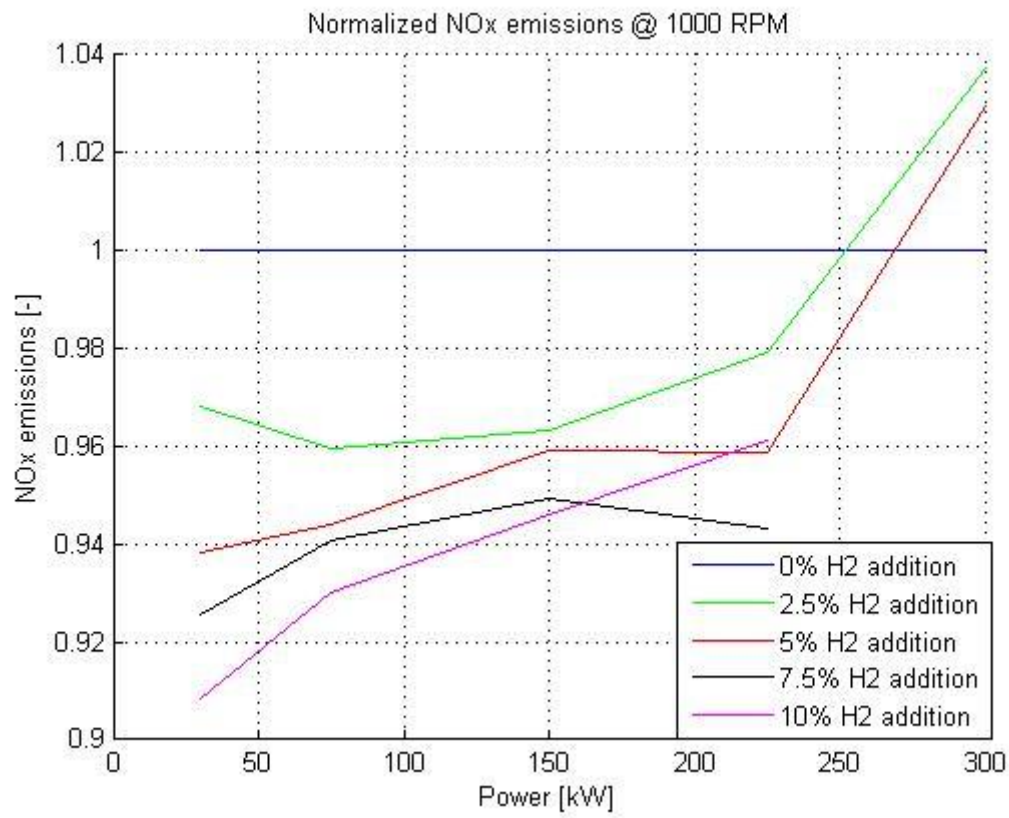


Figure 6.15: Normalized specific NO_x emissions at 1000 RPM

6.5 Cylinder pressure

The raw pressure data was not mathematically smoothed or fitted in any way in post-processing. Instead the average was taken of the 20-30 cycles recorded per cylinder. These 4 traces (4 cylinders) were checked for irregularities, and then averaged again to get the mean cylinder pressure.

After this procedure, it turns out that there is little difference in pressure trace between the baseline measurement and the various amounts of hydrogen addition. Only when zooming in closely on the area around TDC we can see that in some cases the peak pressure increases slightly (and proportionally) with hydrogen addition percentage. This occurs mostly at higher loads, at low loads the effect is insignificant.

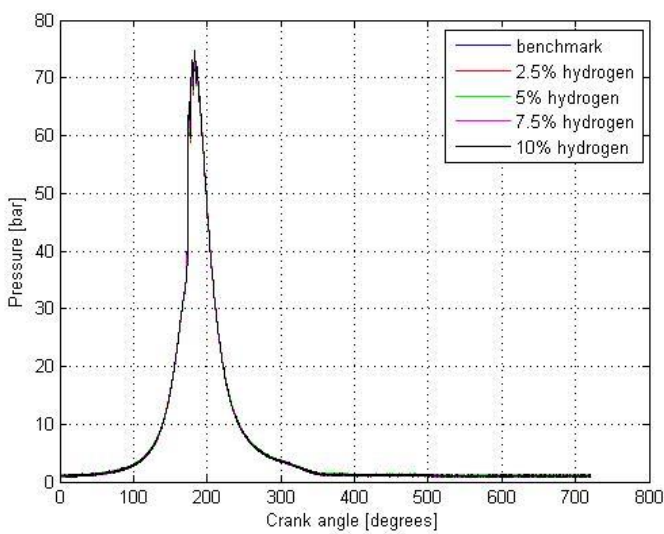


Figure 6.16: Cylinder pressure at 700 RPM, 103 kW

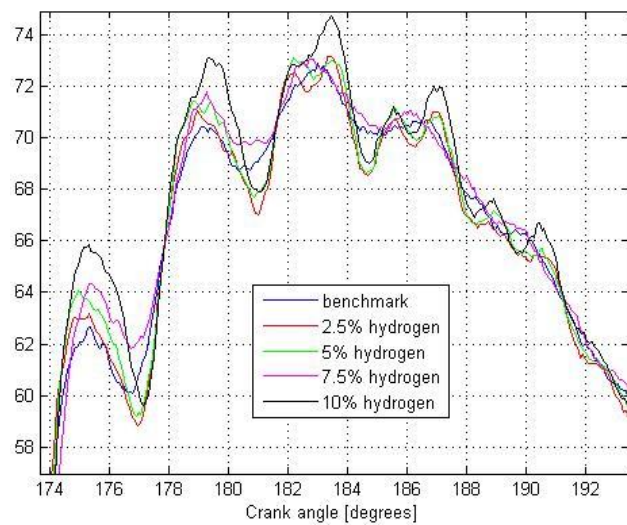


Figure 6.17: Zoom in cylinder pressure around TDC, 700 RPM, 103 kW

For instance, at 700 RPM and 103 kW the increase in peak pressure ranges from 0.1-0.3 bar at the lowest hydrogen addition percentage of 2,5% to approx. 2-3 bar at the highest hydrogen addition percentage of 10%.

If we take a look at a lower load point of 30 kW (figures 12 and 13), we see no difference in peak pressure with hydrogen addition.

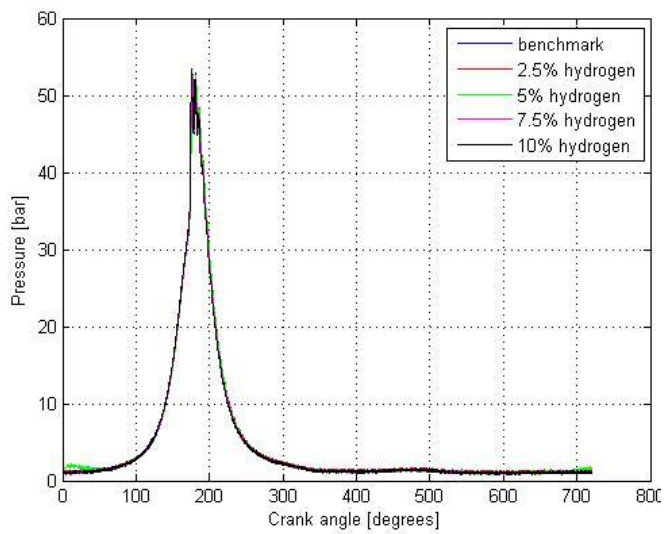


Figure 6.18: Cylinder pressure at 850 RPM, 30 kW

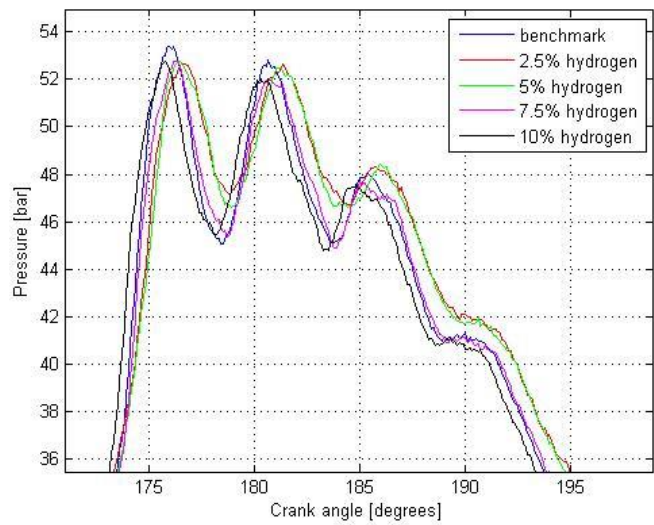


Figure 6.19: Zoom in cylinder pressure around TDC, 850 RPM, 30kW

Finally at the highest load point of 300 kW we see increases in peak pressure of 2-3 bar at 2,5% and 5% hydrogen addition (figure 14 and 15). This is similar to the effect at 7,5% and 10% hydrogen addition at 103 kW, indicating that both increasing load and higher hydrogen addition percentage have an effect on the peak pressure increase. Unfortunately the 7,5 and 10% addition at 300 kW are missing as mentioned before, but all the data so far suggests that peak pressure increase would be even higher here.

Figure 6.20: Cylinder pressure at 1000 RPM, 300 kW

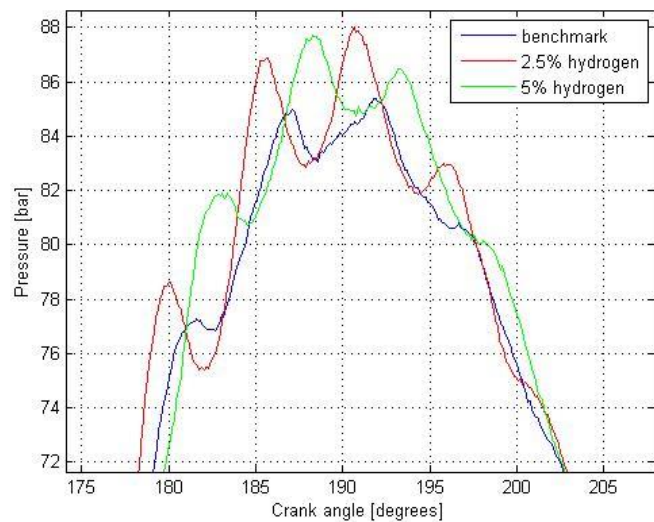
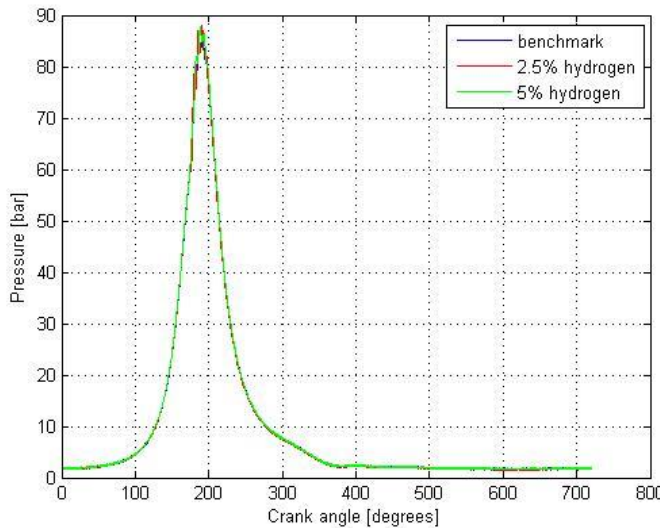


Figure 6.21: Zoom in cylinder pressure around TDC, 1000 RPM, 300kW

This result is consistent with previous results, as other researchers ([Sandalci, 2014] and [Zhou, 2014]) have also found that adding hydrogen increased peak pressure. The effect is however fairly small, a 3-5% increase in peak pressure that can only be seen at high load. At lower loads, no effect is found at all.

Chapter 7: Cylinder pressure analysis results

7.1 Introduction

This chapter will display the results of the cylinder pressure analysis. It covers the following subjects:

- Heat release rate (paragraph 7.2);
- Vibe parameters (paragraph 7.3);
- Seiliger parameters (paragraph 7.4).

7.2 Heat release rate

As explained in chapter 3.1, the heat release rate (HRR) and its integral the reaction coordinate (RCO) are calculated by the Heat Release Calculation Model [Ding, 2011] using the measured pressure. In figures 7.1 and 7.2 below examples are given of the results of these calculations.

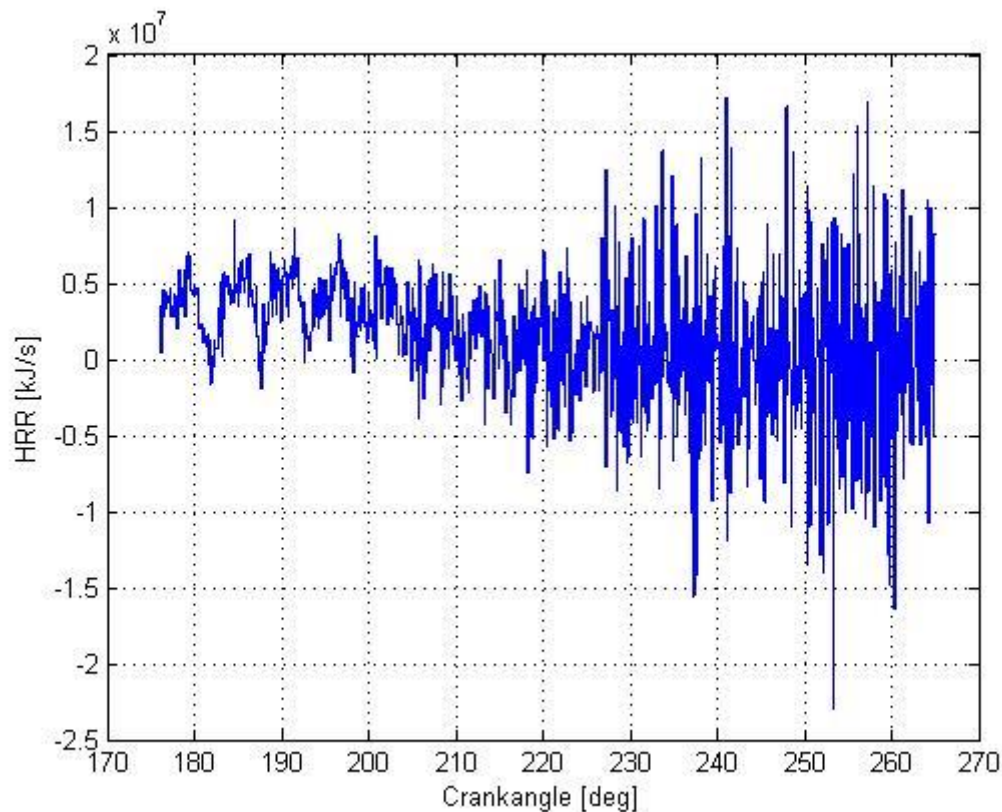


Figure 7.1: raw HRR as calculated by HRR model (1000 rpm, 300 kW) [Ding, 2011]

As mentioned before, due to the noisy nature of the input pressure signal the HRR is also very messy. If the signal is integrated however, the result is quite nice (figure 7.2). The RCO is normalized, so that it represents the progression of the combustion.

Theoretically the normalized reaction coordinate should reach unity for complete combustion. This is however not a fixed value that can be easily calculated, but rather the result of a complex calculation. One of the most difficult parts is estimating the heat loss to the cylinder head, walls and

piston crown correctly. As mentioned before this is done using an empirical Woschni model, resulting in uncertainty when calculating the RCO. Underestimating over overestimating heat loss results in the final RCO under- or overshooting unity. This is an effect reported by multiple other researchers as well ([He, 1990], [Hua, 1984], and [Lapuerta, 2000]).

From this graph the initial estimates of SOC can be adjusted as well (figure 39). Here we can also see the RCO overshoot unity, indicating more fuel is burned. This indicates that most likely the heat release to the wall was underestimated, and this will iteratively be adjusted by changing the constant in the Woschni model.

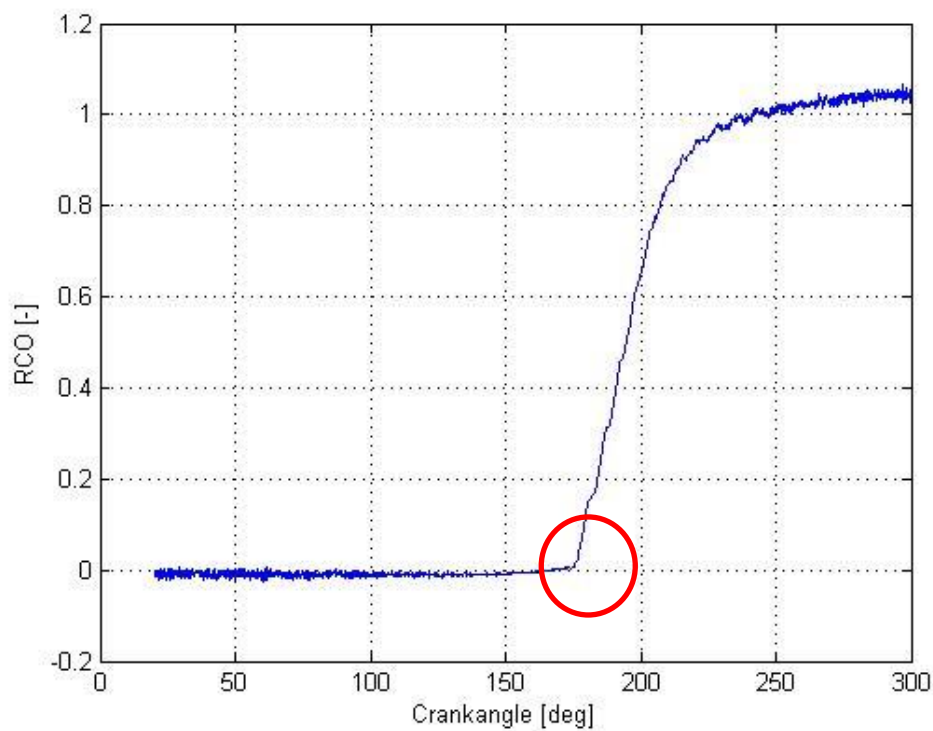


Figure 7.2: RCO, result of integrating the HRR (1000 rpm, 300kW)

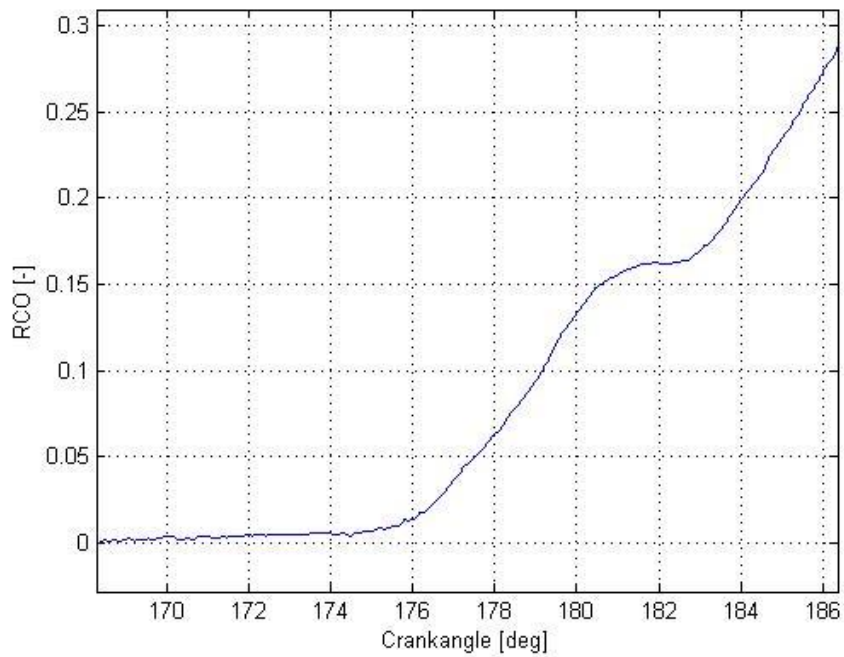


Figure 7.3: Zoom-in of RCO around SOC (1000 rpm, 300 kW)

After correcting any errors the final RCO (from SOC to EOC) is ready to be fitted. This is done with both single, double and triple Vibe functions as explained in chapter 3.2.

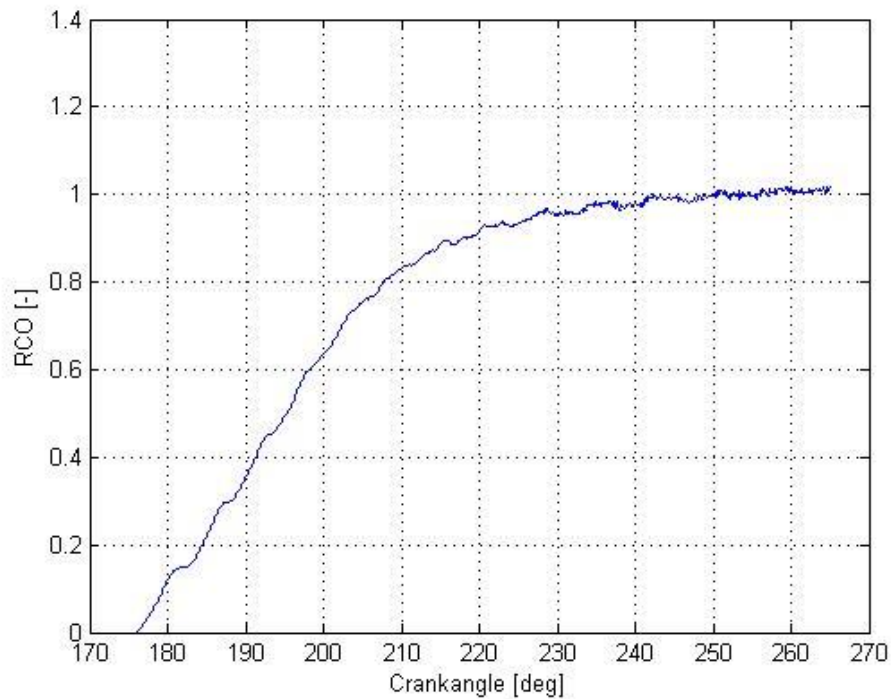


Figure 7.4: RCO graph from SOC (176 degrees CA) to EOC (265 degrees CA) (1000 rpm, 300 kW)

In the figure below the RCO has been fitted using single, double and triple Vibe functions. The y-axis still has the dimensionless RCO, representing combustion progress. The x-axis represents the combustion duration from SOC to EOC. This duration has also been normalized since the Vibe fit requires values between 0 and 1. The actual duration is the same as the figures above, SOC at 176 and EOC at 265 degrees CA since it is the same operation point (1000 rpm, 300 kW).

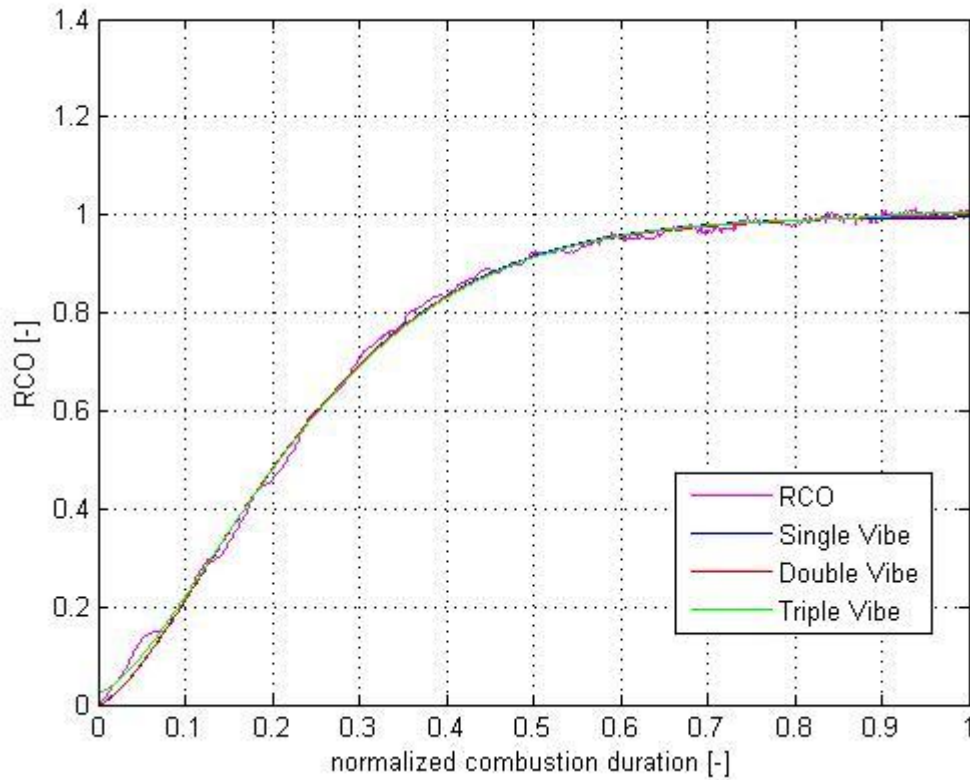


Figure 7.5: RCO fitted with single, double and triple Vibe (1000 rpm, 300 kW)

Now that the Vibe fits are complete, the Vibe parameters are known. Using these, the HRR can be constructed using equation 3.11 from chapter 3.2:

$$Z = b \cdot (a \cdot (m + 1) \cdot \tau^m \cdot e^{-a \cdot \tau^{m+1}}) \quad (3.18)$$

τ in this formula is the normalized combustion duration mentioned above, and a , b and m are the shape parameters.

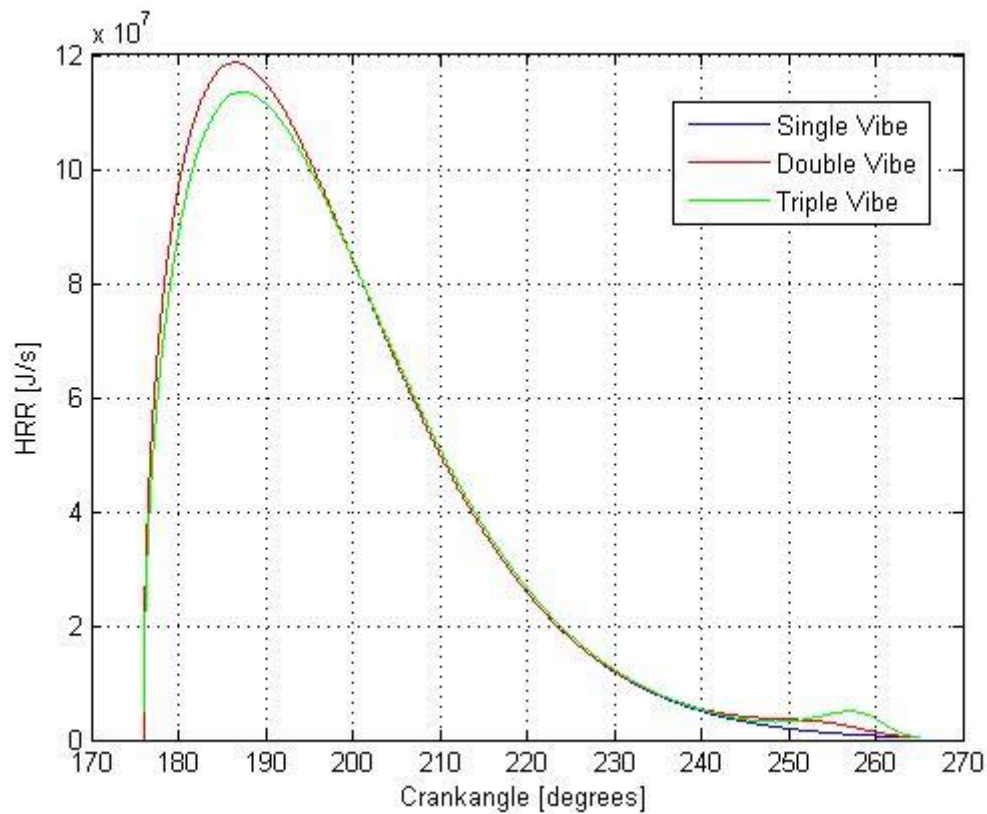


Figure 7.6: HRR calculated using single, double and triple Vibe (1000 rpm, 300 kW)

This process is executed for each operating point, and for each step of hydrogen addition per operating point. The best fit at each point is selected using a number of *goodness of fit* criteria, namely R-squared, SSE (sum of squares due to error) and RMSE (root mean squared error). This is not necessarily the triple Vibe fit, as sometimes a single or double Vibe fit produces the same results without the extra parameters.

Showing all the results here is pointless, but a selection will be made to show the results throughout the entire operational envelope of the engine, and to compare benchmark and hydrogen operation.

7.2.1 Benchmark Vibe fits (no hydrogen addition)

What is immediately evident is that at this low load point of 700 rpm, 30 kW the HRR does not start at zero but has a high initial value. This is due to the parameter m assuming a negative value. This problem was also encountered by Ding in his thesis, and although physically this phenomenon is not realistic (infinite reaction rate at the start of combustion is impossible), Ding argued that the quality of fit was significantly worse if the parameter m was forced to have a positive value. This was confirmed in this research, so similarly to Ding a negative value for m will be allowed.

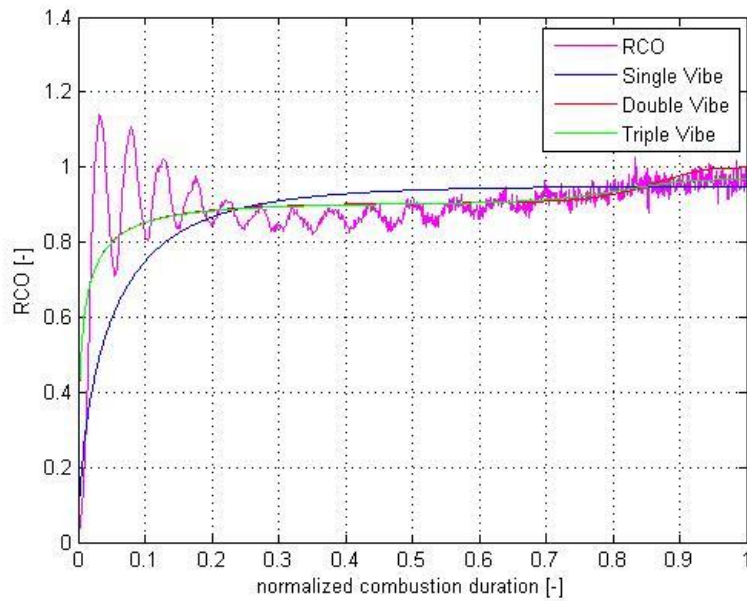


Figure 7.7: RCO at 700 rpm, 30 kW

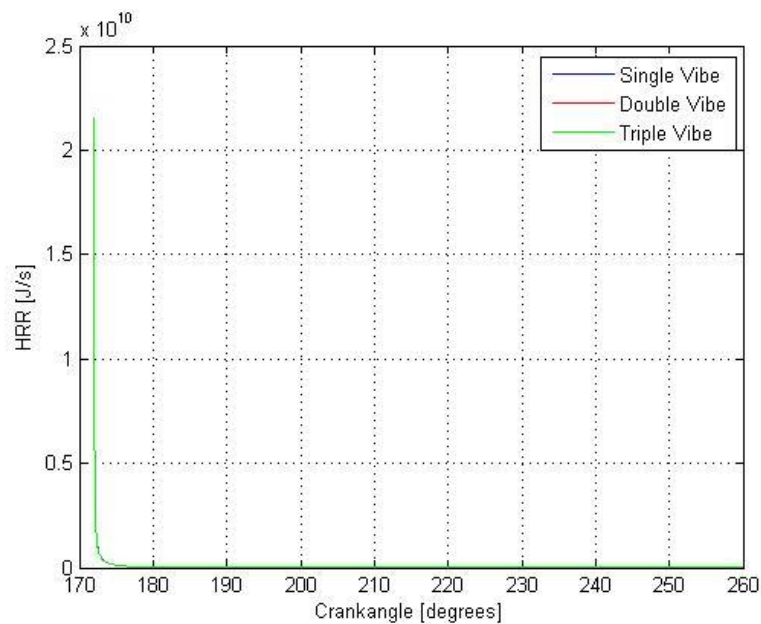


Figure 7.8: HRR at 700 rpm, 30 kW

At this load point there is basically no difference between the single, double and triple Vibe functions. The engine is basically idling, and very little fuel is being burned. To see some results, the engine must be loaded some more.

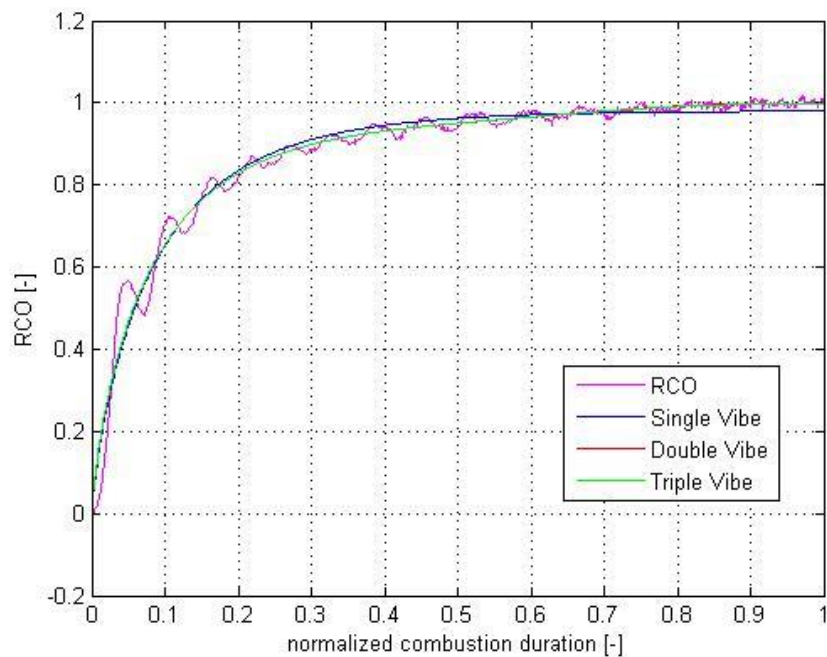


Figure 7.9: RCO at 700 rpm, 103 kW

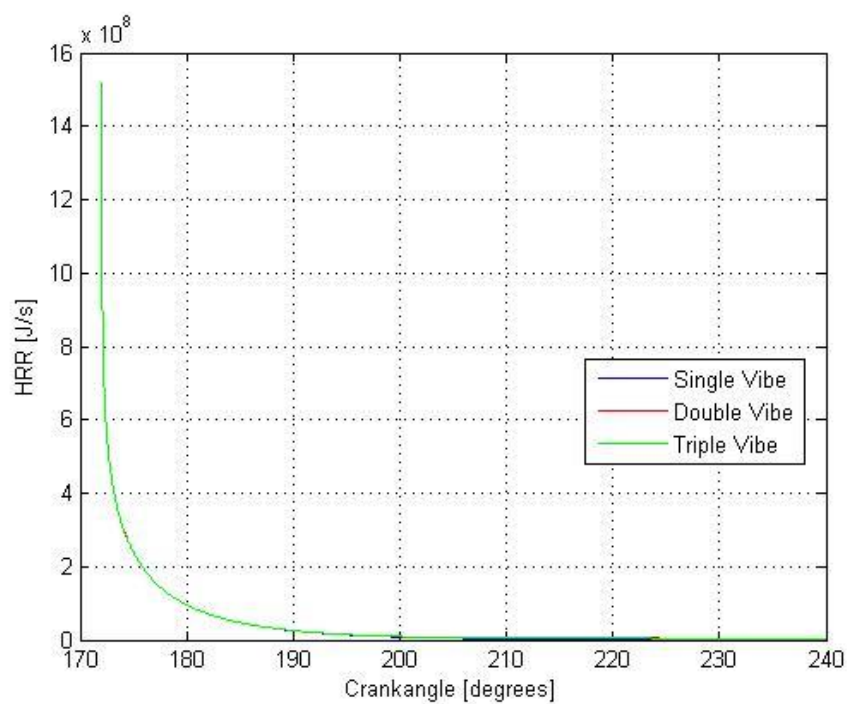


Figure 7.10: HRR at 700 rpm, 103 kW

At this low load point of 700 rpm, 103 kW the HRR is similar to the previous point of 700 rpm, 30 kW but has some more “flesh” to it. More fuel is being burned so differences become clearer. There is some small effect from the additional Vibe functions, resulting in a slightly better fit and some late combustion around 205 to 225 degrees crank angle.

	Single Vibe	Double Vibe	Triple Vibe
R-square	.9716	.9756	.9756
SSE	6.4009	5.4966	5.4954
RMSE	.0307	.0284	.0284

From the goodness of fit results it is clear that a third Vibe adds almost no accuracy, so a double Vibe seems optimal. This fit incorporates a small fraction of late combustion. The fit overall is also quite good, with R-square at .9756.

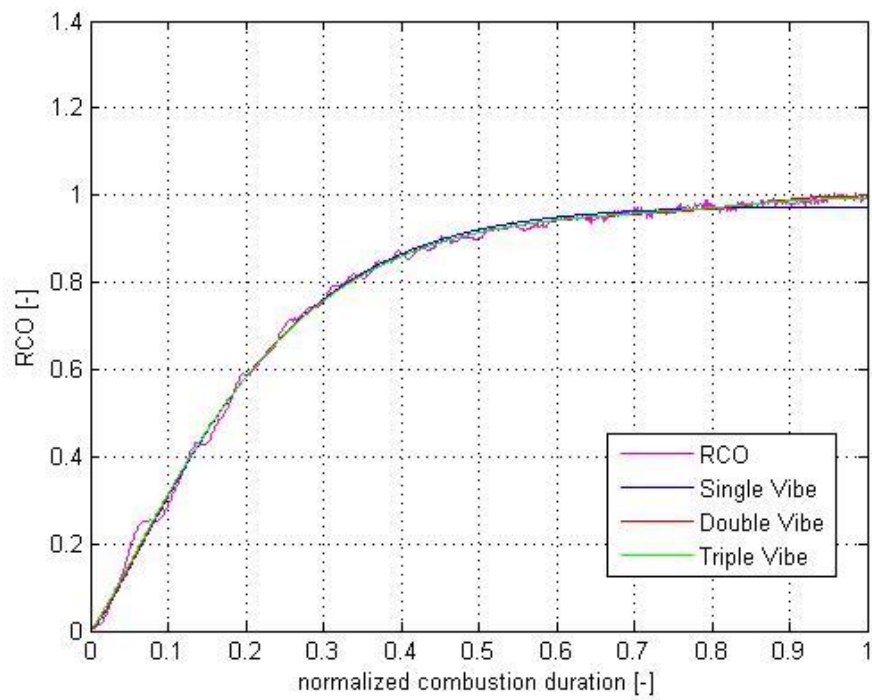


Figure 7.11: RCO at 1000 rpm, 225 kW

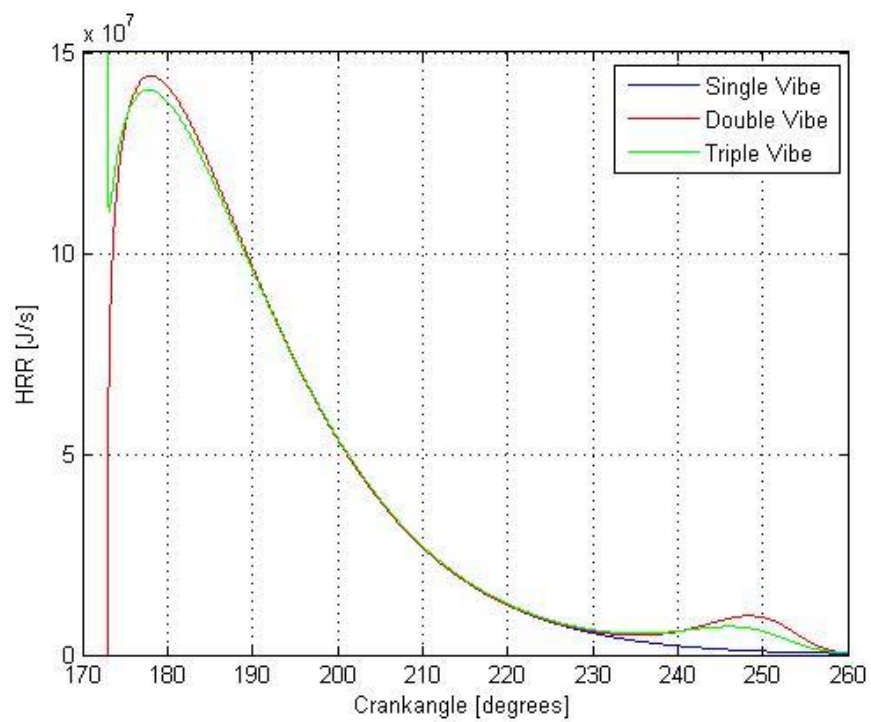


Figure 7.12: HRR at 1000 rpm, 225 kW

This medium load point has some more pronounced late combustion in the double and triple Vibe functions, but the triple Vibe also adds a little bit of early combustion in the form of a negative m parameter. This seems unlikely for this operating point, and since the goodness of fit of the double and triple are fairly similar, the double Vibe function will be selected as the best fit.

	Single Vibe	Double Vibe	Triple Vibe
R-square	.9973	.9980	.9982
SSE	1.6726	1.2091	1.1318
RMSE	.0139	.0118	.0114

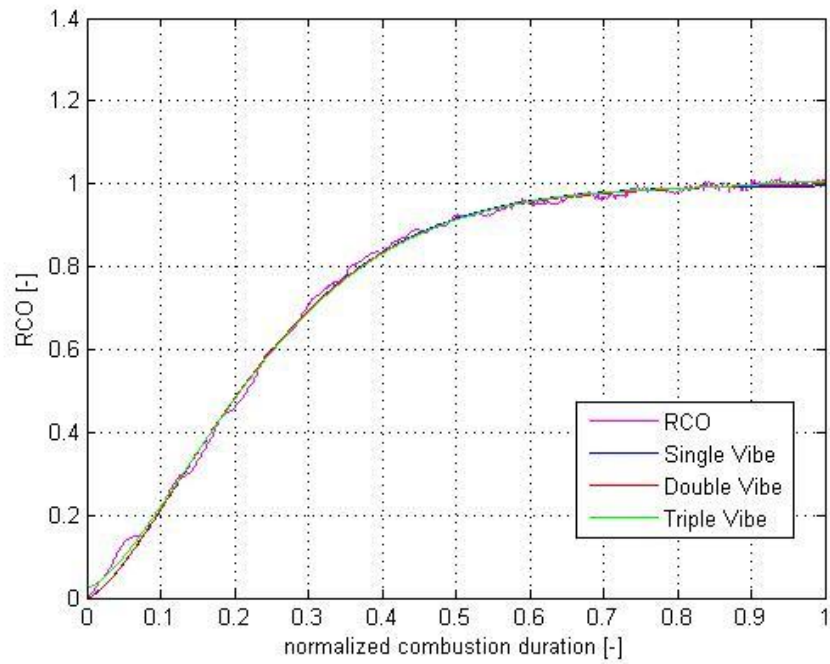


Figure 7.13: RCO at 1000 rpm, 300 kW

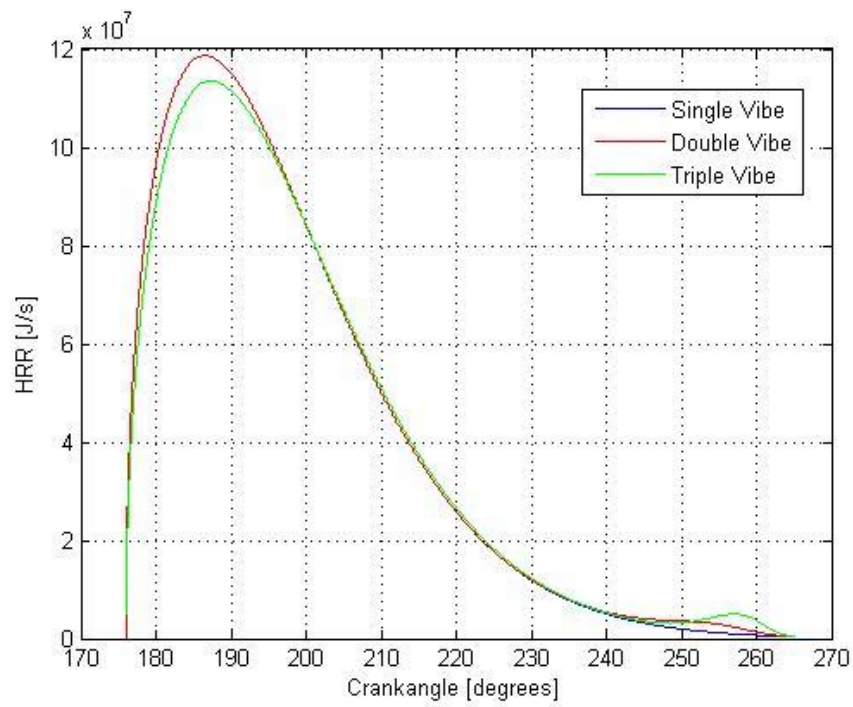


Figure 7.14: HRR at 1000 rpm, 300 kW

At this highest (and nominal) load point of 1000 rpm, 300 kW all 3 of the Vibe fits are fairly close together. Single and double Vibe have a similar initial behaviour but double Vibe adds a little bit of late combustion. Additionally the triple Vibe reduces the early combustion for some extra late combustion.

In terms of goodness of fit all 3 are fairly close together, so picking the best fit is difficult. Physically all 3 fits are quite possible, but mathematically the triple Vibe fit is slightly better. Therefore this fit is chosen.

	Single Vibe	Double Vibe	Triple Vibe
R-square	.9982	.9983	.9987
SSE	1.6726	1.2091	1.1318
RMSE	.0139	.0118	.0114

7.2.2 Hydrogen addition Vibe fits

The same engine operating points as above will be discussed, but here the differences in HRR due to hydrogen addition will be discussed. The operating points with hydrogen have also been fitted using both single, double and triple Vibe and the best fit has been selected for each point. These fits will now be compared to each other.

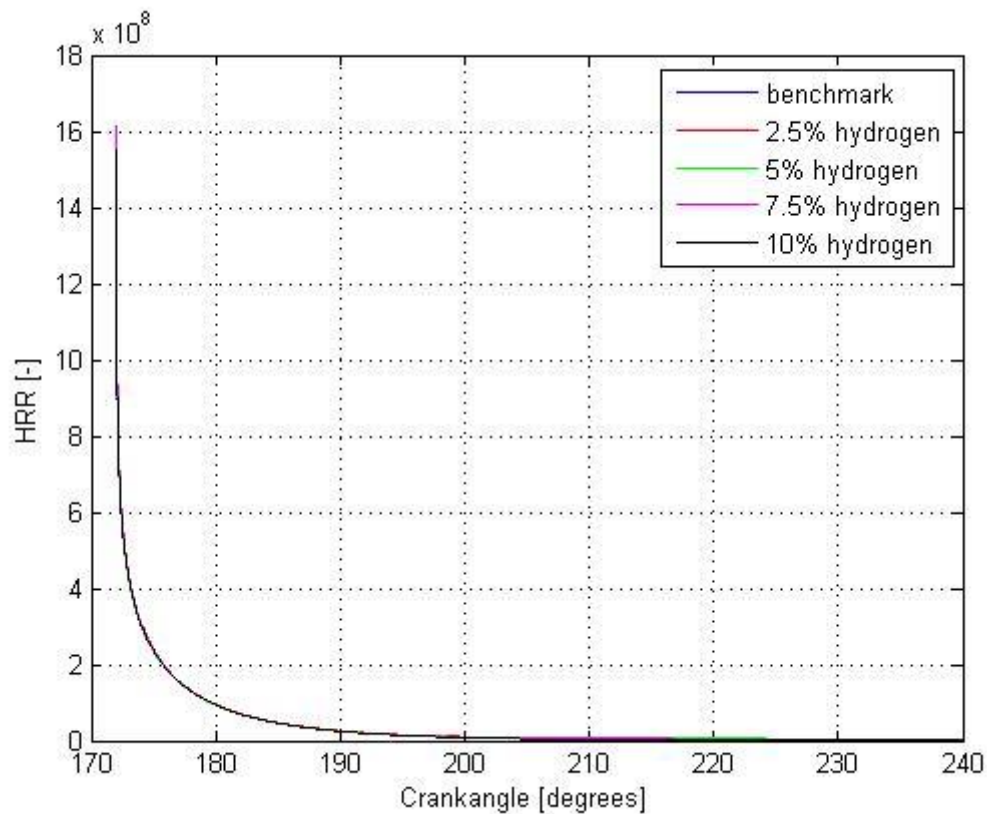


Figure 7.15: HRR at 700 rpm, 103 kW with hydrogen addition

The HRR's at this operating point are all as good as identical. There is no difference between benchmark and the various percentages of hydrogen addition.

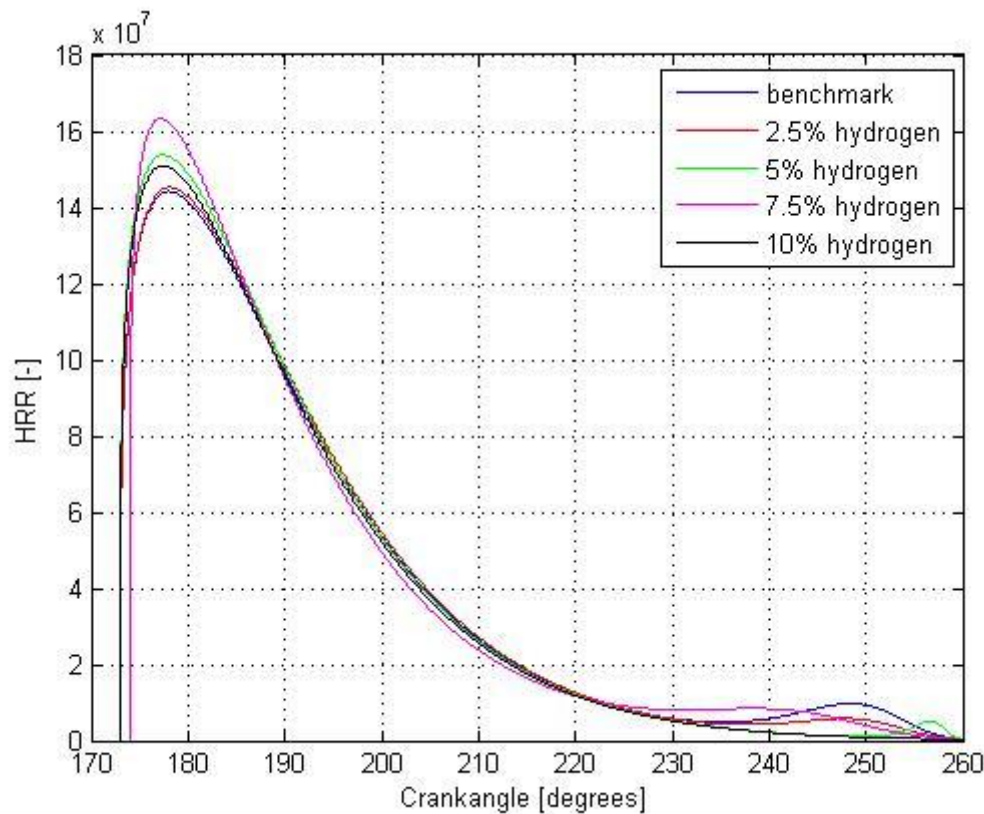


Figure 7.16: HRR at 1000 rpm, 225 kW with hydrogen addition

At this operating point it is clear that the addition of hydrogen has a distinct effect on the HRR. Pre-mixed combustion is increased with hydrogen addition, fairly substantial in some cases with large hydrogen addition percentages (7,5% for example). This seems plausible, since the hydrogen is in the charge air it is well mixed and available for combustion immediately. As soon as a small pilot of diesel ignites and the required temperature is reached this hydrogen-air mixture can ignite.

Additionally the late combustion component that is present in the benchmark HRR is reduced. This could be either because there is simply less diesel to be burned because it is replaced by hydrogen, or because hydrogen has increased the combustion speed.

In a single case the timing of the combustion is also different. The 7,5% hydrogen addition curve has the combustion retarded by 1 crank angle degree. This is contrary to what other researchers ([Zhou, 2014], [Sandalc, 2014]) have found, where adding hydrogen has advanced the start of combustion. This is only a single point where this happened and at 10% hydrogen addition the effect is not present, so this might just be an error in the fit or a fluke occurrence.

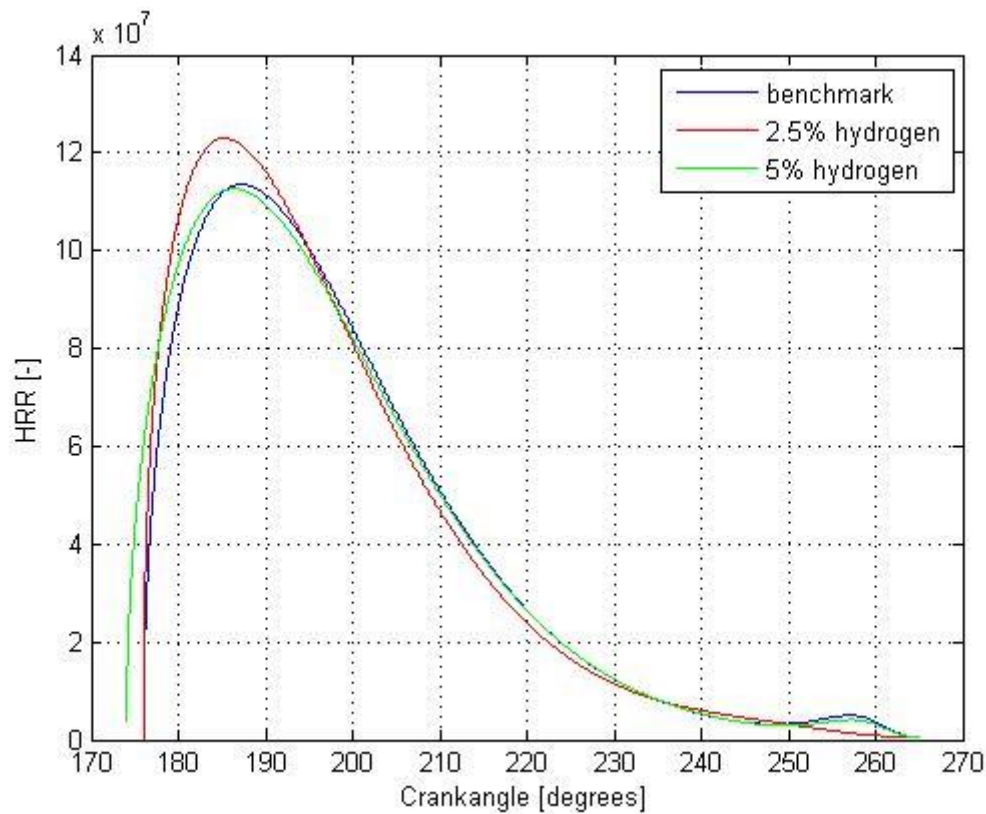


Figure 7.17: HRR at 1000 rpm, 300 kW with hydrogen addition

At this highest and nominal operating point, we see similar effects to the previous operation point of 1000 rpm, 225 kW. Pre-mixed combustion is increased with hydrogen addition of 2,5% and late combustion somewhat reduced.

More interestingly however, the SOC is advanced by two degrees crank angle for the 5% hydrogen addition fit. This is the type of effect that some other researchers have also found. The only point where this research was able to reproduce this result is at nominal load of 300 kW. It is unfortunate that the 7,5% and 10% hydrogen addition tests were not performed at this point , since it would have been very interesting to see if the start of combustion would advance even more, but practical considerations prevented these points from being measured.

All results regarding the Vibe fits of all measured points can be found in Appendix C.

7.3 Seiliger fit

In addition to the Vibe parameters, the combustion process can also be described using the Seiliger cycle and parameters. These parameters are found by fitting a Seiliger cycle to an actual measured engine cycle (or a modelled engine cycle based on Vibe parameters, to compare these 2 methods).

The Seiliger fit method that is used in this thesis is based on the procedure outlined in [Ding, 2010], paragraph 3.3. This was done since the same engine is used in both researches and the results Ding achieves in his thesis are excellent with this method.

In order to fit the Seiliger process to the real diesel engine cycle, equivalence criteria must be selected first on which the fit is based. These equivalence criteria relate the Seiliger process to the measured engine parameters that are deemed important. Therefore they should be selected in such a way that they describe the engine performance as completely as possible.

Additional focus is put on the parameters which are likely influenced by hydrogen addition (as indicated in table 2.2 in Chapter 2), so that any effects of the hydrogen addition will also be visible in the Seiliger fit.

The following criteria are selected:

- Q_{in}
- W_i
- P_{max}
- T_{EO}
- T_{max}

Q_{in} , W_i : Work and heat input are the main indicators of an engines output, and their ratio describes the efficiency of the engine. This is one of the most important parameters when looking at engine performance, and therefore these 2 are included as equivalence criteria.

P_{max} : the maximum pressure represents the mechanical load an engine is put under. It is very important when dimensioning the engine and its parts (mainly the crankshaft, connecting rod and cylinder heads) for safe operation. It is also one of the parameters which is suspected to react the most to hydrogen addition, and therefore of extra interest.

T_{EO} : The temperature at exhaust opens is very important, since it is the last point of the in-cylinder process and therefore defines the starting conditions for the gas entering the turbine of the turbocharging system. Pressure at EO could also be selected as criterion, but since they are related by the gas law and the mass is constant, only one of the two is used.

Maximum temperature (T_{max}) is also mentioned here. It represents the thermal load of the engine, and therefore could be considered as an equivalence criteria. However, the maximum temperature only occurs for a very short time, and has more effect on for instance emissions (NOx). We also already have a criterium that monitors the load on the engine, P_{max} .

On the other hand this parameter is expected to react to hydrogen addition, and is therefore quite interesting. In total only 4 equivalence criteria are required, but given the situation the fits will be performed using both T_{EO} and T_{max} , and results will be compared.

These 5 equivalence criteria will be used to obtain the Seiliger parameters α , b , c and n_{exp} .

7.3.1 Seiliger fit results

In the figures below, the results of the Seiliger fit are plotted. The red lines indicate the Seiliger cycle, fitted over the measured (blue) cycle. The Vibe (green) cycle is also plotted as a reference.

7.3.1.1 Operating point 700 RPM, 103 kW

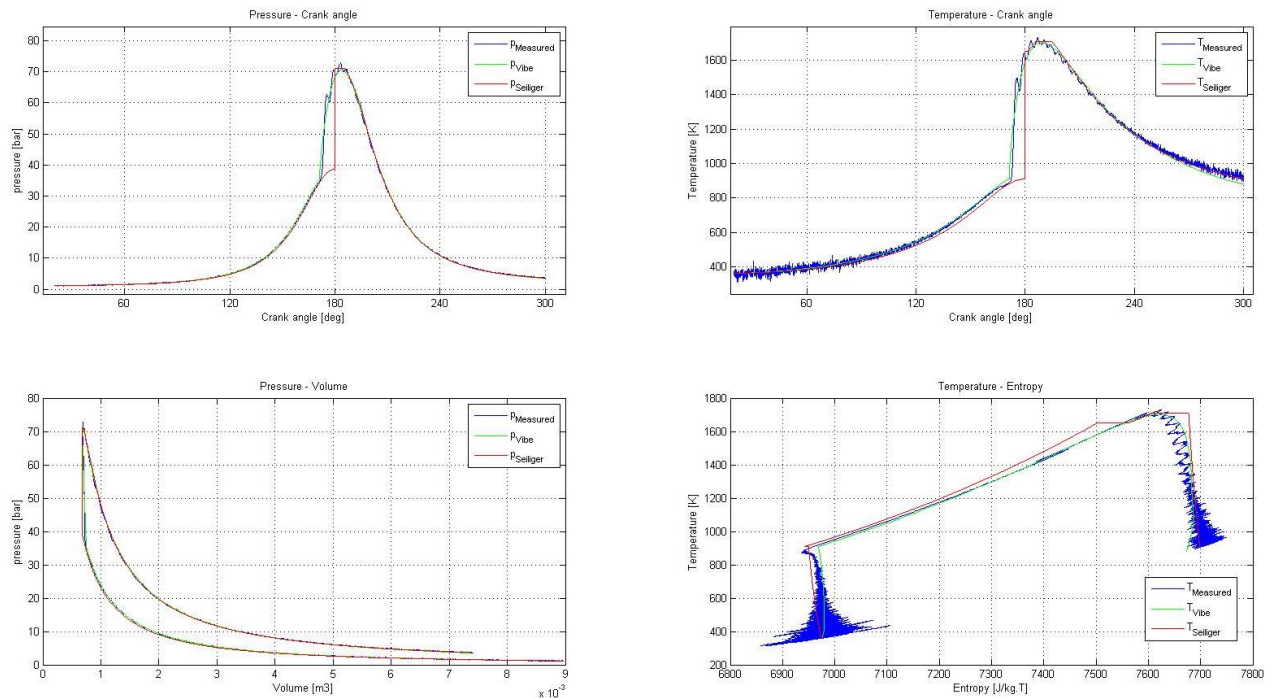


Figure 7.18: Seiliger fit at 700 RPM, 103 kW, benchmark (0% H₂)

Overall the fit of the Seiliger cycle to the measured engine cycle is fairly good, although the temperature during compression is slightly low. The pressure fit is good, but it is visible that the Seiliger cycle assumes combustion at 180 degrees crank angle, whereas SOI and SOC in the actual engine cycle are slightly before 180 degrees crank angle. This is consistent with results shown in [Ding, 2010].

In terms of equivalence criteria the fit results are shown in table 7-1 and 7-2 below. Both the fit using T_{max} and the fit using T_{EO} as equivalence criteria show very good results at this operating point. The fit using maximum temperature performs slightly better, since it estimates temperature at exhaust opens accurate as well.

Table 7-1: Result of Seiliger fit at 700 RPM, 103 kW using T_{max} as equivalence criteria

Equivalence Criteria	Relative error (%)	Absolute error
Q_{in}	$8.13 \cdot 10^{-5}$	0.6867 J
W_i	$3.00 \cdot 10^{-4}$	1.3681 J
P_{max}	0	0 Pa
T_{EO}	0.0045	-5.6085 K
T_{max}	0.0018	0.3234 K

Table 7-2: Result of seiliger fit at 700 RPM, 103 kW using T_{EO} as equivalence criteria

Equivalence Criteria	Relative error (%)	Absolute error
Q_{in}	$4.80 \cdot 10^{-4}$	-4.0522 J
W_i	$4.82 \cdot 10^{-4}$	-2.1991 J
P_{max}	0	0 Pa
T_{EO}	$4.82 \cdot 10^{-5}$	-0.1608 K
T_{max}	0.0306	-52.4406 K

The results in terms of Seiliger parameters are as follows:

Tabel 7.1: Seiliger parameters at 700 RPM, 103 kW

	Benchmark	2.5% H_2	5% H_2	7,5% H_2	10% H_2
Seiliger param.					
a	1.8409	1.8704	1.8693	1.8643	1.8555
b	1.0366	1.0371	1.0362	1.0359	1.0357
c	1.2005	1.1284	1.1826	1.2217	1.2085
n_{exp}	1.2906	1.2814	1.2949	1.3063	1.3039

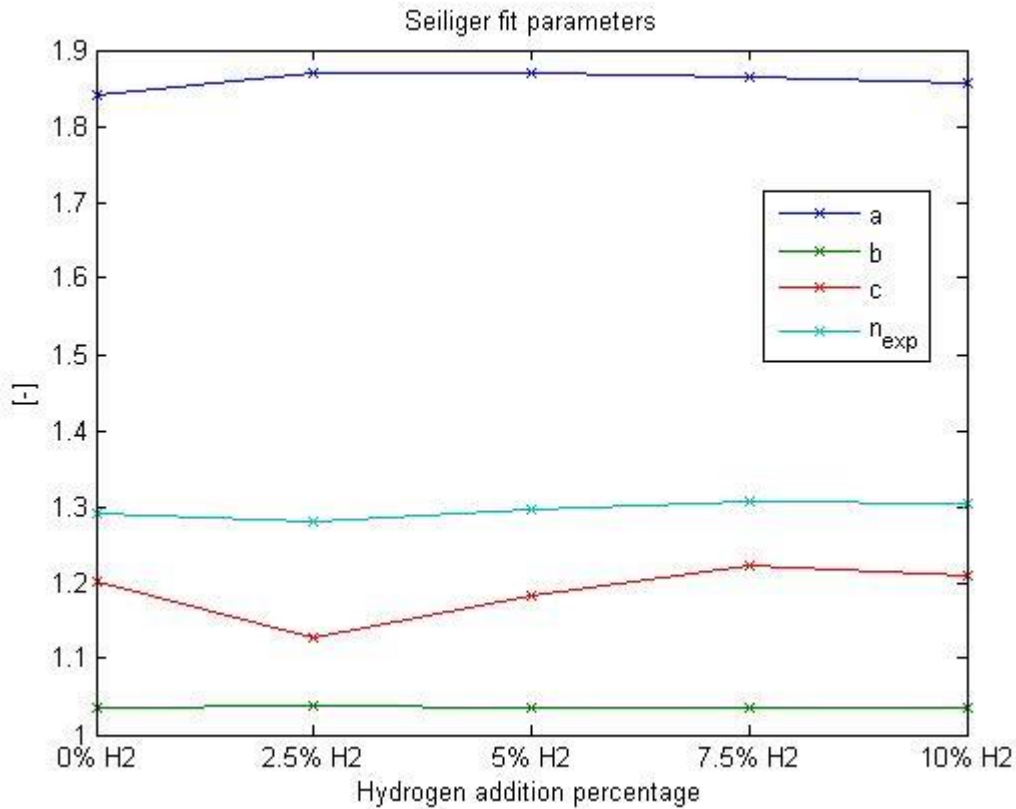


Figure 7.19: Seiliger fit parameters 700 RPM, 103 kW

The fit parameters vary very little, and this was to be expected. As we have seen with the Vibe fits the effect of hydrogen addition at low loads is very small, often not even visible. We can conclude here that at low load, most of the combustion occurs early during the a phase (as expected). Hydrogen addition seems to increase the a parameter slightly, but not proportionally with hydrogen addition percentage.

Due to the low load and therefore small amounts of energy combusted, there is almost no late combustion in the form of b and c .

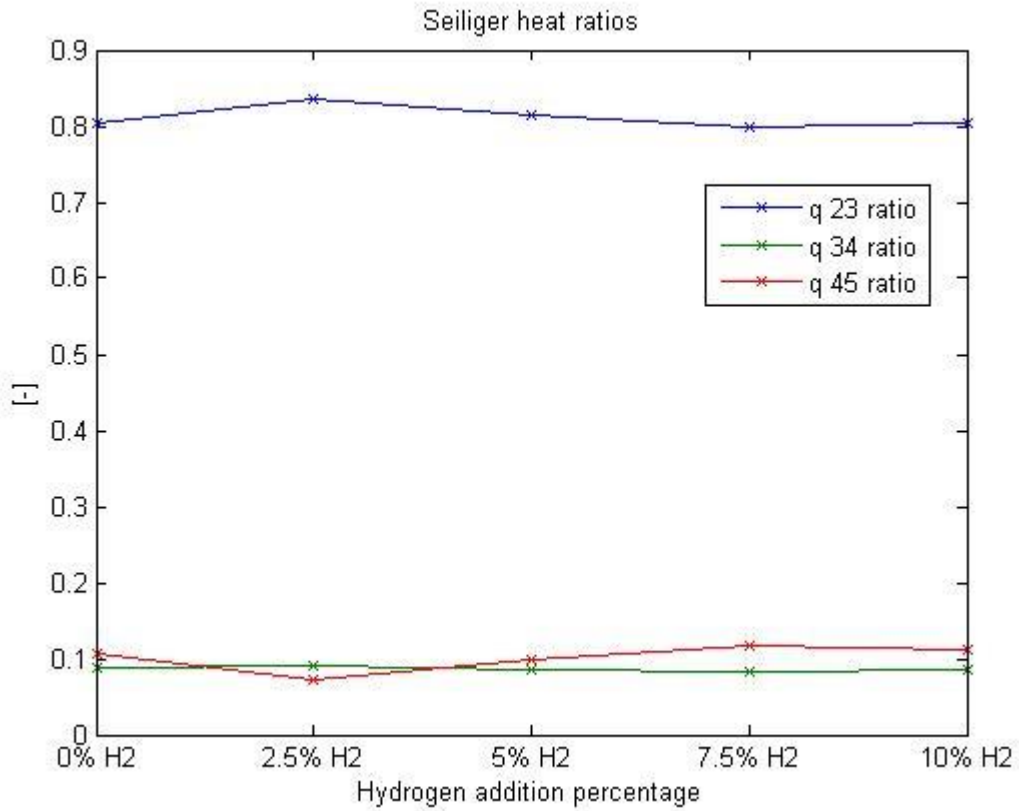


Figure 7.20: Heat ratios at 700 RPM, 103 kW

In addition to the a , b , c and n_{exp} parameters we can also review how much of the total heat of the fuel is combusted in what specific part of the process. The numbering refers to the points of the Seiliger process. We can see that at this low operating point, the ratios remain constant with hydrogen addition, and that most of the energy is released in the early phases of combustion (stage 2-3).

7.3.1.2 Operating point 850 RPM, 150 kW

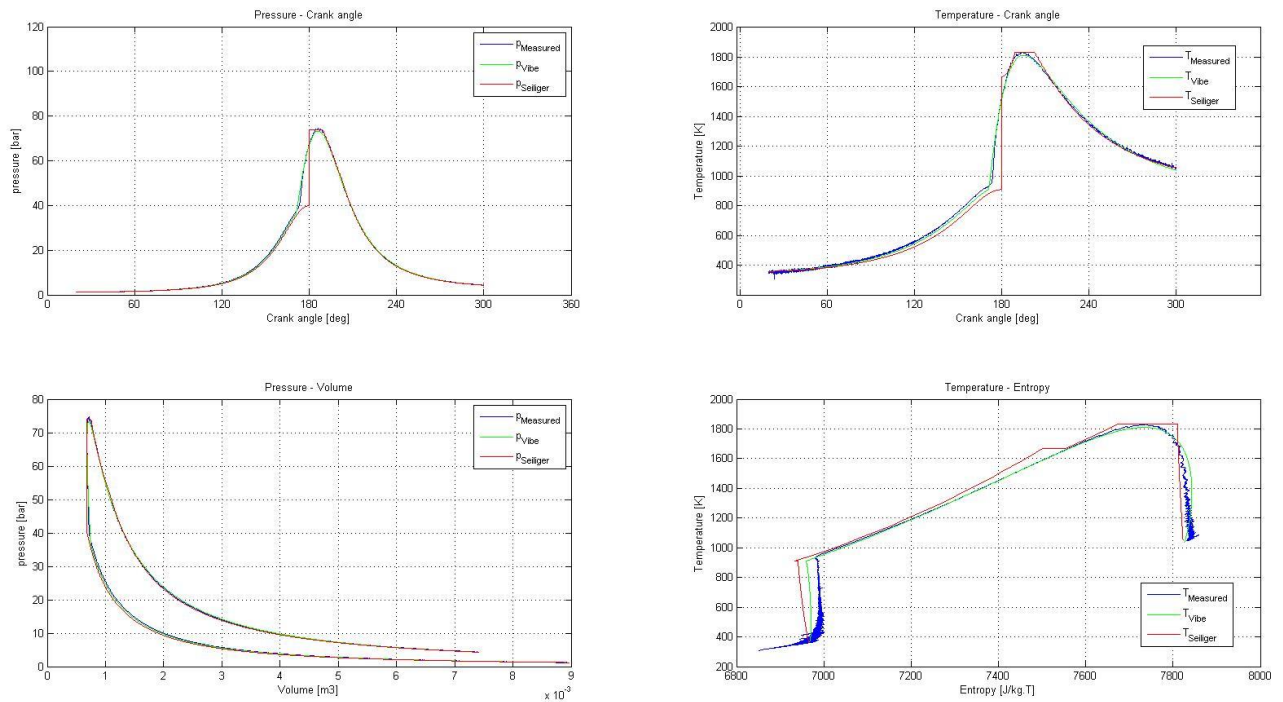


Figure 7.21: Seiliger fit at 850 RPM, 150 kW

The fit shows similar characteristics as the previous figure, where the temperature during compression is lower than the actual data, and the combustion occurs at exactly at 180 degrees crankangle. The temperature – entropy graph (bottom right) has some differences between Seiliger and measured values during compression, but overall the angle of this initial part of the graph is still as expected (slightly angled to the left). Overall the fit is quite good.

In terms of equivalence criteria the fit results are shown in table 7-3 and 7-4 below. Again the fit using T_{max} is slightly better, since it estimates both the maximum temperature and temperature at exhaust opens fairly accurately.

Table 7-3: Result of Seiliger fit at 850 RPM, 150 KW using T_{max} as equivalence criteria

Equivalence Criteria	Relative error (%)	Absolute error
Q_{in}	$1.13 \cdot 10^{-4}$	1.2687 J
W_i	$3.04 \cdot 10^{-4}$	-1.7994 J
P_{max}	0	0 Pa
T_{EO}	0.0029	-3.1007 K
T_{max}	$4.87 \cdot 10^{-4}$	0.8888 K

Table 7-4: Result of Seiliger fit at 850 RPM, 150 K using T_{EO} as equivalence criteria

Equivalence Criteria	Relative error (%)	Absolute error
Q_{in}	$7.50 \cdot 10^{-4}$	-8.4124 J
W_i	$7.34 \cdot 10^{-4}$	-4.3461 J
P_{max}	0	0 Pa
T_{EO}	$3.0 \cdot 10^{-4}$	-0.3183 K
T_{max}	0.014	-25.6915 K

The results in terms of Seiliger parameters are as follows:

Table 7-5: Seiliger parameters at 850 RPM, 150 kW

	Benchmark	2.5% H_2	5% H_2	7,5% H_2	10% H_2
Seiliger param.					
a	1.8553	1.8400	1.8545	-	-
b	1.0990	1.0990	1.1014	-	-
c	1.4335	1.4726	1.4535	-	-
n_{exp}	1.2864	1.2861	1.2876	-	-

Unfortunately the measured data for 7.5% and 10% did not converge to a fit using either option of equivalence criteria. Why this only occurred at these 2 points is not clear, but most likely has to do with a problem during initial data logging.

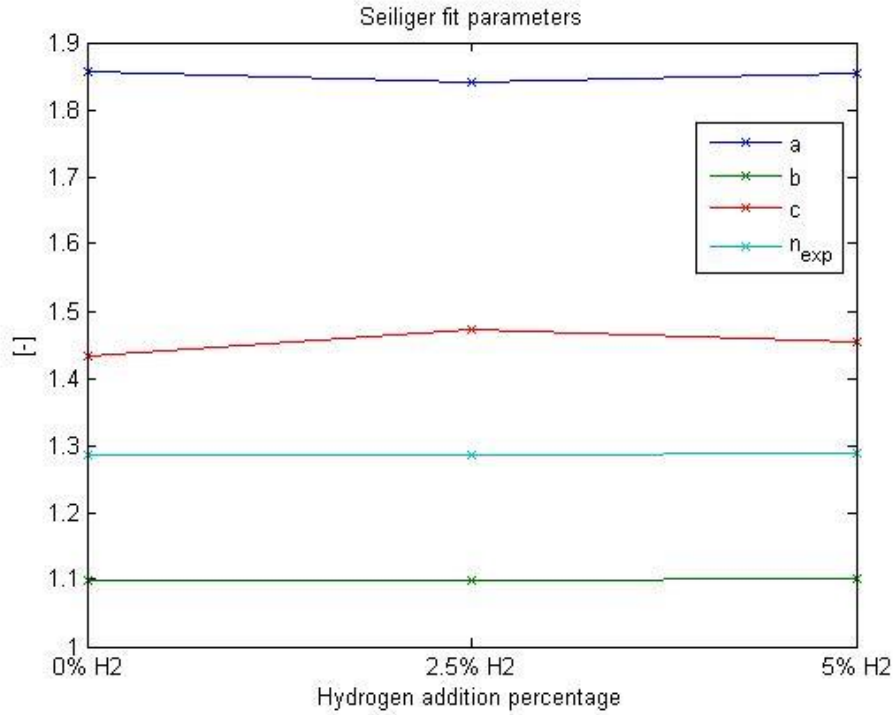


Figure 7.22: Seiliger fit parameters, 850 RPM, 150 kW

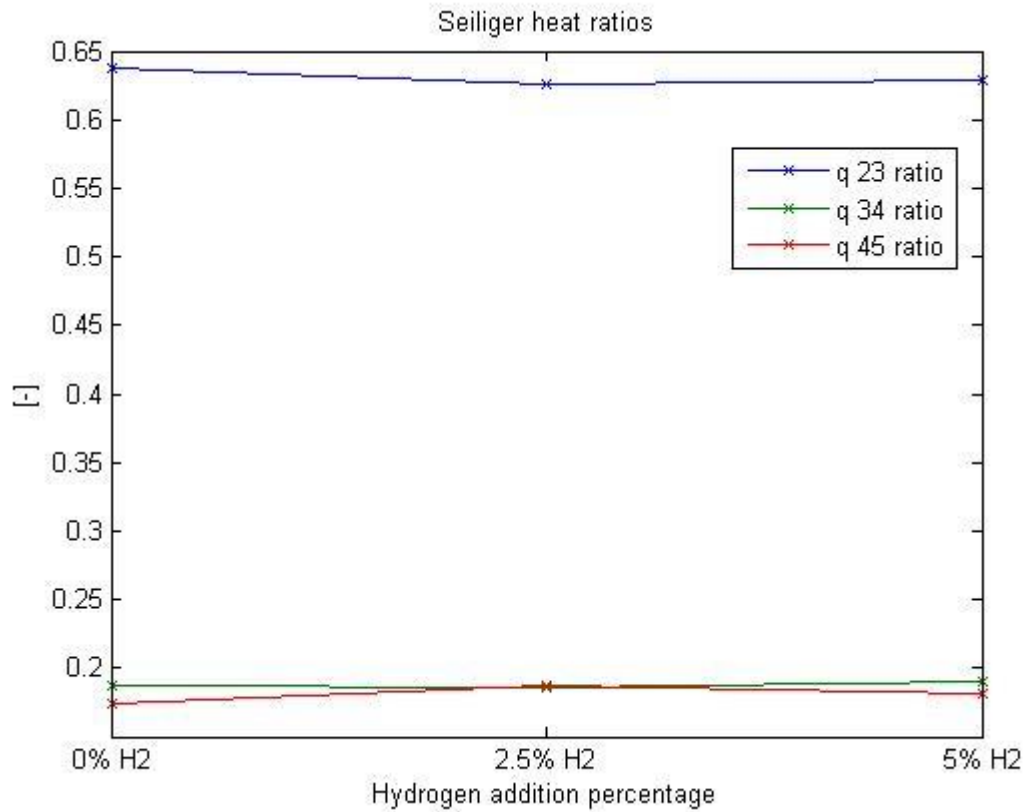


Figure 7.23: Heat ratios at 850 RPM, 150 kW

In terms of heat ratios, we see a similar picture as the previous point at 700 RPM and 103 kW. Stage 2-3 is responsible for the largest part of the delivered fuel heat, with both stages 3-4 and 4-5 equally sharing the rest.

7.3.1.3 Operating Point 1000 RPM, 225 kW

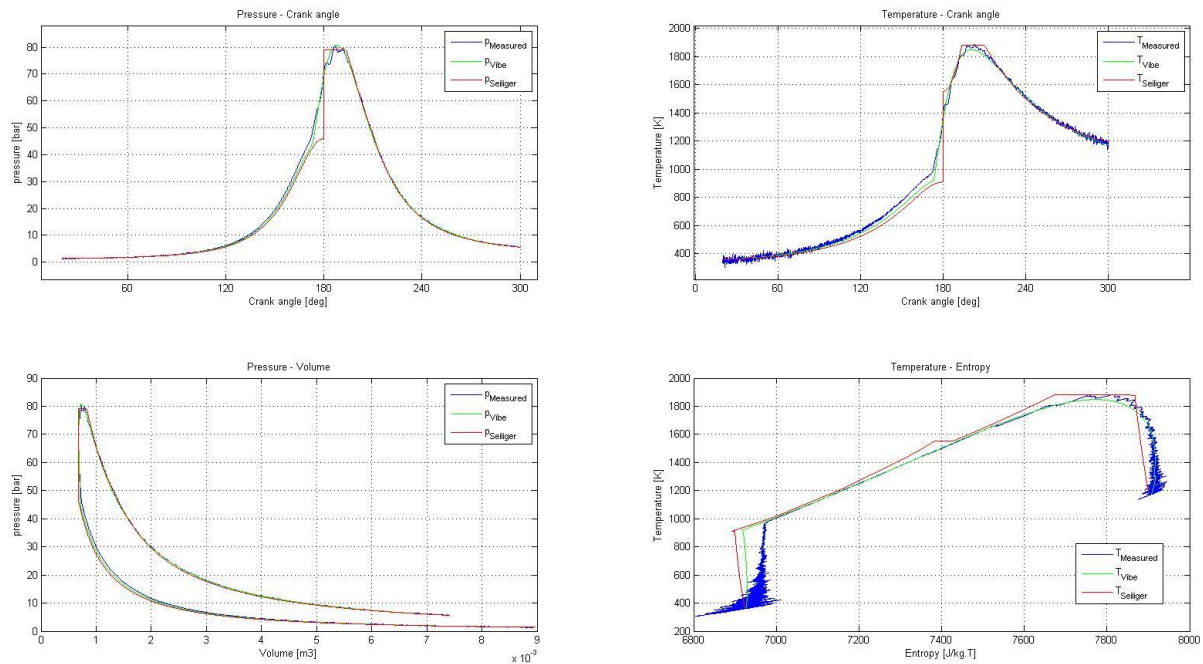


Figure 7.24: Seiliger fit at 1000 RPM, 225 kW

The figure above illustrates the Seiliger fit at 1000 RPM, 225 kW at benchmark operation (no hydrogen addition). The fit is quite good, although similar issues mentioned before still persist. Additionally the entropy during compression is not fitted very well. It leans slightly to the right, whereas the Seiliger and Vibe fit predict an angle to the left. This is a problem that occurs only at higher loads. Adjusting the polytropic compression coefficient results in a better fit, and additionally has a positive effect on the temperature during compression. In figure 7.25 below the polytropic compression factor has been increased from the standard value of 1.36 to 1.39, and it is clear that this results in a much better fit.

The reason as to why this occurs only at high loads is not 100% clear, but most likely to do with practical issues during testing. The order of testing was such that the high load points were always performed last, so the engine could reach operating temperature of each testing point quickly while progressing from low to high load throughout the day. This meant that when testing the high load points, the ambient temperature was quite high in the engine room, and the engine had been running for almost a full day. This could have potentially resulted in higher temperatures of cooling water, ambient temperatures, and perhaps even some overheating due to the age of the engine.

This in turn could have resulted in some extra heat input to the cylinder, resulting in the effect seen in the graphs.

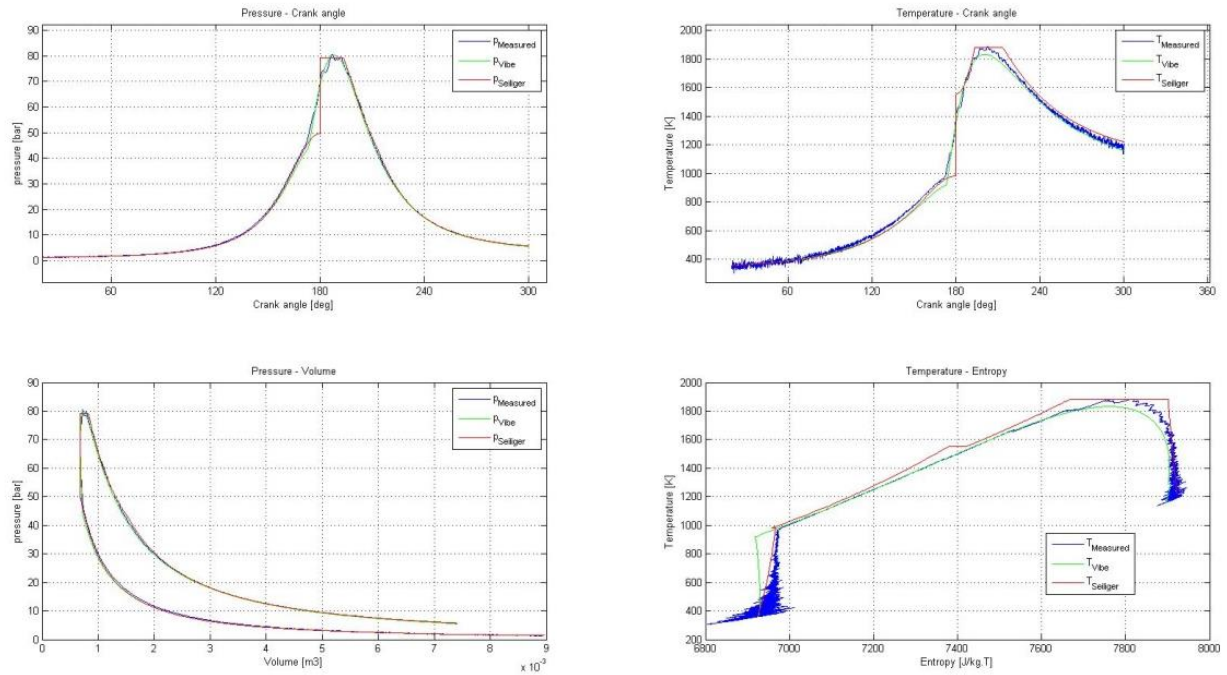


Figure 7.25: Seiliger fit at 1000 RPM, 225 kW with $n_{comp} = 1.39$

The results in terms of the equivalence criteria are shown below, in tables 7-6 and 7-7.

Table 7-6: Result of Seiliger fit at 1000 RPM, 225 KW using T_{max} as equivalence criteria

Equivalence Criteria	Relative error (%)	Absolute error
Q_{in}	$1.5 \cdot 10^{-4}$	2.2955 J
W_i	$2.42 \cdot 10^{-4}$	1.8775 J
P_{max}	0	0 Pa
T_{EO}	0.0240	27.8108 K
T_{max}	$1.72 \cdot 10^{-4}$	0.3223 K

Table 7-7: Result of Seiliger fit at 1000 RPM, 225 KW using T_{EO} as equivalence criteria

Equivalence Criteria	Relative error (%)	Absolute error
Q_{in}	$1.5 \cdot 10^{-4}$	-2.3358 J
W_i	$2.0 \cdot 10^{-4}$	-1.5821 J

P_{max}	0	0 Pa
T_{EO}	$9.1 \cdot 10^{-5}$	-0.1058 K
T_{max}	0.0618	115.5507 K

At higher loads the difference between both Seiliger fit methods becomes more clearly visible. While work and heat input are accurate in both fits, the temperatures vary quite a bit between the two methods. When using T_{EO} as equivalence criteria the maximum temperature is estimated way too high (115 K), and when using T_{max} as equivalence criteria T_{EO} is overestimated by 27 K. Overall however when using T_{max} as equivalence criteria the error is smaller, and the overall fit better.

Table 7-8: Seiliger parameter at 1000 RPM, 225 kW

	Benchmark	2.5% H_2	5% H_2	7,5% H_2	10% H_2
Seiliger param.					
a	1.7233	1.7270	1.7270	1.7808	1.7871
b	1.2129	1.1907	1.1910	1.1801	1.1791
c	1.6393	1.6811	1.6773	1.6983	1.6442
n_{exp}	1.2687	1.2787	1.2793	1.2955	1.2872

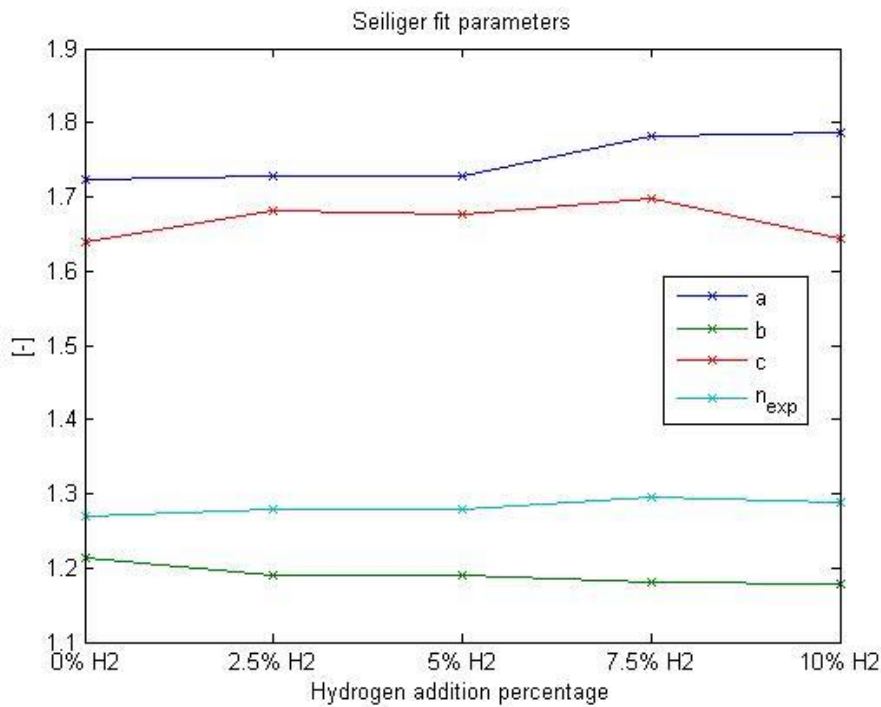


Figure 7.26: Seiliger fit parameters, 1000 RPM, 225 kW

From figure 7.23 we can see that with increasing hydrogen addition percentage, Seiliger parameter a increases as well. Parameter b decreases proportionally as well, indicating that combustion shifts towards more early combustion. Results for parameter c seem inconsistent, since the value

increases at first but then decreases for the final 10% hydrogen addition point. n_{exp} varies only very slightly, and no real conclusions can be drawn here.

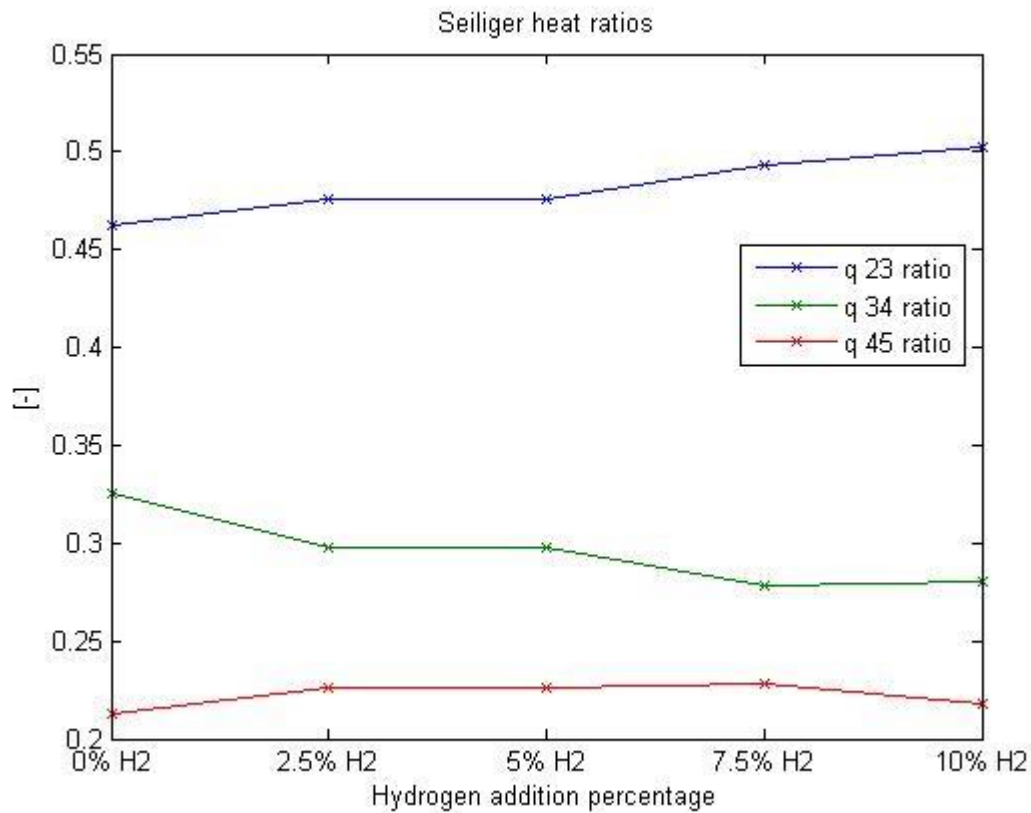


Figure 7.27: Heat ratios at 1000 RPM, 225 kW

This is the first heat ratio figure where the addition of hydrogen results in a different distribution of the delivered heat. It is clear that increasing hydrogen fraction results in more heat during the early stage 2-3, a result that was both expected and also visible in figure 7.25 in the Seiliger parameters. Most of this early combustion is compensated by less heat in stage 3-4, while very late combustion in stage 4-5 is also decreased slightly.

Operating point 1000 RPM, 300 kW (nominal point)

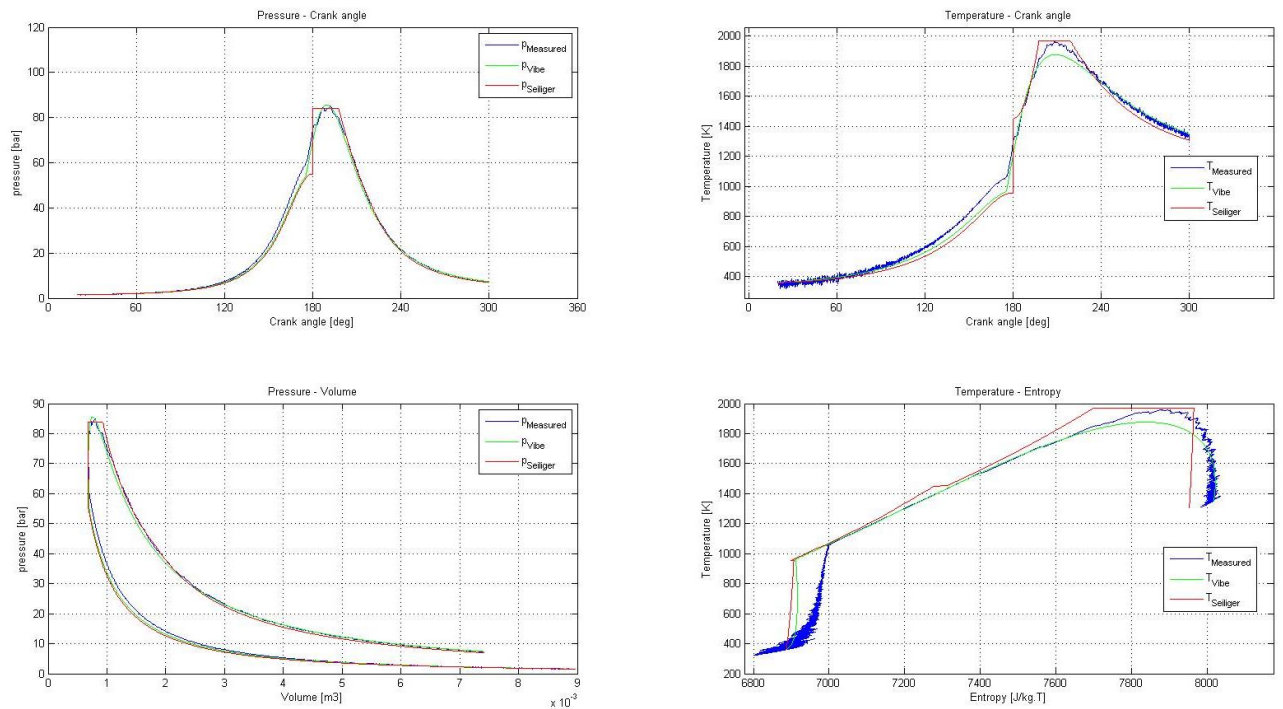


Figure 7.28: Seiliger fit at 1000 RPM, 300 kW

The figure above illustrates the Seiliger fit at 1000 RPM, 300 kW at benchmark operation. The fit has the same problems mentioned before during the compression stroke, where pressure and temperature are higher in the measured data than both the Vibe and Seiliger fit predict. Additionally the temperature-entropy plot shows the same behaviour as mentioned before at the 225 kW operating point. Again the polytropic compression factor was increased to improve the fit, and an increase to 1.42 from the previous 1.36 was required. The result is shown in figure 7.29 below.

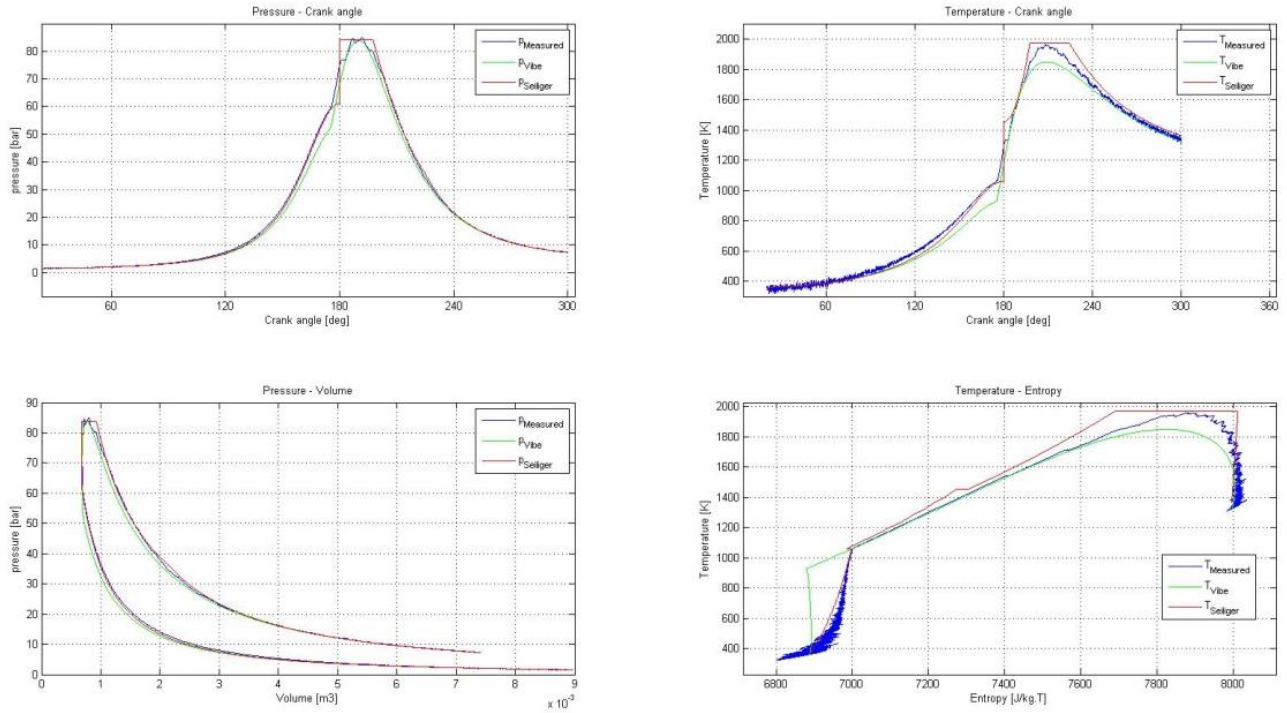


Figure 7.29: Seiliger fit at 1000 RPM, 300 kW with $n_{comp} = 1.42$

Table 7-9: Result of Seiliger fit at 1000 RPM, 300 kW using T_{max} as equivalence criteria

Equivalence Criteria	Relative error (%)	Absolute error
Q_{in}	$3.70 \cdot 10^{-5}$	0.7318 J
W_i	$6.76 \cdot 10^{-5}$	0.6547 J
P_{max}	0	0 Pa
T_{EO}	0.0213	-28.13 K
T_{max}	$2.92 \cdot 10^{-5}$	0.0571 K

Table 7-10: Result of Seiliger fit at 1000 RPM, 300 kW using T_{EO} as equivalence criteria

Equivalence Criteria	Relative error (%)	Absolute error
Q_{in}	$4.0378 \cdot 10^{-5}$	-0.7985 J
W_i	$4.8357 \cdot 10^{-5}$	-0.4681 J
P_{max}	0	0 Pa
T_{EO}	$2.0239 \cdot 10^{-5}$	-0.0268 K
T_{max}	0.0382	-74.6068 K

Similar results to previous fits: using maximum temperature as equivalence criteria instead of temperature at exhaust opens results in an overall better fit.

Tabel 7.2: Seiliger parameters at 1000 RPM, 300 kW

	Benchmark	2.5% H_2	5% H_2	7,5% H_2	10% H_2
Seiliger param.					
a	1.3757	1.3781	1.3786	-	-
b	1.3574	1.3325	1.3410	-	-
c	2.3012	2.3702	2.4599	-	-
n_{exp}	1.2953	1.3093	1.3163	-	-

As mentioned before the 7,5% and 10% points where not tested due to practical issues.

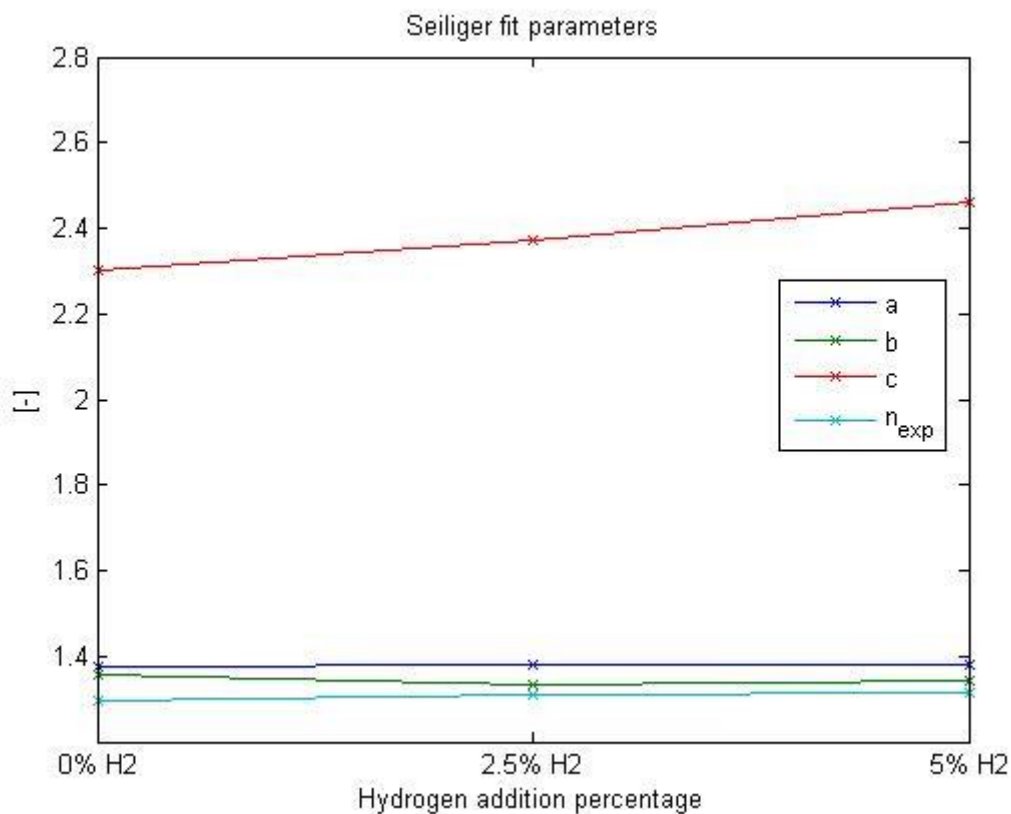


Figure 7.30: Seiliger fit parameters, 1000 RPM, 300 kW

The most suprising result at this nominal operating point is the increase in late combustion, parameter c. Parameter a remains practically constant, while b decreases slightly. This would indicate that combustion shifts from medium towards late combustion. The effect on n_{exp} is also a small increase, again indicating some extra late combustion.

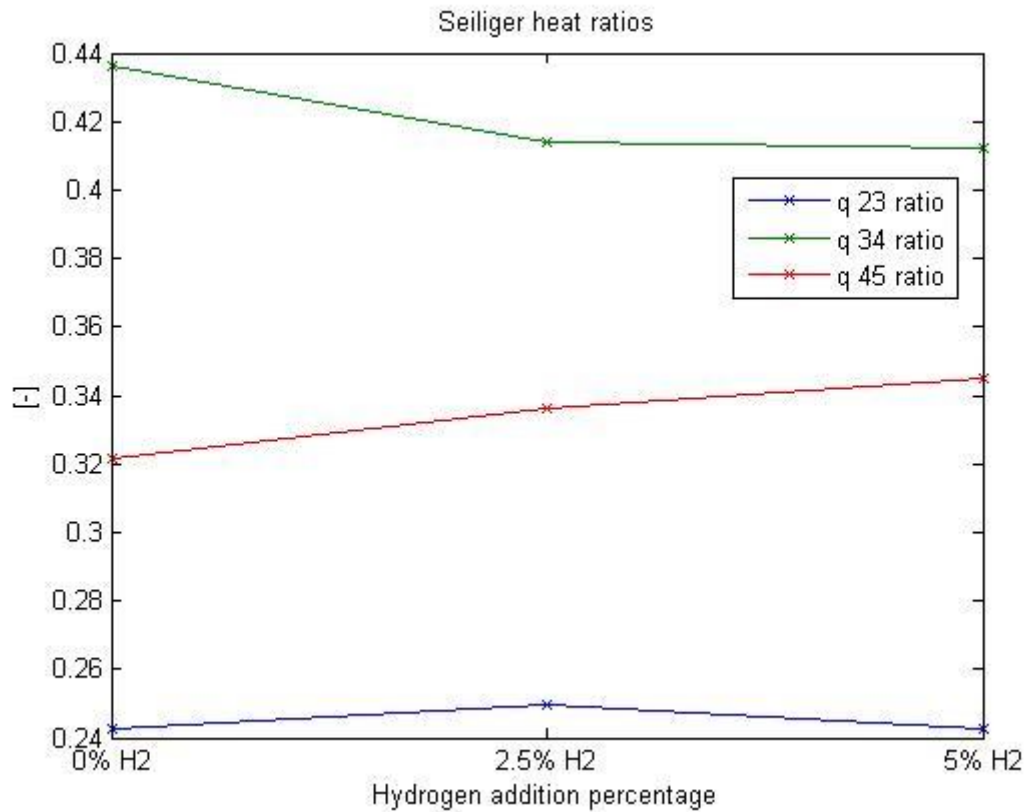


Figure 7.31: Heat ratios at 1000 RPM, 300 kW

Similarly to the surprising results of figure 7.30, figure 7.31 also has some interesting results. Early combustion seems fairly constant, which corresponds to the constant Seiliger parameter a we saw earlier. Heat release in the late phase 4-5 is increased, which of course means that the ratio 3-4 needs to decrease to maintain unity. These results are consistent with figure 7.28,

Chapter 8: Matching results

8.1 Introduction

In this chapter the results of the Vibe fits and Seiliger fits will be compared to each other in more detail. We will discuss both low load and high load scenario's, as well as investigating the effect of hydrogen addition on both methods to see if they are influenced differently. Paragraphs are as follows:

- Low load scenario's (paragraph 8.2);
- High load scenario's (paragraph 8.3);
- Hydrogen addition effect (paragraph 8.4);

8.2 Low load scenario's

In the figures below a low load scenario (700 RPM, 103 kW) is illustrated. 103 kW corresponds to about 33% load, and at 700 RPM this point lies on the propeller curve of the engine. This makes it a real word operating point.

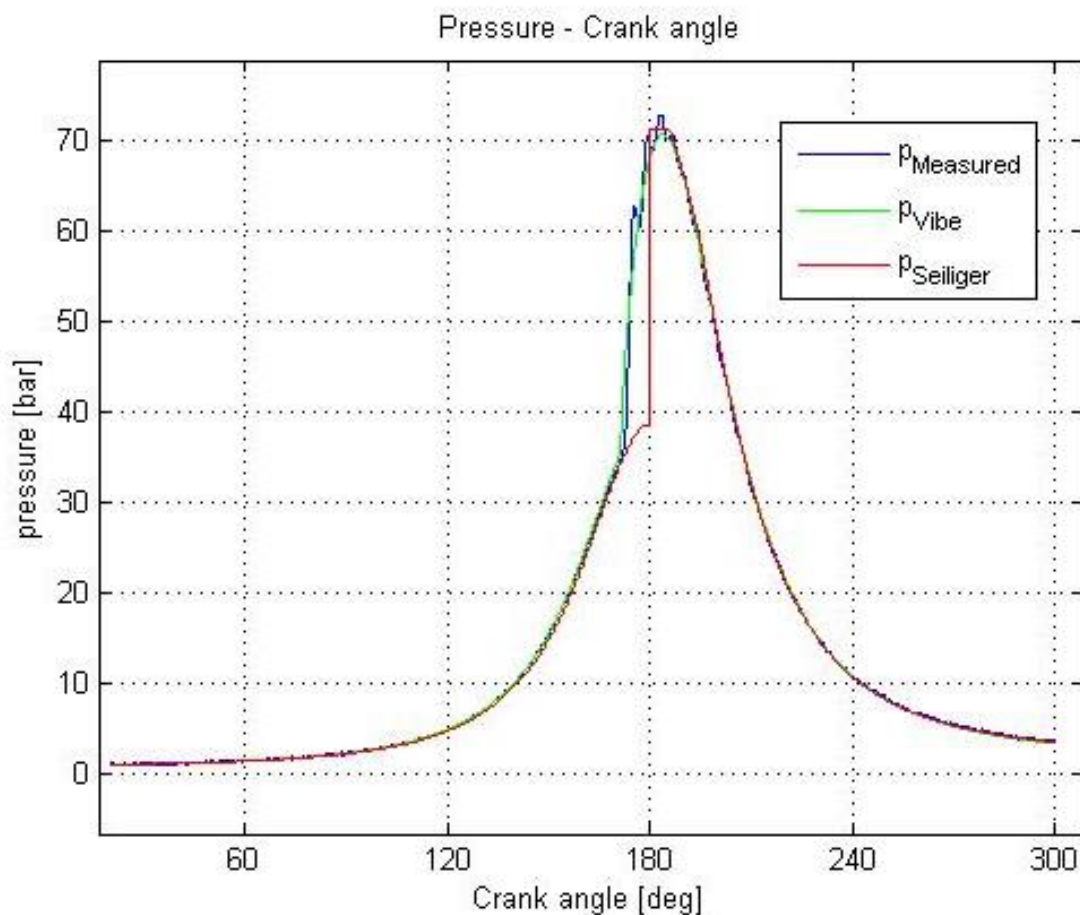


Figure 8.1: Pressure - crankangle at 700 RPM, 103 kW

It is clear that both the Vibe fit and the Seiliger fit produce a very accurate result at this point. Compression and expansion are modelled very well, and maximum pressure is also accurately fit. The only downside of the Seiliger fit that is clear from this figure is that it assumes start of combustion (SOC) at exactly 180 degrees. The Vibe fit is based on the actual heat release in the cylinder, and is therefore much more accurate in this area. From figure 8.1 it is clear that during combustion the Vibe fit follows the measured data very closely.

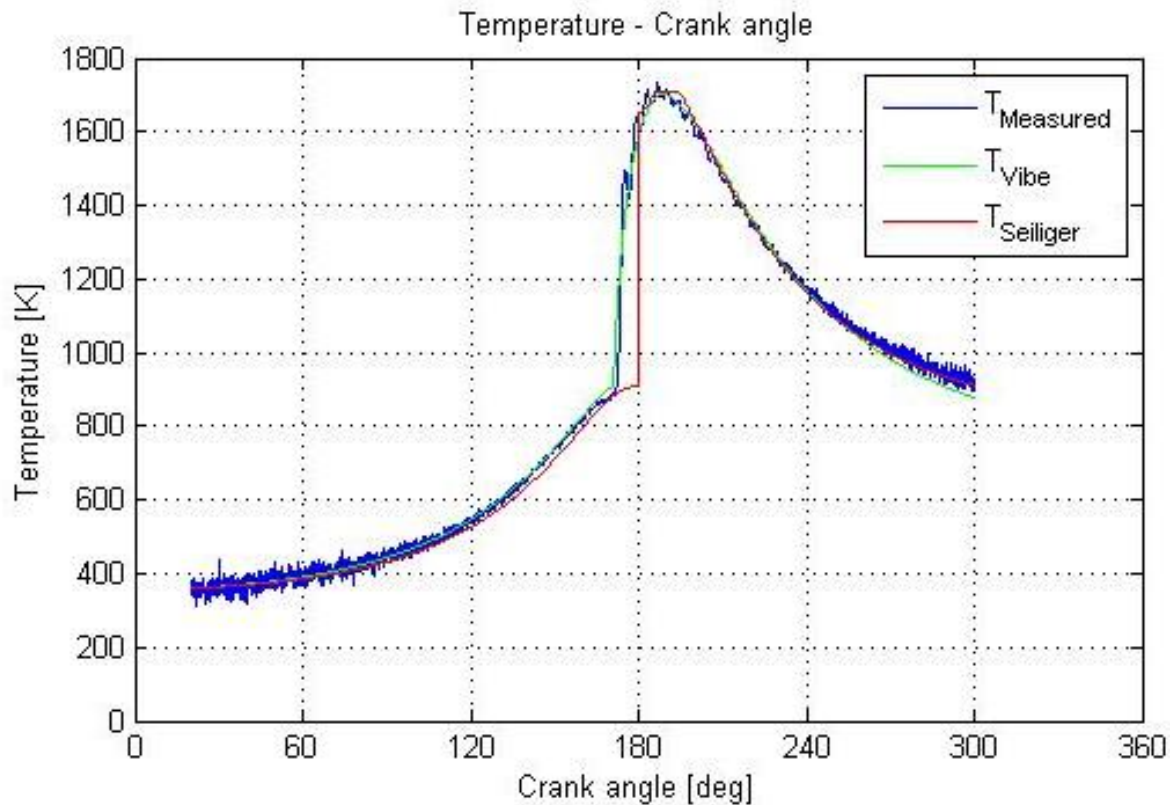


Figure 8.2: Temperature - crankangle at 700 RPM, 103 kW

In the temperature – crankangle plot the same effect that was mentioned before can be seen again, where combustion is assumed at 180 degrees crankangle (exactly TDC) in the Seiliger cycle. Maximum temperature is accurate for both methods, but the temperature at exhaust opens (EO) is slightly underestimated by the Vibe fit. The Seiliger fit can adjust the value for the polytropic expansion coefficient to model additional heat loss or heat input during late expansion, whereas the Vibe uses an empirical formula (the Woschni model) to calculate/estimate heat loss. It is possible to adjust a parameter in this formula manually to increase the fit accuracy, but this can affect other areas as well and is very much a trial-and-error approach to fitting, and therefore not really preferred.

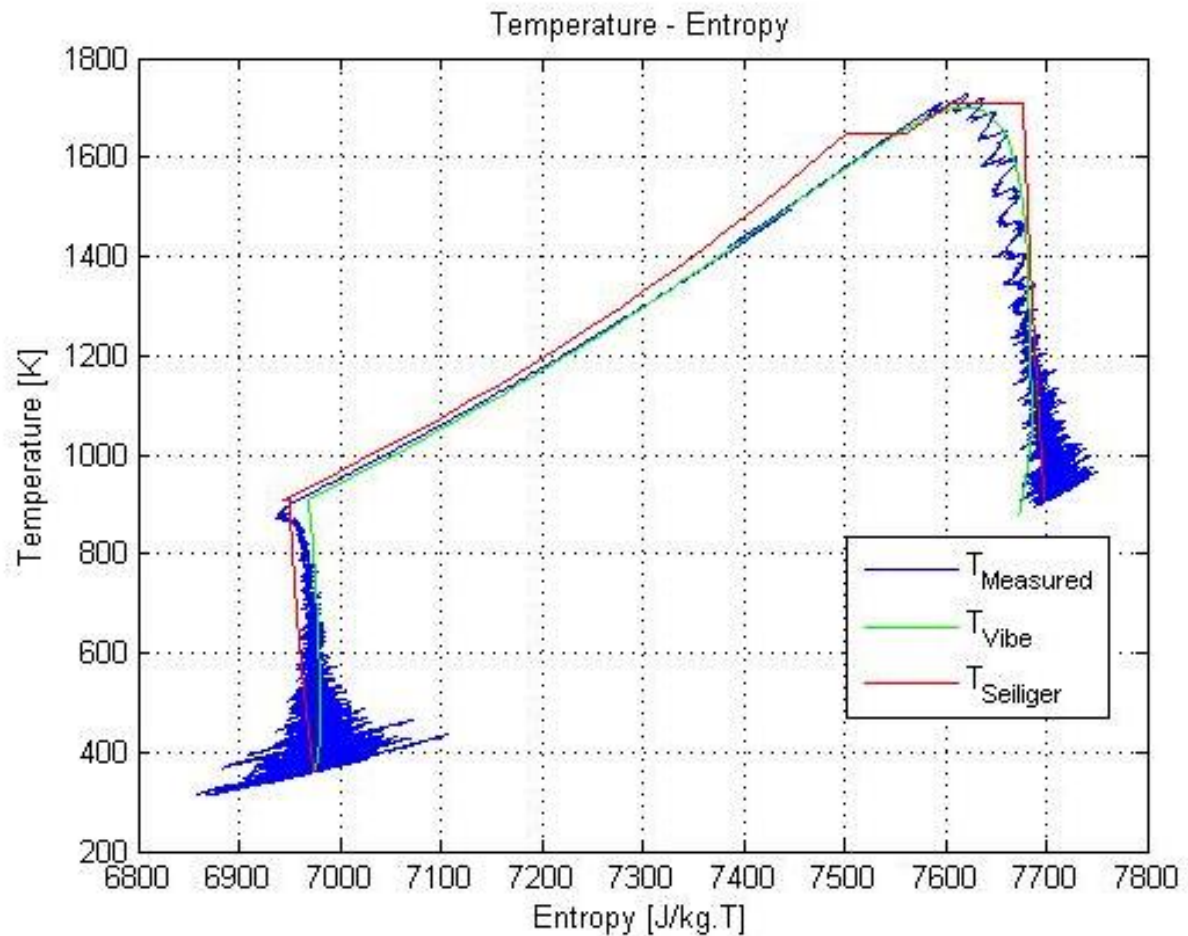


Figure 8.3: Temperature - entropy at 700 RPM, 103 kW

At this operating point both methods appear to be quite accurate. Both methods model compression fairly well, correctly showing a slight angle to the left. This indicates heat input (from the hot wall), but as soon as the gas temperature rises above the cylinder wall temperature, this will change to heat loss to the wall. Vibe models the middle section of the graph very accurately, while Seiliger slightly overestimates. Vibe fitting is also much more fluent, whereas in the Seiliger fit it is very clearly visible where the 'stations' are that separate the different parts of the combustion process in the Seiliger cycle.

8.3 High load scenario's

In the figures below a high load scenario (1000 RPM, 300 kW) is illustrated. This point corresponds to the engines nominal operating point (100% load), and is therefore peak load.

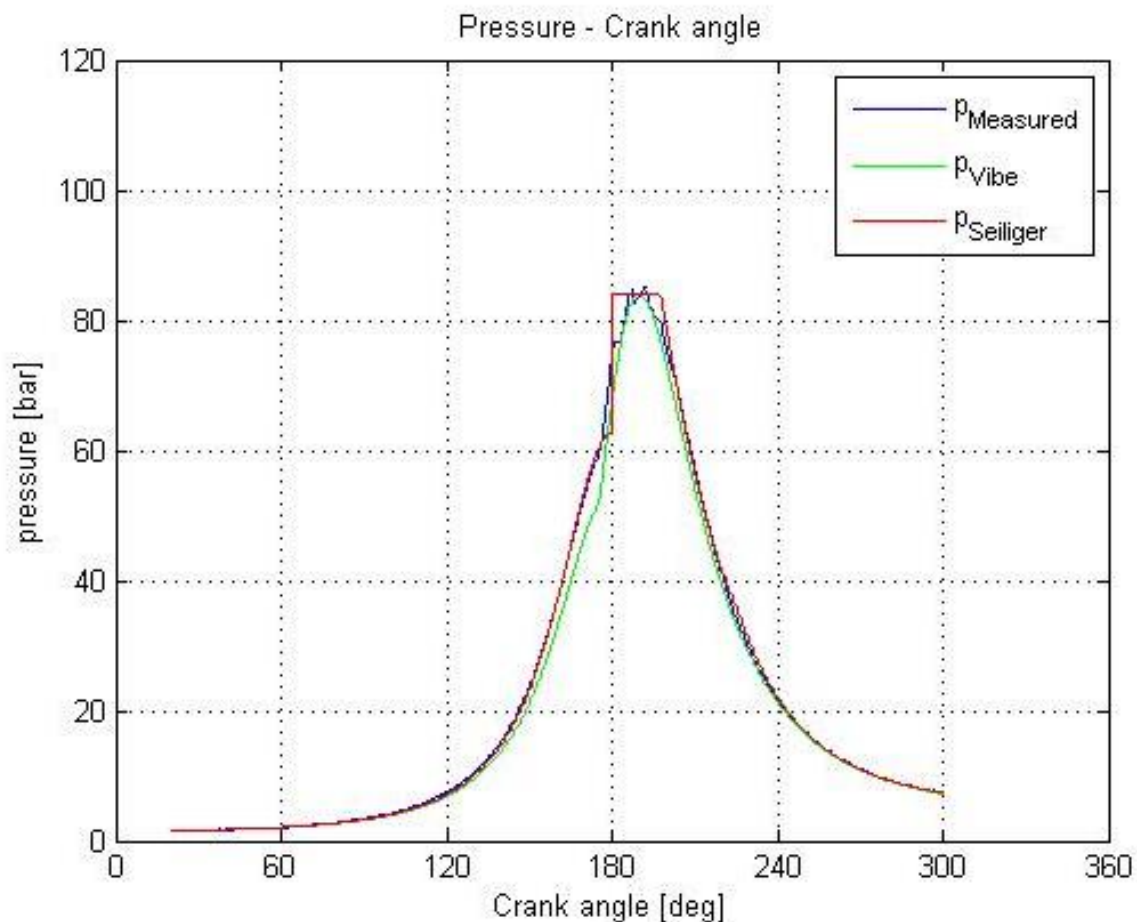


Figure 8.4: Pressure - crank angle at 1000 RPM, 300 kW

From 8.4 a number of clear differences are visible between the Vibe and Seiliger fit. Starting with compression, the Vibe fit underestimates the pressure here quite significantly. As mentioned before in chapter 7, the polytropic compression exponent was adjusted from the base value of 1.36 to 1.42. This makes it possible to adjust the Seiliger fit to certain aspects of a particular engine, such as in this case where extra heat input occurred during these measurements. This is an advantage of the Seiliger cycle that the Vibe fit method does not have. Although a parallel could be drawn with the Woschni heat loss parameter mentioned in paragraph 8.2 which can also be adjusted manually, doing so with a Seiliger fit is much more straightforward and quick.

Continuing, the fit around TDC is much better using Vibe fitting. The Seiliger cycle clearly shows the different combustion stages in straight lines, whereas the Vibe fit (based on actual heat release) can follow the measured data very closely. This is a clear advantage for Vibe fitting if accuracy in this area around TDC is required. Finally the expansion stage is quite similar for both methods.

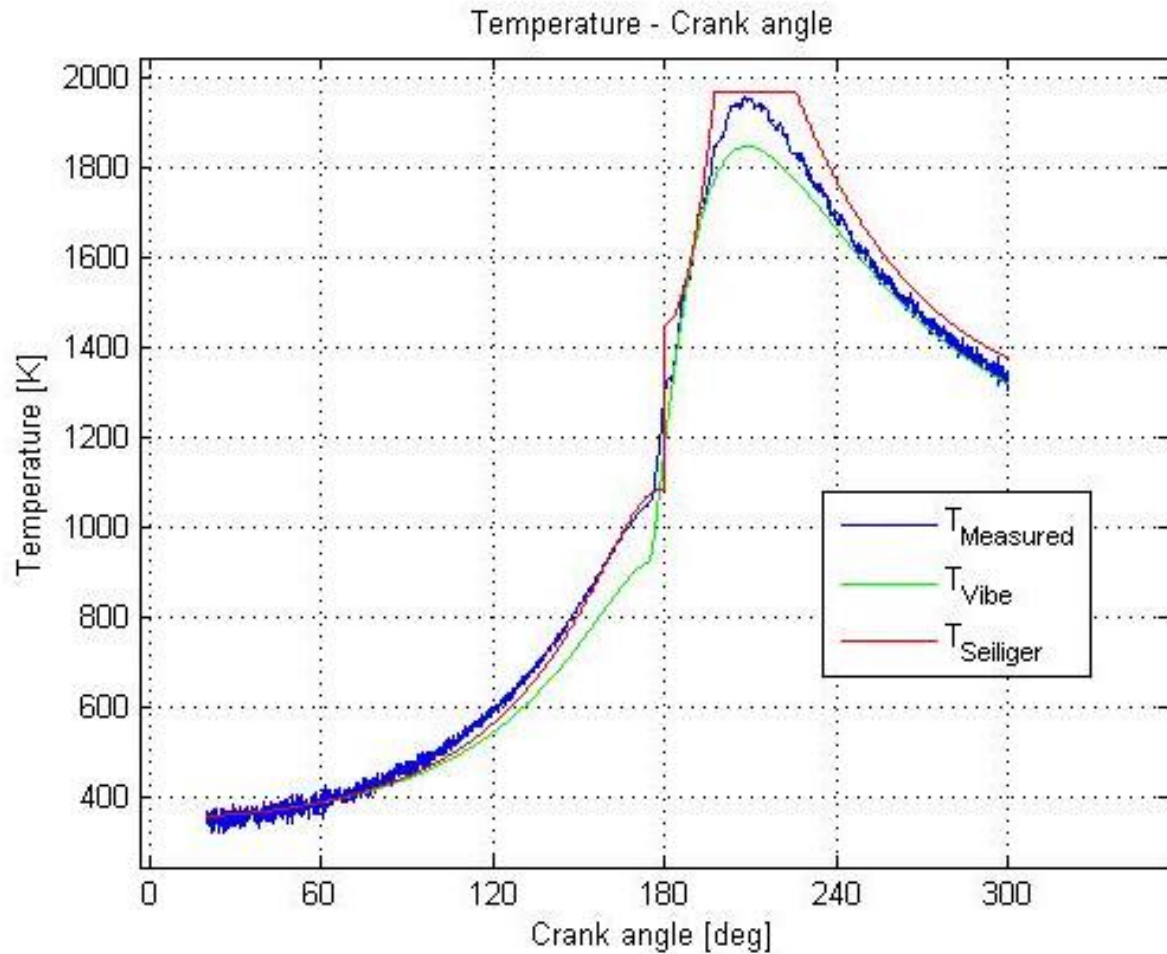


Figure 8.5: Temperature - crank angle at 1000 RPM, 300 kW

During compression the same effect is visible as mentioned before, where the Vibe fit could not be adjusted for the additional heat input. A more interesting area is around TDC, where there are quite some differences between fit methods.

The Vibe fit underestimates the peak temperature around TDC, which is probably due to the fact it assumes a lower temperature after compression. This is therefore basically another symptom of the problem mentioned before, where the extra heat input during compression is not accounted for. The difference in temperature around 180 degrees crankangle is about equivalent to the difference in peak temperature. The temperature at exhaust opens however is spot on, which is very impressive.

The Seiliger method on the other hand fits peak temperature almost perfectly. Given that this was an equivalence criteria during this particular fit that was to be expected, but in return the temperature at exhaust opens (300 degrees crankangle) is overestimated. This is a downside of Seiliger fitting, where only a number of specific equivalence criteria can be selected on which the fit is based. Seiliger fit versions with more equivalence criteria are available, but they increase in complexity and do not always converge to a solution reliably.

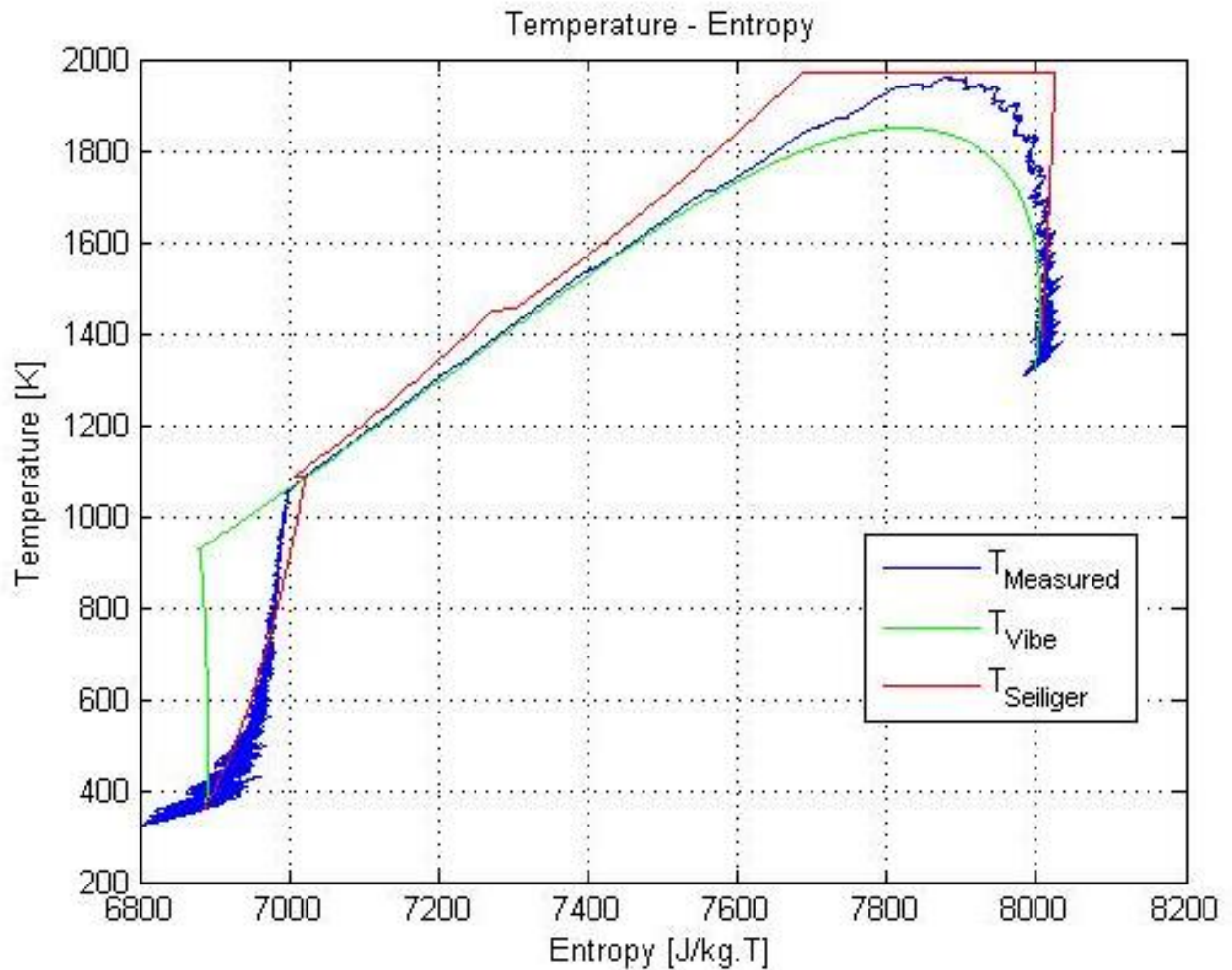


Figure 8.6: Temperature - entropy at 1000 RPM, 300 kW

As mentioned, at this high load point heat loss dominates during compression and therefore the entropy is angled towards the right. Seiliger can follow, Vibe cannot as has been explained before.

In the middle section however the Vibe fit is quite accurate, whereas Seiliger again overestimates. And, again, the Vibe fit is much more fluent here while the Seiliger fit clearly shows the different combustion stages.

As shown in figure 8.5 the maximum temperature is underestimated by Vibe, due to the same reasons mentioned there. Seiliger fits the maximum temperature almost perfectly, but the question is if this results in an overall better fit? The temperature just before and after the peak is quite overestimated, which could mean the overall estimate for work done is not accurate.

On the same note it can be said that Vibe fitting underestimates the peak temperature. However, since an extra area is overestimated during compression, the total work done is more accurate than the Seiliger fit.

Overall the Seiliger fit method is faster and simpler, and allows for some quick adjustments if there are some unexpected problems. For instance the increased heat intake during compression: this is a quirk of the particular engine that was used for the tests, combined with ambient conditions. While Seiliger allows for quick adjustments to only a certain part of the overall fit (adjusting just the polytropic compression exponent), Vibe does not.

On the other hand: when the engine performs as it should, the fit provided by the Vibe method is very accurate at all stages of combustion, including around TDC where Seiliger falters. It requires some more work because an accurate heat release rate must be obtained, but this also results in a very accurate overall fit.

Both methods have their use cases. Seiliger provides quite a good fit during compression and expansion, and is very well suited for finding mean values such as peak pressure, peak temperature, etc. When the entire cycle is of importance, and especially if the area around TDC is subject of the investigation, a Vibe fit is much more valuable and accurate.

Chapter 9: Conclusions and recommendations

9.1 Conclusions

The objective of this thesis was to study the effect of small amounts (max 10% total energy added) of hydrogen addition in turbocharged marine diesel engines on engine performance and emissions.

In paragraph 2.8, table 2-2, the expected effect on certain parameters and expected results were summarized. This table can now be reviewed and adjusted if necessary. A green color indicates that the expected result was confirmed, whereas a red color indicates the opposite. Where the effect remains unclear, yellow is used.

Table 9-1: Results at various loads and hydrogen addition percentages

	Low (partial) load		High (full) load	
	Low H ₂ addition	High H ₂ addition	Low H ₂ addition	High H ₂ addition
Brake thermal efficiency, η_e	-	-	=	?/+
Peak pressure, p_{max}	=/+	=/+	++	++
Start of combustion, SOC	=	=	=	-
Ignition delay	=/?	=/?	-	-
CO ₂ emissions	-	-	-	-
CO emissions	-	-	-	-
NO _x emissions	-	-	+	+
Pre-mixed combustion	+	+	+	+
Diffuse combustion	-	-	-	-

The results will be discussed in detail below.

9.1.1 Low (partial) load

Measurements of fuel consumption indicate that addition of 2,5% to 10% hydrogen (of total energy consumption) at low loads does not result in more efficient operation (higher brake thermal efficiency). SOC and ignition delay all remain fairly constant at these operation points.

Peak pressure increased slightly with increasing load: at 30 kW the effect was not visible, but at 103 kW a slight increase was apparent. The increase was constant for all hydrogen addition percentages.

The reduction of CO and CO₂ emissions was proportional to the reduction in carbon based fuel, but no extra reduction was found. NO_x emissions also reduced proportionally with hydrogen addition, as expected.

The expected effect of hydrogen on heat release rate, where combustion shifts from diffuse to pre-mixed combustion, was not witnessed at low load points. Only when approaching higher loads (approx 150 kW) this effect started occurring.

9.1.2 High (full) load

Unfortunately the full load point was not tested with 7,5% and 10% hydrogen addition. For this reason most of these cells are yellow. Some of the expected results in terms of emissions are still colored green however, since the effect at 2,5% and 5% is such that the effect at higher hydrogen percentage is almost certainly similar.

At full load measurements of fuel consumption indicate that addition of 2,5% and 5% hydrogen (of total energy consumption) results in more efficient operation (reduced energy consumption of about 1.5-2%). This effect was initially only expected at higher hydrogen addition percentages, but was already visible here.

Peak pressure increased about 2-3 bar at high loads as expected. Interestingly both increasing load and increasing hydrogen addition percentage have a positive effect on increasing peak pressure.

SOC remained constant most of the time, but at full load and 5% hydrogen addition SOC advanced with 2 crankangle degrees. This effect was only witnessed at this point, but is what was expected based on literature.

No effect on ignition delay was observed, contrary to the expectations (with the exception of the full load 5% hydrogen addition point mentioned before). This could indicate that simply not enough hydrogen was present to consistently reduce the delay and advance combustion as expected. If this is indeed the case the 7,5% and 10% points would have performed better.

In terms of emissions, CO and CO₂ reduced proportionally with the amount of carbon-based fuel (diesel) replaced with hydrogen. This is similar to the low load points. At 100% load however this reduction increased, resulting in an extra reduction not based on the substitution of fuel. This indicates a catalytic effect of the hydrogen addition.

NO_x emissions decreased at low and medium loads proportionally with hydrogen addition percentage as mentioned before, but increased significantly at 100% load. This effect is expected to be even greater with 7,5% and 10% hydrogen addition, due to even higher peak pressure and temperatures.

Investigation of the heat release rate indicates that at higher loads (225 kW and 300 kW) Vibe fitting showed that hydrogen addition results in a slight increase in early combustion, at the cost of some late combustion. This is the result we also expected at low loads, but only occurred here at higher loads.

This effect could also be seen when using the Seiliger fit method at 225 kW, but unfortunately not at 300 kW. It is not clear if this is a measurement error, or some other effect is in play here.

9.1.3 Overall conclusions

From this thesis it is clear that any expected gains are to be found at high loads, around the nominal operating point of the specific engine. Percentage-wise results of 1.5% to 2% increased fuel efficiency have been found at 100% load. Supporting these results with HRR measurement proved to be difficult due to the small differences between benchmark operation and operation with hydrogen addition, but has shown some preliminary results.

Further research aimed specifically at operation at or around 100% load with small amounts of hydrogen (practically speaking up to 5%) is required for a conclusive answer. A number of recommendations for further research are mentioned below.

9.2 Recommendations

Recommendations are split up in a number of categories:

9.2.1.1 Testing equipment

One of the most useful additions to the testing equipment would be the ability to measure hydrogen in the exhaust gas. This thesis estimates hydrogen combustion efficiency based on literature review, but this can vary per engine and more importantly even per operational point. Also scavenging losses were estimated due to this reason, but could be measured from the exhaust gasses if such a sensor was available.

Another solution to scavenging losses would be to inject the hydrogen directly into the cylinder, similar to the diesel fuel. This does however pose other problems regarding the practical cost and difficulty of installing such a system, as well as the effect this has on hydrogen combustion.

Furthermore the in-cylinder pressure measurement is extremely important, since the entire heat release rate and Vibe fit depends on this parameter. The sensor is currently placed in such a way that pressure waves occur, which have a negative effect on the quality of the measurement. Fixing this problem and increasing the quality of the pressure measurement directly influences all other calculations.

9.2.1.2 Modelling

To improve the modelling of hydrogen/diesel combustion, a dual-fuel model could be developed. Vibe-fitting is very suited for this purpose, since separate Vibe fits can be made for diesel and hydrogen combustion, which can then be easily combined. Currently the model assumes just a single fuel with adapted properties such as lower heating value, density, etc. that are averaged between the two fuels.

Further investigation regarding heat loss of hydrogen combustion is also recommended. Currently the Woschni model is used, but some research indicated that hydrogen has a much higher heat loss

to the cylinder wall than a diesel flame due to higher burning velocity and shorter quenching distance [Shudo and Suzuki, 2002]. Another method to estimate this heat loss could improve the modelling of hydrogen combustion significantly.

9.2.1.3 Further research

As mentioned before further research should be specifically aimed at operation at high loads and small percentages of hydrogen. Practical issues with hydrogen supply become to much of an issue if the percentage of hydrogen addition is increased over 5% of total energy, and the effect at low loads is negligible.

Also the use of a more modern engine could have some added effects. The engine used in this thesis is fairly old and due to that reason has a fair share of late combustion due to its design. Additionally an engine with variable valve control could research the effect of early or late combustion with hydrogen addition in greater detail.

References

- An, H., Yang, W. M., Maghbouli, a., Li, J., Chou, S. K., & Chua, K. J. (2013). A numerical study on a hydrogen assisted diesel engine. *International Journal of Hydrogen Energy*, 38(6), 2919–2928. <http://doi.org/10.1016/j.ijhydene.2012.12.062>
- Bari, S., & Mohammad Esmaeil, M. (2010). Effect of H₂/O₂ addition in increasing the thermal efficiency of a diesel engine. *Fuel*, 89(2), 378–383. <http://doi.org/10.1016/j.fuel.2009.08.030>
- Bueno, A. V., Velásquez, J. A., & Milanez, L. F. (1985). Internal combustion engine. *Environment International*, 11(5), IV. [http://doi.org/10.1016/0160-4120\(85\)90256-9](http://doi.org/10.1016/0160-4120(85)90256-9)
- Cassidy, J. F. (1977). *Emissions and total energy consumption of a multicylinder piston engine running on gasoline and a hydrogen-gasoline mixture*.
- Das, L. (2002). Hydrogen engine: research and development (R&D) programmes in Indian Institute of Technology (IIT), Delhi. *International Journal of Hydrogen Energy*, 27(9), 953–965. [http://doi.org/10.1016/S0360-3199\(01\)00178-1](http://doi.org/10.1016/S0360-3199(01)00178-1)
- Dhole, a. E., Yarasu, R. B., Lata, D. B., & Baraskar, S. S. (2014). Mathematical modeling for the performance and emission parameters of dual fuel diesel engine using hydrogen as secondary fuel. *International Journal of Hydrogen Energy*, 39(24), 12991–13001. <http://doi.org/10.1016/j.ijhydene.2014.06.084>
- Gatts, T., Li, H., Liew, C., Liu, S., Spencer, T., Wayne, S., & Clark, N. (2010). An experimental investigation of H₂ emissions of a 2004 heavy-duty diesel engine supplemented with H₂. *International Journal of Hydrogen Energy*, 35(20), 11349–11356. <http://doi.org/10.1016/j.ijhydene.2010.06.056>
- Ghazal, O. H. (2013). Performance and combustion characteristic of CI engine fueled with hydrogen enriched diesel. *International Journal of Hydrogen Energy*, 38(35), 15469–15476. <http://doi.org/10.1016/j.ijhydene.2013.09.037>
- Hamdan, M. O., Selim, M. Y. E., & Elnajjar, E. (2014). Hydrogen supplement co-combustion with diesel in compression ignition engine. *Renewable Energy*, 1–7. <http://doi.org/10.1016/j.renene.2014.08.019>
- Haragopala Rao, B. (1983). Hydrogen for dual fuel engine operation. *International Journal of Hydrogen Energy*, 8(5), 381–384. [http://doi.org/10.1016/0360-3199\(83\)90054-X](http://doi.org/10.1016/0360-3199(83)90054-X)
- Hoehn, F. W., & Dowdy, M. W. (1974). Feasibility Demonstration of a Road Vehicle Fueled with Hydrogen-Enriched Gasoline. In *Ninth Intersociety Energy Conversion Engineering Conference* (pp. 956–964).
- Köse, H., & Ciniviz, M. (2013). An experimental investigation of effect on diesel engine performance and exhaust emissions of addition at dual fuel mode of hydrogen. *Fuel Processing Technology*, 114, 26–34. <http://doi.org/10.1016/j.fuproc.2013.03.023>
- Lata, D. B., Misra, A., & Medhekar, S. (2012). Effect of hydrogen and LPG addition on the efficiency and emissions of a dual fuel diesel engine. *International Journal of Hydrogen Energy*, 37(7), 6084–6096. <http://doi.org/10.1016/j.ijhydene.2012.01.014>
- Liew, C., Li, H., Nuszowski, J., Liu, S., Gatts, T., Atkinson, R., & Clark, N. (2010). An experimental

- investigation of the combustion process of a heavy-duty diesel engine enriched with H₂, 5(Ci), 0–8. <http://doi.org/10.1016/j.ijhydene.2010.06.023>
- Lilik, G. K., Zhang, H., Herreros, J. M., Haworth, D. C., & Boehman, A. L. (2010). Hydrogen assisted diesel combustion. *International Journal of Hydrogen Energy*, 35(9), 4382–4398. <http://doi.org/10.1016/j.ijhydene.2010.01.105>
- Masood, M., Ishrat, M., & Reddy, a. (2007). Computational combustion and emission analysis of hydrogen–diesel blends with experimental verification. *International Journal of Hydrogen Energy*, 32(13), 2539–2547. <http://doi.org/10.1016/j.ijhydene.2006.11.008>
- Miao, R., Li, J., Shi, L., Deng, K., & Tbp, G. (2013). Study of Top Dead Center Measurement and Correction Method in a Diesel Engine, 6(6), 1101–1105.
- Miyamoto, T., Hasegawa, H., Mikami, M., Kojima, N., Kabashima, H., & Urata, Y. (2011). Effect of hydrogen addition to intake gas on combustion and exhaust emission characteristics of a diesel engine. *International Journal of Hydrogen Energy*, 36(20), 13138–13149. <http://doi.org/10.1016/j.ijhydene.2011.06.144>
- Nguyen, T. A., & Mikami, M. (2013). Effect of hydrogen addition to intake air on combustion noise from a diesel engine. *International Journal of Hydrogen Energy*, 38(10), 4153–4162. <http://doi.org/10.1016/j.ijhydene.2013.01.082>
- Olsen, R. A. (2013). Analysis and Simulation of the Rate of Heat Release (ROHR) in Diesel Engines, (June).
- Pan, H., Pournazeri, S., Princevac, M., Miller, J. W., Mahalingam, S., Khan, M. Y., ... Welch, W. a. (2014). Effect of hydrogen addition on criteria and greenhouse gas emissions for a marine diesel engine. *International Journal of Hydrogen Energy*, 39(21), 11336–11345. <http://doi.org/10.1016/j.ijhydene.2014.05.010>
- Rajkumar, K., & Govindarajan, P. (2011). Impact of Oxygen Enriched Air Intake on the Exhaust of a Single Cylinder Diesel Engine, 7(2), 136–140.
- Sandalcı, T., & Karagöz, Y. (2014). Experimental investigation of the combustion characteristics, emissions and performance of hydrogen port fuel injection in a diesel engine. *International Journal of Hydrogen Energy*, 39(32), 18480–18489. <http://doi.org/10.1016/j.ijhydene.2014.09.044>
- Saravanan, N., Nagarajan, G., Sanjay, G., Dhanasekaran, C., & Kalaiselvan, K. M. (2008). Combustion analysis on a DI diesel engine with hydrogen in dual fuel mode. *Fuel*, 87(17-18), 3591–3599. <http://doi.org/10.1016/j.fuel.2008.07.011>
- Science, M. O. F. (2014). CHARACTERIZING THE OPERATION OF A DUAL-FUEL DIESEL-HYDROGEN ENGINE NEAR THE KNOCK LIMIT, (May).
- Shudo, T., & Suzuki, H. (2002). Applicability of heat transfer equations to hydrogen combustion, 23, 303–308.
- SinghYadav, V., Soni, S. L., & Sharma, D. (2012). Performance and emission studies of direct injection C.I. engine in duel fuel mode (hydrogen-diesel) with EGR. *International Journal of Hydrogen Energy*, 37(4), 3807–3817. <http://doi.org/10.1016/j.ijhydene.2011.04.163>
- Szwaja, S., & Grab-Rogalinski, K. (2009). Hydrogen combustion in a compression ignition diesel engine. *International Journal of Hydrogen Energy*, 34(10), 4413–4421.

<http://doi.org/10.1016/j.ijhydene.2009.03.020>

Tyagi, R. K., & Ranjan, R. (2013). Effect of hydrogen and gasoline fuel blend on the performance of SI engine, 4(November), 125–130. <http://doi.org/10.5897/JPTAF2013.0095>

Yi, H. S., Min, K., & Kim, E. S. (2000). The optimised mixture formation for hydrogen fuelled engines, 25, 685–690.

Zhou, J. H., Cheung, C. S., & Leung, C. W. (2014). Combustion, performance, regulated and unregulated emissions of a diesel engine with hydrogen addition. *Applied Energy*, 126(x), 1–12. <http://doi.org/10.1016/j.apenergy.2014.03.089>

Appendix A: MAN 4L20/27 Technical details and measured parameters

Pressure sensor

The pressure sensor used in the measurement system is a KISTLER 7061B, which is a water-cooled precision pressure sensor especially suited for duty in internal combustion engines for high-precision thermodynamic measurement. The technical data of this sensor is shown below.

Table A-0-1: Kistler 7061B Pressure sensor Technical Data

Parameters	Unit	Value
Range	bar	0 – 250
Calibrated partial ranges	bar	0 – 50 0 – 5
Overload	bar	300
Sensitivity	pC/bar	≈ -80
Natural frequency	kHz	≈ 45
Linearity all ranges (cooling)	%FSO	$\leq \pm 0.5$
Acceleration sensitivity (axial) with cooling	bar/g	< 0.01
Operating temperature range Without cooling	°C	-50 – 350
Sensitivity shift		
cooled 50 ± 35 °C	%	$\leq +2$
non-cooled 200 ± 150 °C	%	$\leq \pm 0.5$
Load-change drift (Drop of zero line after cutting the ignition)	bar/s	$\leq \pm 0.5$

Table A-2: Measured parameters on MAN 4L20/27

	Parameter	Unit
1	Atmosphere Pressure	mbar
2	Fuel Leakage	--
3	Fuel Control Rod	--
4	Fuel Vessel	--
5	CO Emission	--
6	CO ₂ Emission	--
7	Cylinder Cool Water Pressure	bar
8	CxHy Emission	--
9	Pressure after Turbine in Exhaust Pipe Point 1	bar
	Parameter	Unit
10	Sea Water Pressure	bar
11	Fuel Pressure before Engine	bar
12	Central Cool Water Pressure	bar
13	Cylinder 1 Pressure	bar
14	Cylinder 2 Pressure	bar
15	Cylinder 3 Pressure	bar
16	Cylinder 4 Pressure	bar
17	Inlet Receiver Pressure	bar
18	Nozzle Pressure	bar
19	Water Brake Pressure	bar
20	Pressure before Turbine in Exhaust Pipe Above	bar
21	Pressure before Turbine in Exhaust Pipe Beneath	bar

22	Total Efficiency	%
23	Fuel Flow	kg/s
24	Central Cool Water Flow for both Cylinder Water Cooler and Lubricating Oil	kg/s
25	Central Cool Water Flow for Inter Cooler	kg/s
26	Cylinder Cool Water Flow	kg/s
27	Lubricating Oil Flow	kg/s
28	Average Torque	N·m
29	Average Temperature for Exhaust	N·m
30	Load	--
31	High Level of Fuel Weighter	--
32	High level of Leakage Tank	--
33	Kisler Cooler	--
34	Torque	N·m

35	Torque Set Point	--
36	Fuel Leakage	--
37	Air consumption	kg/s
38	NOx Emission	--
39	DO Tank Level	--
40	HFO Tank Level	--
41	O2 Emission	--
42	Governor	--
43	Relative Humidity	%
44	SFC	
45	Lubricating Oil Pressure	bar
46	Fly Wheel Signal	--
47	Inlet Air Temperature	°C
48	Temperature after Turbine in Exhaust Pipe	°C
49	Fuel Temperature Before Engine	°C
50	Central Cool Water Temperature after Cylinder Water Cooler	°C
51	Central Cool Water Temperature after Inter Cooler	°C
52	Central Cool Water Temperature after Lubricating Oil Cooler	°C
53	Central Cool Water Temperature Before Cylinder Cool Water Cooler	°C
54	Central Cool Water Temperature before Inter Cooler	°C
55	Central Cool Water Temperature before Lubricating Oil Cooler	°C
56	Cylinder Cool Water Temperature after Cooler	°C
57	Cylinder Cool Water Temperature after Engine	°C

Appendix B: Hydrogen addition percentage calculator

	A	B	C	D	E	F	G	H	I	J	K	L	M	N	O						
1	Diesel LHV:	42.7 MJ/kg					2.5% Hydrogen addition														
2	Hydrogen LHV	120 MJ/kg					Engine load [kW] Hydrogen energy [MJ/sec]														
3	F-76 density (liquid)	850 kg/m ³					[kg/sec] [g/min]									m ³ /min	Flowmeter setting	massa percentage			
4	Hydrogen density (gas) @ 200 bar	16.83 kg/m ³					103									0.0068	0.0001	0.0034	0.0399	7.99%	0.89%
5	Rated engine power	300 kW					184									0.0118	0.0001	0.0059	0.0694	13.89%	0.89%
6							150									0.0097	0.0001	0.0048	0.0568	11.35%	0.89%
7							225									0.0146	0.0001	0.0073	0.0855	17.10%	0.89%
8	Engine load [kW]	SFC [g/kWh]	Fuel consumption [kg/sec]	[MJ/sec]			75									0.0051	0.0000	0.0026	0.0301	6.02%	0.89%
9		103	222.85	0.0064	0.2723	echt	5% Hydrogen addition														
10		184	217	0.0111	0.4736	echt	Engine load [kW] Hydrogen energy [MJ/sec]														
11		150	217.6	0.0091	0.3871	echt	[kg/sec] [g/min]														
12		225	218.55	0.0137	0.5833	echt	103									0.0136	0.0001	0.0068	0.0798	15.96%	1.78%
13		75	230.8	0.0048	0.2053	echt	184									0.0237	0.0002	0.0118	0.1389	27.77%	1.78%
14							150									0.0194	0.0002	0.0097	0.1135	22.70%	1.78%
15							225									0.0292	0.0002	0.0146	0.1710	34.20%	1.78%
16							75									0.0103	0.0001	0.0051	0.0602	12.04%	1.78%
17							7% Hydrogen addition														
18							Engine load [kW] Hydrogen energy [MJ/sec]														
19	Duration of 1 measurement cycle:		10 minutes				[kg/sec] [g/min]														
20	No. of measurement runs:		1 [-]				103									0.0204	0.0002	0.0102	0.1197	23.95%	2.67%
21	Total hydrogen consumption:		6.44 kg				184									0.0356	0.0003	0.0178	0.2083	41.66%	2.67%
22	Volume @ 200 bar		382.41 liter				150									0.0290	0.0002	0.0145	0.1703	34.05%	2.67%
23	Total time of measurements		14.2 hours				225									0.0437	0.0004	0.0219	0.2565	51.30%	2.67%
24	No. of cylinders H2 (@ 50liter)		7.65 [-]				75									0.0154	0.0001	0.0077	0.0903	18.06%	2.67%
25							10% Hydrogen addition														
26							Engine load [kW] Hydrogen energy [MJ/sec]														
27							[kg/sec] [g/min]														
28							103									0.0272	0.0002	0.0136	0.1596	31.93%	3.56%
29							184									0.0474	0.0004	0.0237	0.2777	55.54%	3.56%
30							150									0.0387	0.0003	0.0194	0.2270	45.40%	3.56%
31							225									0.0583	0.0005	0.0292	0.3420	68.40%	3.56%
32							75									0.0205	0.0002	0.0103	0.1204	24.08%	3.56%
33	density @ normal						Total consumption if each measurement point lasts 1 minute:									0.2402			2.8170		
34		0.085286512																			
35																					
36																					

Appendix C: Vibe parameters

Operating point	Vibe function	Vibe 1		Vibe 2		Vibe 3	
		b_1	m_1	b_2	m_2	b_3	m_3
3A	First order	.9808	-0.1996	-	-	-	-
	Second order	0.9629	-0.2182	0.0371	4.699	-	-
	Third order	0.9626	-0.2185	0.03636	4.531	2.223e-14	1
Adjusted R-square		0.9716		0.9756		0.9756	
Optimal Vibe function		Second order Vibe function					

Operating point	Vibe function	Vibe 1		Vibe 2		Vibe 3	
		b_1	m_1	b_2	m_2	b_3	m_3
3B25	First order	0.9858	-0.1948	-	-	-	-
	Second order	0.9608	-0.2201	0.0391	3.486	-	-
	Third order	0.9615	-0.2195	0.01032	18.98	0.04059	3.748
Adjusted R-square		0.9529		0.9583		0.9587	
Optimal Vibe function		Second order Vibe function					

Operating point	Vibe function	Vibe 1		Vibe 2		Vibe 3	
		b_1	m_1	b_2	m_2	b_3	m_3
3B50	First order	0.9675	-0.2002	-	-	-	-
	Second order	0.9493	-0.2195	0.0507	6.367	-	-
	Third order	0.9461	-0.2225	0.0434	4.615	2.23e-14	1
Adjusted R-square		0.9498		0.9550		0.9555	
Optimal Vibe function		<i>Second order Vibe function</i>					

Operating point	Vibe function	Vibe 1		Vibe 2		Vibe 3	
		b_1	m_1	b_2	m_2	b_3	m_3
3B75	First order	0.9761	-0.2124	-	-	-	-
	Second order	0.965	-0.2239	0.035	7.385	-	-
	Third order	0.9621	-0.2266	0.02908	4.769	2.262e-14	1
Adjusted R-square		0.9702		0.9726		0.9729	
Optimal Vibe function		Second order Vibe function					

Operating point	Vibe function	Vibe 1		Vibe 2		Vibe 3	
		b_1	m_1	b_2	m_2	b_3	m_3
3B100	First order	0.9546	-0.2195	-	-	-	-
	Second order	0.9512	-0.2231	0.0488	35.15	-	-
	Third order	0.9424	-0.2321	0.01631	122.3	0.02612	5.248
Adjusted R-square		0.9367		0.9374		0.9393	
Optimal Vibe function		Third order Vibe function					

Operating point	Vibe function	Vibe 1		Vibe 2		Vibe 3	
		b_1	m_1	b_2	m_2	b_3	m_3
11A	First order	1	-0.005583	-	-	-	-
	Second order	1	-0.005582	0	5	-	-
	Third order	-	-	-	-	-	-
Adjusted R-square		0.8044		0.8044		-	
Optimal Vibe function		First order Vibe function					

Operating point	Vibe function	Vibe 1		Vibe 2		Vibe 3	
		b_1	m_1	b_2	m_2	b_3	m_3
11B25	First order	0.9995	-0.07415	-	-	-	-
	Second order	1	-0.07372	0	17.5	-	-
	Third order	0.9995	-0.07416	6.723e-08	17.5	2.323e-14	1
Adjusted R-square		0.8030		0.8030		0.8029	
Optimal Vibe function		First order Vibe function					

Operating point	Vibe function	Vibe 1		Vibe 2		Vibe 3	
		b_1	m_1	b_2	m_2	b_3	m_3
11B50	First order	0.9811	-0.04609	-	-	-	-
	Second order	0.9808	-0.04632	0.0191	290.5	-	-
	Third order	0.9808	-0.04632	0.01672	290.5	2.237e-14	1
Adjusted R-square		0.8930		0.8930		0.8929	
Optimal Vibe function		First order Vibe function					

Operating point	Vibe function	Vibe 1		Vibe 2		Vibe 3	
		b_1	m_1	b_2	m_2	b_3	m_3
11B75	First order	0.9883	-0.05552	-	-	-	-
	Second order	0.9877	-0.05612	0.0123	95.05	-	-
	Third order	0.9877	-0.05611	0.01601	98.87	3.493e-10	-9
Adjusted R-square		0.8549		0.8550		0.8549	
Optimal Vibe function		First order Vibe function					

Operating point	Vibe function	Vibe 1		Vibe 2		Vibe 3	
		b_1	m_1	b_2	m_2	b_3	m_3
11B100	First order	0.9725	-0.1532	-	-	-	-
	Second order	0.9711	-0.1546	0.0289	69.47	-	-
	Third order	0.9711	-0.1546	0.02719	69.47	2.455e-14	1
Adjusted R-square		0.7926		0.7929		0.7928	
Optimal Vibe function		First order Vibe function					

Operating point	Vibe function	Vibe 1		Vibe 2		Vibe 3	
		b_1	m_1	b_2	m_2	b_3	m_3
12A	First order	0.9695	-0.04241	-	-	-	-
	Second order	0.9461	-0.0677	0.0539	4.695	-	-
	Third order	0.9381	-0.0743	0.04635	2.848	2.337e-14	1
Adjusted R-square		0.9139		0.9157		0.9167	
Optimal Vibe function		Second order Vibe function					

Operating point	Vibe function	Vibe 1		Vibe 2		Vibe 3	
		b_1	m_1	b_2	m_2	b_3	m_3
12B25	First order	0.9723	-0.004368	-	-	-	-
	Second order	0.9418	-0.03691	0.0581	3.961	-	-
	Third order	0.9388	-0.03927	0.05134	3.169	2.304e-14	1
Adjusted R-square		0.9105		0.9134		0.9138	
Optimal Vibe function		Second order Vibe function					

Operating point	Vibe function	Vibe 1		Vibe 2		Vibe 3	
		b_1	m_1	b_2	m_2	b_3	m_3
12B50	First order	0.9748	-0.01575	-	-	-	-
	Second order	0.9439	-0.0482	0.0561	3.745	-	-
	Third order	0.9422	-0.04946	0.05062	3.217	2.259e-14	1
Adjusted R-square		0.9034		0.9066		0.9067	
Optimal Vibe function		Second order Vibe function					

Operating point	Vibe function	Vibe 1		Vibe 2		Vibe 3	
		b_1	m_1	b_2	m_2	b_3	m_3
12B75	First order	0.9725	-0.00534	-	-	-	-
	Second order	0.9451	-0.03485	0.0549	4.169	-	-
	Third order	0.9421	-0.03724	0.04717	3.242	2.298e-14	1
Adjusted R-square		0.9416		0.9441		0.9446	
Optimal Vibe function		Second order Vibe function					

Operating point	Vibe function	Vibe 1		Vibe 2		Vibe 3	
		b_1	m_1	b_2	m_2	b_3	m_3
12B100	First order	0.9754	-0.01668	-	-	-	-
	Second order	0.9484	-0.04523	0.0516	4.108	-	-
	Third order	0.9469	-0.0464	0.0464	3.536	2.228e-14	1
Adjusted R-square		0.9079		0.9107		0.9109	
Optimal Vibe function		Second order Vibe function					

Operating point	Vibe function	Vibe 1		Vibe 2		Vibe 3	
		b_1	m_1	b_2	m_2	b_3	m_3
13A	First order	0.984	-0.01251	-	-	-	-
	Second order	0.978	-0.01972	0.022	9.887	-	-
	Third order	0.7539	0.0972	0.01058	13.55	0.2308	-0.3513
Adjusted R-square		0.9873		0.9877		0.9890	
Optimal Vibe function		First order Vibe function					

Operating point	Vibe function	Vibe 1		Vibe 2		Vibe 3	
		b_1	m_1	b_2	m_2	b_3	m_3
13B25	First order	0.9868	0.04458	-	-	-	-
	Second order	0.9862	0.04387	0.0138	96.38	-	-
	Third order	0.9862	0.04386	0.01433	96.38	2.221e-14	1
Adjusted R-square		0.9981		0.9981		0.9981	
Optimal Vibe function		First order Vibe function					

Operating point	Vibe function	Vibe 1		Vibe 2		Vibe 3	
		b_1	m_1	b_2	m_2	b_3	m_3
13B50	First order	0.9799	0.02977	-	-	-	-
	Second order	0.9714	0.01957	0.0286	10.05	-	-
	Third order	0.9707	0.01884	0.02546	8.53	2.224e-14	1
Adjusted R-square		0.9882		0.9893		0.9893	
Optimal Vibe function		First order Vibe function					

Operating point	Vibe function	Vibe 1		Vibe 2		Vibe 3	
		b_1	m_1	b_2	m_2	b_3	m_3
13B75	First order	0.9913	0.01219	-	-	-	-
	Second order	0.991	0.01187	0.009	163.7	-	-
	Third order	0.991	0.01186	0.01189	164.8	3.496e-10	-9
Adjusted R-square		0.9859		0.9859		0.9859	
Optimal Vibe function		First order Vibe function					

Operating point	Vibe function	Vibe 1		Vibe 2		Vibe 3	
		b_1	m_1	b_2	m_2	b_3	m_3
13B100	First order	0.9859	0.03415	-	-	-	-
	Second order	0.9813	0.02875	0.0187	12.97	-	-
	Third order	0.9811	0.02854	0.01656	11.52	5.332e-12	1
Adjusted R-square		0.9962		0.9967		0.9967	
Optimal Vibe function		First order Vibe function					

Operating point	Vibe function	Vibe 1		Vibe 2		Vibe 3	
		b_1	m_1	b_2	m_2	b_3	m_3
14A	First order	0.9752	0.2599	-	-	-	-
	Second order	0.967	0.2489	0.033	13.62	-	-
	Third order	0.9303	0.274	0.02517	11.41	0.03778	-0.3037
Adjusted R-square		0.9973		0.9980		0.9982	
Optimal Vibe function		First order Vibe function					

Operating point	Vibe function	Vibe 1		Vibe 2		Vibe 3	
		b_1	m_1	b_2	m_2	b_3	m_3
14B25	First order	0.9853	0.2597	-	-	-	-
	Second order	0.9802	0.2529	0.0191	14.27	-	-
	Third order	0.9801	0.2528	0.01833	13.29	5.229e-14	1
Adjusted R-square		0.9984		0.9987		0.9987	
Optimal Vibe function		First order Vibe function					

Operating point	Vibe function	Vibe 1		Vibe 2		Vibe 3	
		b_1	m_1	b_2	m_2	b_3	m_3
14B50	First order	0.9954	0.2262	-	-	-	-
	Second order	0.9949	0.2256	0.0051	50.49	-	-
	Third order	0.9949	0.2256	0.00545	50.49	2.221e-14	1
Adjusted R-square		0.9946		0.9946		0.9946	
Optimal Vibe function		First order Vibe function					

Operating point	Vibe function	Vibe 1		Vibe 2		Vibe 3	
		b_1	m_1	b_2	m_2	b_3	m_3
14B75	First order	0.9771	0.1926	-	-	-	-
	Second order	0.9611	0.172	0.0389	7.304	-	-
	Third order	0.8052	0.2959	0.02511	11.33	0.1679	-0.2982
Adjusted R-square		0.9944		0.9960		0.9971	
Optimal Vibe function							

Operating point	Vibe function	Vibe 1		Vibe 2		Vibe 3	
		b_1	m_1	b_2	m_2	b_3	m_3
14B100	First order	0.9859	0.2377	-	-	-	-
	Second order	0.9759	0.2247	0.0241	7.95	-	-
	Third order	0.9081	0.253	0.02227	8.651	0.06968	-0.09052
Adjusted R-square		0.9982		0.9988		0.9989	
Optimal Vibe function		First order Vibe function					

Operating point	Vibe function	Vibe 1		Vibe 2		Vibe 3	
		b_1	m_1	b_2	m_2	b_3	m_3
15A	First order	0.9959	0.4584	-	-	-	-
	Second order	0.9928	0.454	.0072	13.21	-	-
	Third order	0.9715	0.4843	0.01046	21.44	0.02373	-1.306
Adjusted R-square		0.9982		0.9983		0.9987	
Optimal Vibe function		First order Vibe function					

Operating point	Vibe function	Vibe 1		Vibe 2		Vibe 3	
		b_1	m_1	b_2	m_2	b_3	m_3
15B25	First order	0.9973	0.4176	-	-	-	-
	Second order	0.9905	0.4082	0.0095	7.327	-	-
	Third order	0.9443	0.4703	0.01316	16.01	0.05233	-0.5667
Adjusted R-square		0.9957		0.9959		0.9969	
Optimal Vibe function		First order Vibe function					

Operating point	Vibe function	Vibe 1		Vibe 2		Vibe 3	
		b_1	m_1	b_2	m_2	b_3	m_3
15B50	First order	0.9862	0.5175	-	-	-	-
	Second order	0.9852	0.516	0.0148	51.21	-	-
	Third order	0.9846	0.5153	0.00772	22.68	7.051e-09	-59
Adjusted R-square		0.9986		0.9986		0.9986	
Optimal Vibe function		First order Vibe function					